ISAS - INTERNATIONAL SCHOOL FOR ADVANCED STUDIES

Lattice Dynamics of Semiconductors from Density-Functional Perturbation Theory.

Thesis submitted for the degree of

"Doctor Philosophiæ"

CANDIDATE

Pasquale Pavone

SUPERVISOR

Prof. Stefano Baroni

November 1991

TRIESTE

SISSA - SCUOLA INTERNAZIONALE SUPERIORE DI STUDI AVANZATI

TRIESTE

Strada Costiera 11

SISSA ISAS

SCUOLA INTERNAZIONALE SUPERIORE DI STUDI AVANZATI
INTERNATIONAL SCHOOL FOR ADVANCED STUDIES

Lattice Dynamics of Semiconductors from Density-Functional Perturbation Theory.

Thesis submitted for the degree of

"Doctor Philosophiæ"

CANDIDATE

Pasquale Pavone

SUPERVISOR

Prof. Stefano Baroni

November 1991

a Vichi

Index

Introduction

Ab-initio methods based on Density-Functional Theory (DFT) are by now common and well established tools for studying structural and vibrational properties of materials on very realistic grounds. The plane-wave pseudopotential method and the Local-Density Approximation (LDA) to DFT have provided a simple framework whose accuracy and predictive power have been convincingly demonstrated in a large variety of systems.[1] The calculation of reliable phonon spectra in semiconductors is well within the reach of DFT. Recently, a very efficient perturbative approach has been developed: the Density Functional Perturbation Theory[2,3] (DFPT). This approach allows to obtain dynamical matrices at arbitrary wavevectors with a computational effort comparable to that of a self-consistent calculation for the unperturbed bulk. It is by now possible to obtain accurate phonon dispersions on a fine grid of wavevectors covering the entire Brillouin zone (BZ),[4] which compare directly with neutron diffraction data, and from which several physical properties of the system (such as heat capacities, thermal expansion coefficients, temperature dependence of the band gap, and so on) can be calculated.

Bulk phonon dispersion spectra are interesting not only for their relevance to the properties of pure materials, but also as ingredients of approximate calculations for complex systems such as semiconductor alloys, superlattices, and other quantum microstructures. Much attention is presently being paid to the vibrational properties of such systems, both because of their fundamental interest, and as a

promising tool for the structural characterization of these new materials.[5,6] Most of the existing theoretical studies heavily rely on information about the force constants of the pure materials.[6] Even when first-principles calculations for the superlattice are available, bulk phonon dispersions of the constituents are very useful for interpreting the calculated spectra, and comparing them with experiments.[7] A detailed account of disorder effects in semiconductor microstructures may require the consideration of (many) systems with a rather high number of atoms per unit cell ($\approx$ 100, or more). A direct first-principles calculation of the phonon spectra for such systems may be very demanding computationally, even with the highly efficient linear-response techniques presently available. On the other hand, calculations based on empirical models such as the shell model, the bond-charge model or others, have a limited predictive power. In fact, the parameters entering these models are fitted to experiments. In the case of AlAs, for instance, experimental information is very poor, and existing semiempirical calculations based on force constants fitted to the phonon spectrum of bulk GaAs produce a longitudinal-optic (LO) band along the ΓX direction which is much wider than calculated from first principles.[7] It is therefore desirable to devise a method to treat both perfect bulk semiconductors and their alloys and microstructures with an affordable amount of computer resources, retaining an accuracy similar to that of direct first-principles calculations.

In this thesis we present the modern methods for calculating the vibrational properties of extended systems and we apply them to pure bulk semiconductors. Furthermore, we develop an approach to describe more complex systems such as superlattices and alloys. To this end, we first give a detailed theoretical description of the DFPT and of the computational techniques necessary to implement it.

We then demonstrate the predictive power of these methods in the case of semiconducting pure crystals, where a wealth of well established experimental results exists. We present the first *ab-initio* calculation of full phonon dispersions of three group IV elements, C, Si and Ge, and four compound semiconductors, GaAs, AlAs, GaSb, and AlSb. In the case of AlAs—whose vibrational properties are poorly known because of the lack of neutron-scattering data—the accuracy of our predictions is confirmed by the excellent agreement between the phonon dispersions calculated for the closely related compound AlSb, and recent neutron-scattering data.[8]

A complete description of harmonic lattice dynamics requires the knowledge of both eigenvalues and eigenvectors of the dynamical matrix. To this purpose we also calculate the eigendisplacements along some high-symmetry lines in diamond and some elemental (Si, Ge) and compound (GaAs, AlAs) semiconductors. The peculiar behaviour of the eigenvectors in the case of diamond is analyzed and discussed in terms of the competition between angular (bond-bending) and radial (bond-stretching) force constants. As a byproduct we calculate the internal strain parameter for these materials.

As a further application, thermal expansion of semiconductors can be calculated within the so-called Quasi Harmonic Approximation. While most of the materials expand upon heating, many tetrahedral semiconductors (e.g. Si, Ge, GaAs) exhibit negative thermal expansions at low temperatures.[9,10] For long time these features have been investigated theoretically only within semi-empirical models. Only recently, the first attempts of *realistic* calculations have been carried out on silicon[11,12,13] and diamond.[13] We improve the previous ab-initio calculation[12] of the thermal expansion coefficient of Si, and extend the application to some other semiconductors (Ge, GaAs, AlAs).

Finally, we focus our interest on mixed semiconductors (superlattices and alloys), particularly on the possibility of using for these systems the informations gained from calculations on pure materials. To this aim, we examine to which extent the interatomic force constants of pure bulk semiconductors are similar to each other, in view of using them to study the vibrational properties of mixed systems, such as alloys, superlattices (both ordered and partially disordered), or other quantum structures. In the case of III-V compounds, we find that the force constants of materials which differ by their cations are rather similar to each other, while this is less so when the materials differ by their anions. The situation is intermediate in the case of elemental semiconductors. Phonon frequencies of thin $(AlAs)_n(GaAs)_n$ (001) superlattices (SL's) are evaluated using the force constants of the corresponding virtual crystal. The values obtained in such an approximation compare very well with those of full ab-initio calculations of the same systems.

The detailed features of the Raman spectra in these systems are still far from being completely understood. A simple approximation has been recently proposed for the Raman intensity in AlAs/GaAs systems,[14] in which the differences of the atomic polarizabilities between the two cationic species are neglected. Though adequate for many qualitative purposes, this approximation fails to reproduce the observed relative intensity of the various peaks. In order to improve the quantitative understanding of Raman spectra in AlAs/GaAs systems, we present a model based on a perturbative expansion of the dielectric susceptibility of the crystal upon composition. In this model the Raman tensor is expressed in terms of a restrict number of parameters which are obtained by a fitting procedure applied to the results of ab-initio calculations of Raman intensities of some short-period SL's. The method which we have developed can then be used to obtain Raman spectra of *any* AlAs/GaAs mixed structure.

Chapter 1

Ab-Initio Lattice Dynamics in Semiconductors

Many important achievement have been obtained by modern solid state physics in the description of the vibrational properties of solids. Model theories of lattice dynamics[15] reached the state in which experimental values can be reproduced with great accuracy by fitting the parameters of the model to experiments. However, these last years have seen increased demand for "parameter-free" approaches, both for the intrinsic theoretical interest and for the fundamental role played when the experimental information is lacking or debated.

In this chapter we first introduce the problem of lattice dynamics of infinite crystals. We show then the details of a method that allows the "first principles" evaluation of the lattice dynamical properties of semiconductors in the framework of the Density Functional Perturbation Theory.

1.1 Lattice dynamics and force constants

Let us consider an extended three-dimensional crystal made by N cells with n atoms in the unit cell. We indicate the position of the i-th atom of the generic

cell, in the undistorted crystal, as:

$$\mathbf{R}_{L,i} = \mathbf{R}_L + \tau_i \qquad i = 1, 2, ..., n \ , \tag{1.1}$$

where the lattice vector $\mathbf{R}_L$ can be expressed in terms of the basis vectors $\{\mathbf{a}_l\}$ as:

$$\mathbf{R}_L = n_1\mathbf{a}_1 + n_2\mathbf{a}_2 + n_3\mathbf{a}_3 \qquad L \equiv \{n_1, n_2, n_3\} \ , \tag{1.2}$$

the $\{n_l\}$ are integer numbers, and the position of the i-th atom in the unit cell is given by:

$$\tau_i = x_1^i\mathbf{a}_1 + x_2^i\mathbf{a}_2 + x_3^i\mathbf{a}_3 \qquad 0 \leq x_l^i < 1. \tag{1.3}$$

In the harmonic approximation small displacements from the equilibrium position are assumed. Therefore the total effective potential energy of the crystal can be expressed in terms of the displacements defined by

$$\mathbf{R}_{L,i} \rightarrow \mathbf{R}_{L,i} + \boldsymbol{u}_i(\mathbf{R}_L) \ , \tag{1.4}$$

as a Taylor expansion up to the second order:

$$\mathcal{E} = \mathcal{E}_0 + \frac{1}{2}\sum_{L,L'}\sum_{i,j} \boldsymbol{u}_i(\mathbf{R}_L) \cdot \boldsymbol{C}_{i,j}(\mathbf{R}_L, \mathbf{R}_{L'}) \cdot \boldsymbol{u}_j(\mathbf{R}_{L'}) + \mathcal{O}(\boldsymbol{u}^3) \ . \tag{1.5}$$

The coefficients $C_{\alpha i,\beta j}(\mathbf{R}_L, \mathbf{R}_{L'})$ appearing in Eq. (1.5) are called *interatomic force constants* and are given by

$$C_{\alpha i,\beta j}(\mathbf{R}_L, \mathbf{R}_{L'}) = \left.\frac{\partial^2\mathcal{E}}{\partial u_{\alpha i}(\mathbf{R}_L)\partial u_{\beta j}(\mathbf{R}_{L'})}\right|_0 , \tag{1.6}$$

where the second derivatives are calculated at the equilibrium. To lighten the notation, in the following we will drop the index L for Bravais lattice vectors when

no possibility of confusion may arise. Differentiation with respect to $u_{\alpha i}(\mathbf{R})$ of Eq. (1.5) allows us to write the force acting on an atom at site $\mathbf{R}_i$:

$$\boldsymbol{F}_i(\mathbf{R}) = -\frac{\partial \mathcal{E}}{\partial \boldsymbol{u}_i(\mathbf{R})} = -\sum_{\mathbf{R}',j} \boldsymbol{C}_{i,j}(\mathbf{R},\mathbf{R}') \cdot \boldsymbol{u}_j(\mathbf{R}') + \mathcal{O}(\boldsymbol{u}^2) \ . \tag{1.7}$$

The atomic force constants defined in Eq. (1.6) are not independent quantities, but they are connected to each other by relations due to the symmetry properties of the crystal. In particular, because of the translational invariance of the crystal, the force constants only depend on the difference $\mathbf{R} - \mathbf{R}'$; furthermore they satisfy the relation:

$$\sum_{\mathbf{R}',j} \boldsymbol{C}_{i,j}(\mathbf{R} - \mathbf{R}') = 0 \ . \tag{1.8}$$

Eq. (1.8) expresses the fact that the potential energy remains unchanged for a uniform translation of the whole crystal. This property is related to the vanishing frequence of the acoustic modes at the Brillouin zone center. According to Eq. (1.7) the classic equations of motion read:

$$M_i \ddot{\boldsymbol{u}}_i(\mathbf{R}) = -\sum_{\mathbf{R}',j} \boldsymbol{C}_{i,j}(\mathbf{R} - \mathbf{R}') \cdot \boldsymbol{u}_j(\mathbf{R}') \ . \tag{1.9}$$

Translational invariance requires that the solution of the infinite set of coupled equations (1.9) can be put in the Bloch-wave form:

$$\boldsymbol{u}_i(\mathbf{R}) = \frac{1}{\sqrt{M_i}} \boldsymbol{u}_i \, \mathrm{e}^{i\mathbf{q}\cdot\mathbf{R} - i\omega t} \ . \tag{1.10}$$

The allowed values of $\mathbf{q}$ are chosen according to the Born-Von Kármán periodic boundary conditions. By substitution of Eq. (1.10) in Eq. (1.9) we obtain the equation:

$$\omega^2 \boldsymbol{u}_i = \sum_j \tilde{\boldsymbol{D}}_{i,j}(\mathbf{q}) \cdot \boldsymbol{u}_j \ , \tag{1.11}$$

where we have introduced the discrete Fourier transform:

$$\widetilde{\boldsymbol{D}}_{i,j}(\mathbf{q}) = \frac{1}{\sqrt{M_i M_j}} \sum_{\mathbf{R}} \boldsymbol{C}_{i,j}(\mathbf{R})\, \mathrm{e}^{-i\mathbf{q}\cdot(\mathbf{R})} \ . \tag{1.12}$$

The matrix $\widetilde{\boldsymbol{D}}_{i,j}(\mathbf{q})$ defined by Eq. (1.12) is called the *dynamical matrix* of the crystal. It is a $3n \times 3n$ hermitian matrix, and has the well-known properties:[16]

$$\widetilde{\boldsymbol{D}}_{i,j}(\mathbf{q}) = \left(\widetilde{\boldsymbol{D}}_{i,j}(\mathbf{q})^*\right)^T \tag{1.13}$$

$$\widetilde{\boldsymbol{D}}_{i,j}(-\mathbf{q}) = \widetilde{\boldsymbol{D}}_{i,j}(\mathbf{q})^* \ . \tag{1.14}$$

The eigenvalue problem in Eq. (1.11) has $3n$ solutions for ω^2 at each point in the Brillouin zone, $\mathbf{q}$; these will be denoted by $\omega_m^2(\mathbf{q})$, where $m = 1, 2, ..., n$, and can be interpreted as the branches of a multivalued function $\omega^2(\mathbf{q})$. The relations expressed by the equations $\omega = \omega_m(\mathbf{q})$ are known as *dispersion relations.*

Due to the hermiticity of $\widetilde{\boldsymbol{D}}_{i,j}(\mathbf{q})$ the eigenvectors $\boldsymbol{u}_{i,\mathbf{q}}^m$ can be chosen in such a way to satisfy the orthonormality and the closure relations

$$\begin{aligned} \sum_i (\boldsymbol{u}_{i,\mathbf{q}}^m)^* \cdot \boldsymbol{u}_{i,\mathbf{q}}^{m'} &= \delta_{mm'} \\ \sum_m (u_{\alpha i,\mathbf{q}}^m)^*\ u_{\alpha' j,\mathbf{q}}^m &= \delta_{ij}\delta_{\alpha\alpha'} \ . \end{aligned} \tag{1.15}$$

1.2 Linear response and lattice dynamics

Since the works of De Cicco and Johnson[17] and of Pick, Cohen, and Martin,[18] it is well known that the harmonic force constants of crystals are determined by their static linear electronic response. In fact, within the adiabatic approximation, the lattice distortion associated with a phonon can be seen as a static perturbation acting on the electrons. It is a simple application of the Hellmann-Feynman

theorem[19] to show that the linear variation of the electron density upon application of an external, static, perturbation determines the energy variation up to second order in the perturbation (up to third order, indeed, as shown in Ref. 20).

Suppose that the *bare* external potential acting on the electrons, $V_{\boldsymbol{\lambda}}$, (which we assume for simplicity to be local) is a continuous function of some parameters $\boldsymbol{\lambda} \equiv \{\lambda_i\}$. The Hellmann-Feynman theorem states that the "force" associated with the variation of the external parameters $\boldsymbol{\lambda}$ is given by the ground-state expectation value of the derivative of $V_{\boldsymbol{\lambda}}$:

$$\frac{\partial \mathcal{E}_{\boldsymbol{\lambda}}}{\partial \lambda_i} = \int n_{\boldsymbol{\lambda}}(\mathbf{r}) \frac{\partial V_{\boldsymbol{\lambda}}(\mathbf{r})}{\partial \lambda_i} \, \mathrm{d}\mathbf{r}, \tag{1.16}$$

where $\mathcal{E}_{\boldsymbol{\lambda}}$ is the electron ground-state energy relative to given values of the $\boldsymbol{\lambda}$ parameters, and $n_{\boldsymbol{\lambda}}$ is the corresponding electron density distribution. Total energy variations are obtained from Eq. (1.16) by integration. In order to have energy variations correct up to second order in $\boldsymbol{\lambda}$, it is necessary that the r.h.s. of Eq. (1.16) be correct to linear order:

$$\frac{\partial \mathcal{E}_{\boldsymbol{\lambda}}}{\partial \lambda_i} = \int \left(n_0(\mathbf{r}) \frac{\partial V_{\boldsymbol{\lambda}}(\mathbf{r})}{\partial \lambda_i} + \sum_j \lambda_j \frac{\partial n_{\boldsymbol{\lambda}}(\mathbf{r})}{\partial \lambda_j} \frac{\partial V_{\boldsymbol{\lambda}}(\mathbf{r})}{\partial \lambda_i} + \right.$$
$$\left. + n_0(\mathbf{r}) \sum_j \lambda_j \frac{\partial^2 V_{\boldsymbol{\lambda}}(\mathbf{r})}{\partial \lambda_i \partial \lambda_j} \right) \mathrm{d}\mathbf{r} + \mathcal{O}(\boldsymbol{\lambda}^2), \tag{1.17}$$

all the derivatives being calculated at $\boldsymbol{\lambda} = 0$. Integration of Eq. (1.17) gives:

$$\mathcal{E}_{\boldsymbol{\lambda}} = \mathcal{E}_0 + \sum_i \lambda_i \int n_0(\mathbf{r}) \frac{\partial V_{\boldsymbol{\lambda}}(\mathbf{r})}{\partial \lambda_i} \, \mathrm{d}\mathbf{r} +$$
$$+ \frac{1}{2} \sum_{ij} \lambda_i \lambda_j \int \left(\frac{\partial n_{\boldsymbol{\lambda}}(\mathbf{r})}{\partial \lambda_j} \frac{\partial V_{\boldsymbol{\lambda}}(\mathbf{r})}{\partial \lambda_i} + n_0(\mathbf{r}) \frac{\partial^2 V_{\boldsymbol{\lambda}}(\mathbf{r})}{\partial \lambda_i \partial \lambda_j} \right) \mathrm{d}\mathbf{r}. \tag{1.18}$$

Suppose now that the $\boldsymbol{\lambda}$ parameters represent ion displacements, $u_{\alpha i}(\mathbf{R})$, then the second derivatives of the energy $\mathcal{E}$ are simply related to the matrix of the force

constants:

$$\frac{\partial^2 \mathcal{E}}{\partial u_{\alpha i}(\mathbf{R}) \partial u_{\beta j}(\mathbf{R}')} = C_{\alpha i,\beta j}(\mathbf{R}-\mathbf{R}') = C^{ion}_{\alpha i,\beta j}(\mathbf{R}-\mathbf{R}') + C^{elec}_{\alpha i,\beta j}(\mathbf{R}-\mathbf{R}'). \quad (1.19)$$

The first term in the r.h.s. of Eq. (1.19) is the ionic contribution to the force constants, which is essentially the second derivative of the ion-ion contribution to the total energy of the system:

$$C^{ion}_{\alpha i,\beta j}(\mathbf{R}-\mathbf{R}') = \frac{\partial^2 \mathcal{E}_{\text{ion}-\text{ion}}}{\partial u_{\alpha i}(\mathbf{R}) \partial u_{\beta j}(\mathbf{R}')} , \quad (1.20)$$

where

$$\mathcal{E}_{\text{ion}-\text{ion}} = \sum_{i,j} \sum_{\mathbf{R},\mathbf{R}'} \frac{e^2 Z_i Z_j}{|\mathbf{R}+\boldsymbol{\tau}_i - \mathbf{R}' - \boldsymbol{\tau}_j|} , \quad (1.21)$$

and eZ_i is the valence charge of the i-th ion in the cell. For finite systems no problems arise in the evaluation of $\mathcal{E}_{\text{ion}-\text{ion}}$. However, in an infinite crystal the sums in Eq. (1.21) do not converge. Similar divergences arise in the expression of the electron-ion and electron-electron terms of the total energy. However, due to the charge neutrality of the crystal all these divergences cancel out. The resulting nonsingular expression of $\mathcal{E}_{\text{ion}-\text{ion}}$, evaluated with the Ewald method, is given in Appendix A. The electronic contribution to the force constants, C^{elec} is given by:

$$C^{elec}_{\alpha i,\beta j}(\mathbf{R}-\mathbf{R}') = \int \left(\frac{\partial n(\mathbf{r})}{\partial u_{\alpha i}(\mathbf{R})} \frac{\partial V_{ion}(\mathbf{r})}{\partial u_{\beta j}(\mathbf{R}')} + n_0(\mathbf{r}) \frac{\partial^2 V_{ion}(\mathbf{r})}{\partial u_{\alpha i}(\mathbf{R}) \partial u_{\beta j}(\mathbf{R}')} \right) \mathrm{d}\mathbf{r}, \quad (1.22)$$

where $V_{ion}(\mathbf{r})$ is the *bare* ionic (pseudo)potential acting on the electrons:

$$V_{ion}(\mathbf{r}) = \sum_{\mathbf{R},i} v_i(\mathbf{r}-\mathbf{R}-\boldsymbol{\tau}_i), \quad (1.23)$$

and $\partial n(\mathbf{r})/\partial u_{\alpha i}(\mathbf{R})$ is the electron density response to the displacement in the α-th direction of the i-th ion in the unit cell at $\mathbf{R}$. The matrix of the force constants is conveniently calculated in reciprocal space:

$$C_{\alpha i,\beta j}(\mathbf{R}) = \frac{1}{N} \sum_{\mathbf{q}} \mathrm{e}^{i\mathbf{q}\cdot\mathbf{R}} \, \widetilde{C}_{\alpha i,\beta j}(\mathbf{q}), \quad (1.24)$$

where N is the number of unit cells in the crystal. For the ionic contribution, one finds:

$$\widetilde{C}^{ion}_{\alpha i,\beta j}(\mathbf{q}) = \frac{4\pi e^2}{\Omega} \sum_{\mathbf{G},\mathbf{q}+\mathbf{G}\neq 0} \frac{\mathrm{e}^{-(\mathbf{q}+\mathbf{G})^2/4\eta}}{(\mathbf{q}+\mathbf{G})^2} Z_i Z_j e^{i(\mathbf{q}+\mathbf{G})\cdot(\boldsymbol{\tau}_i-\boldsymbol{\tau}_j)}(\mathrm{q}_\alpha+\mathrm{G}_\alpha)(\mathrm{q}_\beta+\mathrm{G}_\beta)$$
$$-\frac{2\pi e^2}{\Omega} \sum_{\mathbf{G}\neq 0} \frac{\mathrm{e}^{-\mathrm{G}^2/4\eta}}{\mathrm{G}^2} \left[Z_i \sum_l Z_l \mathrm{e}^{i\mathbf{G}\cdot(\boldsymbol{\tau}_i-\boldsymbol{\tau}_l)} \mathrm{G}_\alpha \mathrm{G}_\beta + \mathrm{c.c.} \right] \delta_{ij}, \quad (1.25)$$

where η is a parameter which is chosen to be large enough to allow the neglect of the real-space term in the Ewald energy (see Appendix A).

The electronic contribution to $\widetilde{C}(\mathbf{q})$ is given by

$$\widetilde{C}^{elec}_{\alpha i,\beta j}(\mathbf{q}) = \int \left(\frac{\partial n(\mathbf{r})}{\partial u_{\alpha i \mathbf{q}}} \right)^* \frac{\partial V_{ion}(\mathbf{r})}{\partial u_{\beta j \mathbf{q}}} \, \mathrm{d}\mathbf{r} + \delta_{ij} \int n_0(\mathbf{r}) \frac{\partial^2 V_{ion}(\mathbf{r})}{\partial u_{\alpha i \mathbf{q}=0} \partial u_{\beta i \mathbf{q}=0}} \, \mathrm{d}\mathbf{r}, \quad (1.26)$$

where $\partial V_{ion}(\mathbf{r})/\partial u_{\alpha i \mathbf{q}}$ is the linear variation of the external ionic pseudopotential upon a lattice distortion of the form:

$$u_{\alpha i}(\mathbf{R}) = u_{\alpha i \mathbf{q}} \, \mathrm{e}^{i\mathbf{q}\cdot\mathbf{R}}, \quad (1.27)$$

and $\partial n/\partial u_{\alpha i \mathbf{q}}$ the corresponding variation of the electron density.

Eq. (1.26) shows that the knowledge of the electron density response to a lattice distortion of the form (1.27) enables one to calculate the harmonic force constants of the crystal. Phonon frequencies are then obtained as shown in Section 1.1 by diagonalization of the dynamical matrix:

$$\widetilde{D}_{i,j}(\mathbf{q}) = \frac{\widetilde{C}_{i,j}(\mathbf{q})}{\sqrt{M_i M_j}}, \quad (1.28)$$

where the M's are ionic masses.

1.3 Density-functional perturbation theory

The considerations made in the previous section are exact. In practice we need a method to evaluate the electron density from the external potential. In principle, this can be achieved by solving the Schrödinger equation (SE) of the system. In practice, however, the solution of the SE for many-electron systems is not possible due to the very large number of degrees of freedom. Density-Functional Theory (DFT) provides a theoretical framework to calculate ground state properties without solving any SE. The practical implementation of DFT requires in turn some approximations (namely the Local Density Approximation) whose ability to cope with many problems in condensed matter physics is by now well assessed.

Here we give first a brief review of the main aspects of DFT, then we will present a method to linearize the DFT with respect to perturbations of arbitrary wavelength.

1.3.1 Density functional theory

In the Born-Oppenheimer approximation, the ground state (GS) properties of a system of interacting electrons in an external potential are given by the Schrödinger equation:

$$H\Psi(\mathbf{r}_1,\mathbf{r}_2,...,\mathbf{r}_N) = \left[-\sum_i \frac{\hbar^2}{2m}\nabla_i^2 + \sum_i V_{\rm ext}(\mathbf{r}_i) + \frac{e^2}{2}\sum_{i\neq j}\frac{1}{|\mathbf{r}_i-\mathbf{r}_j|}\right]\Psi = E\Psi \ . \tag{1.29}$$

where the $\mathbf{r}_i$ denote both particle coordinates and spins. The Schrödinger equation implies that all the GS properties of the system are functionals of the external potential $V_{\rm ext}(\mathbf{r})$. In particular $V_{\rm ext}(\mathbf{r})$ determines the GS electron density $n(\mathbf{r})$.

The Hohenberg-Kohn (HK) theorem[21] states the invertibility (up to a trivial constant) of the correspondence between the external potential $V_{\rm ext}$ and the density $n(\mathbf{r})$ in the ground state. As a consequence, we can express any physical property of the system in the ground state as a functional of the electronic density. In particular this holds for the total ground state energy that can be written in the following way:

$$E[n] = \min\left(F[n] + \int V_{\rm ext}(\mathbf{r})n(\mathbf{r})\mathrm{d}\mathbf{r}\right) , \tag{1.30}$$

where the minimum search is constrained by the condition that the total number of electron is fixed, $\int n(\mathbf{r})\mathrm{d}\mathbf{r} = N$, and $F[n]$ is a universal functional (i.e. it is independent on $V_{\rm ext}$) whose form is in general unknown. It is useful to separate in the expression of $F[n]$ the Hartree term, due to the classical electrostatic interaction between the electrons, and a term, $T_0[n]$, defined as the kinetic energy of a noninteracting electron system with density $n(\mathbf{r})$. We have then:

$$F[n] = T_0[n] + \frac{e^2}{2}\int \frac{n(\mathbf{r})n(\mathbf{r}')}{|\mathbf{r}-\mathbf{r}'|}\mathrm{d}\mathbf{r}\mathrm{d}\mathbf{r}' + E_{XC}[n] . \tag{1.31}$$

In fact, Eq. (1.31) defines the *exchange-correlation energy* $E_{XC}[n]$ as the difference between the unknown functional $F[n]$ and the known terms in its r.h.s.

Following this approach, a set of self-consistent single particle equations can be obtained[22] from the variational principle for the total ground state energy $E[n]$:

$$\left[-\frac{\hbar^2}{2m}\nabla^2 + V_{SCF}(\mathbf{r})\right]\psi_i(\mathbf{r}) = \epsilon_i\psi_i(\mathbf{r}) , \tag{1.32}$$

where the self-consistent (SCF) DFT potential, V_{SCF}, for a system of electrons moving in the external potential of the ions is given by:

$$V_{SCF}(\mathbf{r}) = V_{ion}(\mathbf{r}) + e^2\int \frac{n(\mathbf{r}')}{|\mathbf{r}-\mathbf{r}'|}\,\mathrm{d}\mathbf{r}' + v_{XC}(\mathbf{r}) , \tag{1.33}$$

with

$$n(\mathbf{r}) = \sum_i |\psi_i(\mathbf{r})|^2 \ , \qquad v_{XC}(\mathbf{r}) = \frac{\delta E_{XC}[n]}{\delta n(\mathbf{r})} \ , \tag{1.34}$$

where the sums are extended only to the first N lowest eigenstates of the single particle equation (1.32). The above equations are known as the Kohn-Sham self-consistent equations.

Due to the unknown exchange-correlation potential the Kohn-Sham equations are of no practical use, unless an approximation for v_{XC} is specified. In practical calculations the most used approximation is the so-called *Local Density Approximation* (LDA). In this approximation the exchange-correlation energy is taken "locally" equal to the one of the homogeneous electron gas at density equal to the local density, $n(\mathbf{r})$:

$$E_{XC}^{\mathrm{LDA}}[n] = \int \epsilon_{XC}\left(n(\mathbf{r})\right) n(\mathbf{r}) \mathrm{d}\mathbf{r} \ , \tag{1.35}$$

where $\epsilon_{XC}(n)$ is the exchange-correlation energy per particle of the electron gas with uniform density n. In this way the potential v_{XC} appearing in Eq. (1.34) is given by

$$v_{XC}(\mathbf{r}) = \mu_{XC}\left(n(\mathbf{r})\right) \qquad \mu_{XC}(n) = \frac{\mathrm{d}}{\mathrm{d}n}\left[n\,\epsilon_{XC}(n)\right] \Big| \ . \tag{1.36}$$

1.3.2 Linear response in DFT

Suppose one has solved the Kohn-Sham equations for a crystal characterized by a (periodic) ionic potential $V_{ion}(\mathbf{r})$. Let us superimpose to $V_{ion}(\mathbf{r})$ a perturbation $\Delta V^{\mathbf{q}}_{bare}$ of given periodicity $\mathbf{q}$. The self-consistent potential will change accordingly: $V_{SCF} \rightarrow V_{SCF} + \Delta V^{\mathbf{q}}_{SCF}$. If $\Delta V^{\mathbf{q}}_{SCF}$ is supposed to be known, the linear variation in

the electron density Δn is obtained by first-order perturbation theory:

$$\Delta\tilde{n}(\mathbf{q}+\mathbf{G}) = \frac{4}{N\Omega}\sum_{\mathbf{k}}\sum_{c,v}\frac{\langle\psi_{v,\mathbf{k}}|e^{-i(\mathbf{q}+\mathbf{G})\mathbf{r}}|\psi_{c,\mathbf{k}+\mathbf{q}}\rangle\langle\psi_{c,\mathbf{k}+\mathbf{q}}|\Delta V^{\mathbf{q}}_{SCF}|\psi_{v,\mathbf{k}}\rangle}{\epsilon_{v,\mathbf{k}}-\epsilon_{c,\mathbf{k}+\mathbf{q}}}, \quad (1.37)$$

where $\Delta\tilde{n}(\mathbf{q}+\mathbf{G})$ is the Fourier transform of $\Delta n(\mathbf{r})$, Ω is the volume of the unit cell, v and c indicate valence and conduction bands respectively, and the sum over $\mathbf{k}$ covers the first Brillouin zone. It is here assumed that the crystal has doubly occupied valence bands and empty conduction bands separated by a gap. On the other hand, if Δn is known, ΔV_{SCF} can be obtained by linearizing Eq. (1.33):

$$\Delta V^{\mathbf{q}}_{SCF}(\mathbf{r}) = \Delta V^{\mathbf{q}}_{bare}(\mathbf{r}) + e^2\int\frac{\Delta n(\mathbf{r}')}{|\mathbf{r}-\mathbf{r}'|}\,d\mathbf{r}' + \Delta n(\mathbf{r})\left[\frac{dv_{XC}}{dn}\right]_{n=n_0(\mathbf{r})}, \quad (1.38)$$

where n_0 is the unperturbed electron density. Eqs. (1.37) and (1.38) form a system which can be solved iteratively. It should be remarked that the linear response to a perturbation of given $\mathbf{q}$ only contains Fourier components of wavevector $\mathbf{q}+\mathbf{G}$: different $\mathbf{q}$'s do not mix at this order of perturbation theory.

For computational convenience, it is desirable to avoid the sum over conduction bands of Eq. (1.37). This can be achieved by rewriting Eq. (1.37) in the following way:

$$\Delta\tilde{n}(\mathbf{q}+\mathbf{G}) = \frac{4}{N\Omega}\sum_{\mathbf{k}}\sum_{v}\langle\psi_{v,\mathbf{k}}|e^{-i(\mathbf{q}+\mathbf{G})\mathbf{r}}P_c G(\epsilon_{v,\mathbf{k}})P_c\Delta V^{\mathbf{q}}_{SCF}|\psi_{v,\mathbf{k}}\rangle, \quad (1.39)$$

where P_c is the projector over the conduction-state manifold, $G(\epsilon) = 1/(\epsilon - H_{SCF})$ is the one-electron Green's function of the unperturbed system, and the superscript in $\Delta V^{\mathbf{q}}_{SCF}$ has been introduced to stress that $\Delta V^{\mathbf{q}}_{SCF}$—when acting on a wavefunction of wavevector $\mathbf{k}$—transforms it into a function of wavevector $\mathbf{k}+\mathbf{q}$. Note that no special difficulties arise in evaluating Eq. (1.39) when $\Delta V^{\mathbf{q}}_{SCF}$ is a nonlocal operator. To evaluate Eq. (1.39), we further rewrite it as:

$$\Delta\tilde{n}(\mathbf{q}+\mathbf{G}) = \frac{4}{N\Omega}\sum_{\mathbf{k}}\sum_{v}\langle\psi_{v,\mathbf{k}}|e^{-i(\mathbf{q}+\mathbf{G})\mathbf{r}}P_c|\Delta\psi_{v,\mathbf{k}+\mathbf{q}}\rangle, \quad (1.40)$$

where $\Delta\psi_{v,\mathbf{k}+\mathbf{q}}$ is solution of the linear system:

$$\left[\epsilon_{v,\mathbf{k}} - H_{SCF}\right]|\Delta\psi_{v,\mathbf{k}+\mathbf{q}}\rangle = P_c \Delta V^{\mathbf{q}}_{SCF}|\psi_{v,\mathbf{k}}\rangle. \tag{1.41}$$

The linear system (1.41) has an infinite number of solutions because the determinant of $[\epsilon_{v,\mathbf{k}} - H_{SCF}]$ vanishes, and the vector on the l.h.s. is orthogonal to the null space of $[\epsilon_{v,\mathbf{k}} - H_{SCF}]$. In practice, $\Delta\psi_{v,\mathbf{k}+\mathbf{q}}$ is defined within a multiple of $\psi_{v,\mathbf{k}}$. As $\Delta\psi_{v,\mathbf{k}+\mathbf{q}}$ enters Eq. (1.40) only through its projection onto the conduction-state manifold, such an indeterminacy does not affect the final result. Depending on the size of the basis set, Eq. (1.41) can be solved either by factorization techniques, or by iterative methods. If factorization techniques are used, the best choice is to tridiagonalize first H_{SCF}, and solve then the system in the basis where it is tridiagonal. The advantage is that this allows one to perform just one factorization for *all* the systems corresponding to different values of $\epsilon_{v,\mathbf{k}}$. In both cases, the calculation of all the needed functions $\Delta\psi_{v,\mathbf{k}+\mathbf{q}}$ requires a numerical labor comparable to that needed for a single SCF iteration for the *unperturbed* system. The method we have so far described is of general validity and applies to any perturbation.

1.3.3 The plane wave pseudopotentials method

In a practical calculation the numerical solution of the self-consistent equations of the previous section is usually done by truncating the Hilbert space of electronic states to a finite subspace spanned by some appropriate finite basis set. When using periodic boundary conditions one of the most used basis sets is that of the plane waves

$$\langle \mathbf{r}|\mathbf{k}+\mathbf{G}\rangle = \frac{1}{\sqrt{V}}\, \mathrm{e}^{i(\mathbf{k}+\mathbf{G})\cdot\mathbf{r}}\,. \tag{1.42}$$

where $\mathbf{k}$ belongs to the Brillouin zone of the crystal, $\mathbf{G}$ is a reciprocal lattice vector and $V = N\Omega$ is the volume of the crystal. The dimension of the basis set is in this case determined by the so called kinetic energy cutoff $E_{\rm cut}$ through the condition:

$$\frac{\hbar^2}{2m}(\mathbf{k}+\mathbf{G})^2 \leq E_{\rm cut} \ . \tag{1.43}$$

This choice presents the advantage of being independent of the structure of the particular solid which has been considered. Furthermore the accuracy of the expansion can be systematically checked and improved simply by increasing the value of the cutoff energy $E_{\rm cut}$.

Plane wave basis sets are convenient only if not too many of them are needed to represent the Kohn-Sham eigenfunctions $\psi_i(\mathbf{r})$ to some target accuracy. This is surely not the case of the *core* eigenfunctions, namely those corresponding to the lowest lying atomic-like eigenstates, which have strong oscillations near the nuclei. Nevertheless, the core electrons do not contribute in general to the bonding properties of the solid and may be considered as *frozen* in the atomic configuration around the nucleus. On the contrary, the chemically active *valence* electrons, corresponding to the higher filled states and well separated energetically from the core states, are described by functions which are quite smooth at distances from the nucleus larger than a certain radius r_c. Inside this radius the valence eigenfunctions oscillate rapidly due to their orthogonality to the core states. The description of such oscillations would also require too large a basis set to be of practical use.

Many attempts have been made in order to overcome this problem and make feasible the study of general electronic and structural properties of multiatomic systems. Among the others, one of the most used methods is to transform the all-electron Schrödinger equation into an effective equation more suitable for the

practical applications. In this case an effective *pseudopotential* is used to simulate the interaction between the valence electrons and the cores (nuclei plus core electrons) such that no core wavefunctions have to be included explicitly and the valence wavefunction no longer have strong oscillations in the core region.

Many schemes for pseudopotential generation have been generated starting from ab-initio calculations on atoms.[23,24,25]. These schemes basically requires that, for a particular reference configuration, energy levels and wavefunctions beyond the core radius match their all-electron counterpart. The condition that all-electron and pseudo wavefunctions are equal outside the core radius is called *norm conservation* and it ensures transferability of the pseudopotentials to the different chemical environments. It has been demonstrated[26] numerically that these norm-conserving pseudopotentials faithfully simulate the all-electron results in typical semiconductors.

The usual form adopted for the pseudopotential is semilocal:

$$v_i(\mathbf{r},\mathbf{r}') = v_{i,loc}(r)\delta(\mathbf{r}-\mathbf{r}') + \sum_l v_{i,l}(\mathbf{r},\mathbf{r}') \ , \tag{1.44}$$

where

$$v_{i,l}(\mathbf{r},\mathbf{r}') = \frac{2l+1}{4\pi} v_{i,l}(r)\, P_l(\hat{\mathbf{r}}\cdot\hat{\mathbf{r}}')\, \delta(r-r'), \tag{1.45}$$

and P_l is the Legendre polynomial of degree l. The expressions of the matrix elements of various terms which involve the pseudopotentials in Eq. (1.44) are reported in Appendix B.

1.3.4 Use of nonlocal potentials for the electron-ion interaction

If the electron-ion interaction is described by a nonlocal potential, Eqs. (1.16) and

(1.18) do not hold and one must use the more general expressions:

$$\frac{\partial \mathcal{E}_{\boldsymbol{\lambda}}}{\partial \lambda_i} = \sum_{\mathbf{k}} \sum_{v} \left\langle \psi_{v,\mathbf{k}} \left| \frac{\partial V_{\boldsymbol{\lambda}}}{\partial \lambda_i} \right| \psi_{v,\mathbf{k}} \right\rangle \ , \tag{1.46}$$

and

$$\frac{\partial^2 \mathcal{E}_{\boldsymbol{\lambda}}}{\partial \lambda_i \partial \lambda_j} = \sum_{\mathbf{k}} \sum_{v} \left(\left\langle \psi_{v,\mathbf{k}} \left| \frac{\partial^2 V_{\boldsymbol{\lambda}}}{\partial \lambda_i \partial \lambda_j} \right| \psi_{v,\mathbf{k}} \right\rangle + \right.$$
$$\left. + \left\langle \frac{\partial \psi_{v,\mathbf{k}}}{\partial \lambda_i} \left| \frac{\partial V_{\boldsymbol{\lambda}}}{\partial \lambda_j} \right| \psi_{v,\mathbf{k}} \right\rangle + \left\langle \psi_{v,\mathbf{k}} \left| \frac{\partial V_{\boldsymbol{\lambda}}}{\partial \lambda_j} \right| \frac{\partial \psi_{v,\mathbf{k}}}{\partial \lambda_i} \right\rangle \right). \tag{1.47}$$

The first term of Eq. (1.47) is a "diagonal" term, which can be calculated without any knowledge of the response of the system; as for the last two terms, one only needs to know the linear response of the system.

In $\mathbf{q}$-space, the two contributions have the form:

$$\begin{aligned} \widetilde{C}^{(1)}_{\alpha i,\beta j}(\mathbf{q}) &= \frac{2}{N} \sum_{\mathbf{R},\mathbf{R}'} \sum_{\mathbf{k}} \sum_{v} \left\langle \psi_{v,\mathbf{k}} \left| \frac{\partial^2 V_{ion}}{\partial u_{\alpha i}(\mathbf{R}) \partial u_{\beta j}(\mathbf{R}')} \right| \psi_{v,\mathbf{k}} \right\rangle \mathrm{e}^{-i\mathbf{q}\cdot(\mathbf{R}-\mathbf{R}')} \\ &= \delta_{ij} \frac{2}{N} \sum_{\mathbf{k}} \sum_{v} \left\langle \psi_{v,\mathbf{k}} \left| \frac{\partial^2 V_{ion}}{\partial u_{\alpha i \mathbf{q}=0} \partial u_{\beta i \mathbf{q}=0}} \right| \psi_{v,\mathbf{k}} \right\rangle \end{aligned} \tag{1.48}$$

and:

$$\begin{aligned} \widetilde{C}^{(2)}_{\alpha i,\beta j}(\mathbf{q}) &= \frac{4}{N} \sum_{\mathbf{R},\mathbf{R}'} \sum_{\mathbf{k}} \sum_{v} \left\langle \frac{\partial \psi_{v,\mathbf{k}}}{u_{\alpha i}(\mathbf{R})} \left| \frac{\partial V_{ion}}{\partial u_{\beta j}(\mathbf{R}')} \right| \psi_{v,\mathbf{k}} \right\rangle \mathrm{e}^{-i\mathbf{q}\cdot(\mathbf{R}-\mathbf{R}')} \\ &= \frac{4}{N} \sum_{\mathbf{k}} \sum_{v} \left\langle \frac{\partial \psi_{v,\mathbf{k}}}{\partial u_{\alpha i \mathbf{q}}} \left| \frac{\partial V_{ion}}{\partial u_{\beta j \mathbf{q}}} \right| \psi_{v,\mathbf{k}} \right\rangle . \end{aligned} \tag{1.49}$$

A factor 2 comes from spin summation. The first term does not depend on $\mathbf{q}$ so it only needs to be calculated once.

1.4 Polar semiconductors

In polar semiconductors, the long-range character of the Coulomb forces gives rise to macroscopic electric fields for LO phonons in the limit $\mathbf{q} \to 0$. For finite $\mathbf{q}$, polar semiconductors are dealt with in the same way as non polar ones. In the long wavelength limit, however, the macroscopic electric field, $\mathbf{E}$, which accompanies the lattice distortion must be treated with care because the corresponding electronic potential, $\Phi(\mathbf{r}) = -\mathbf{E} \cdot \mathbf{r}$, is not lattice-periodic. Within linear response theory, electric fields can be dealt with during the self-consistent process performed to determine the density response to ionic displacements.[2] A more convenient way of dealing with long wavelength vibrations in polar semiconductors is to exploit the known analytic properties of the dynamical matrix. In the long wavelength limit, the matrix of the force constants can be written as the sum of analytic and non analytic contributions:[27,28]

$$\widetilde{C}_{\alpha i,\beta j} = \widetilde{C}^{an}_{\alpha i,\beta j} + \widetilde{C}^{na}_{\alpha i,\beta j} \ , \tag{1.50}$$

where the analytic part, $\widetilde{C}^{an}$ is the matrix obtained from the response to a zone-center phonon, calculated with electric boundary conditions (EBC) corresponding to zero macroscopic electric field (*zero EBC*). Zero EBC are implicitly assumed in any electronic-structure calculations with periodic boundary conditions for the electronic wavefunctions. The non analytic part has the general form:[28]

$$\widetilde{C}^{na}_{\alpha i,\beta j} = \frac{4\pi e^2}{\Omega} \frac{\sum_\gamma Z^*_{i,\gamma\alpha} \mathrm{q}_\gamma \sum_\nu Z^*_{j,\nu\beta} \mathrm{q}_\nu}{\sum_{\gamma,\nu} \mathrm{q}_\gamma \epsilon^\infty_{\gamma\nu} \mathrm{q}_\nu} = \frac{4\pi e^2}{\Omega} \frac{(\mathbf{q} \cdot \mathbf{Z}^*{}_i)_\alpha (\mathbf{q} \cdot \mathbf{Z}^*{}_j)_\beta}{\mathbf{q} \cdot \boldsymbol{\epsilon}^\infty \cdot \mathbf{q}}, \tag{1.51}$$

where $\epsilon^\infty_{\alpha\beta}$ is the high-frequency static dielectric tensor (i.e. the electronic contribution to the static dielectric tensor), and $Z^*_{i,\alpha\beta}$ is the Born effective charge tensor for the i-th atom in the unit cell. Eq. (1.51) shows that all the information

necessary to deal with the non analytic part of the dynamical matrix is contained in the macroscopic dielectric constant of the system, and in the Born effective charges Z^*, whereas the analytic contribution can be calculated just ignoring any macroscopic polarization associated with the phonon. All these quantities can be easily obtained within our framework.

1.4.1 Calculation of the dielectric tensor

The dielectric tensor relates the screened electric field (with clamped nuclei) $\mathbf{E}$ to the bare electric field $\mathbf{E}_0$: $\mathbf{E}_0 = \epsilon^\infty \cdot \mathbf{E}$. The matrix elements of the bare electrostatic potential, $\Phi_0(\mathbf{r}) = -\mathbf{E}_0 \cdot \mathbf{r}$, are ill-defined in an infinite solid with periodic boundary conditions. They can be cast in a boundary-insensitive form by using the following relation:[29]

$$\langle \psi_{v,\mathbf{k}} | \mathbf{r} | \psi_{c,\mathbf{k}} \rangle = \frac{\langle \psi_{v,\mathbf{k}} | [H_{SCF}, \mathbf{r}] | \psi_{c,\mathbf{k}} \rangle}{\epsilon_{v,\mathbf{k}} - \epsilon_{c,\mathbf{k}}}, \tag{1.52}$$

where

$$[H_{SCF}, \mathbf{r}] = \frac{-i\hbar\mathbf{p}}{m} + [V_{ion}, \mathbf{r}], \tag{1.53}$$

$\mathbf{p}$ is the momentum operator, and m is the electron mass. For a finite system, Eq. (1.52) is an identity. When periodic boundary conditions are used, however, the l.h.s. is no longer well defined, whereas the r.h.s is still so and does not give any problem when passing to the thermodynamic limit. Note that commutator $[V_{ion}, \mathbf{r}]$ does not vanish if the electron-ion interaction is described by a nonlocal potential, in fact the matrix elements of the nonlocal pseudopotential contribution to $[H, \mathbf{r}]$ between plane waves are

$$\langle \mathbf{k}_1 | [v_{i,l}, r_\alpha] | \mathbf{k}_2 \rangle = \frac{1}{\Omega} \int \mathrm{e}^{-i\mathbf{k}_1 \cdot \mathbf{r}} \, v_{i,l}(\mathbf{r}, \mathbf{r}') \, (r'_\alpha - r_\alpha) \, \mathrm{e}^{i\mathbf{k}_2 \cdot \mathbf{r}'} \, \mathrm{d}\mathbf{r} \, \mathrm{d}\mathbf{r}'$$

$$= -i\left(\frac{\partial}{\partial k_{1\alpha}} + \frac{\partial}{\partial k_{2\alpha}}\right)\frac{1}{\Omega}\int \mathrm{e}^{-i\mathbf{k}_1\cdot\mathbf{r}}\, v_{i,l}(\mathbf{r},\mathbf{r}')\,\mathrm{e}^{i\mathbf{k}_2\cdot\mathbf{r}'}\,\mathrm{d}\mathbf{r}\,\mathrm{d}\mathbf{r}'$$
$$= -i\left(\frac{\partial}{\partial k_{1\alpha}} + \frac{\partial}{\partial k_{2\alpha}}\right)\widetilde{v}_{i,l}(\mathbf{k}_1,\mathbf{k}_2). \qquad (1.54)$$

For practical purposes, we calculate once and for all and store the auxiliary functions:

$$|\phi^{\alpha}_{v,\mathbf{k}}\rangle = P_c r_\alpha |\psi_{v,\mathbf{k}}\rangle = \sum_c |\psi_{c,\mathbf{k}}\rangle \frac{\langle\psi_{c,\mathbf{k}}\,|[H,r_\alpha]|\,\psi_{v,\mathbf{k}}\rangle}{\epsilon_{c,\mathbf{k}} - \epsilon_{v,\mathbf{k}}} =$$
$$-P_c G_0\big(\epsilon_{v,\mathbf{k}}\big) P_c[H,r_\alpha]|\psi_{v,\mathbf{k}}\rangle. \qquad (1.55)$$

When an external electric field is applied, the bare perturbing potential has only a "macroscopic" ($\mathbf{G} = 0$) component, whereas the screened potential has both "macroscopic" and "microscopic" ($\mathbf{G} \neq 0$) components. The latter are given as usual by Eqs. (1.38) and (1.39). The former is proportional to the electronic contribution to the macroscopic polarization per unit volume $\mathbf{P}$:[30]

$$\frac{\partial \mathbf{P}}{\partial E_\alpha} = \frac{e}{N\Omega}\int \mathbf{r}\frac{\partial n(\mathbf{r})}{\partial E_\alpha}\,\mathrm{d}\mathbf{r}, \qquad (1.56)$$

which can be recast into the form:[30,31]

$$\frac{\partial \mathbf{P}}{\partial E_\alpha} = \frac{4e}{N\Omega}\sum_{\mathbf{k}}\sum_{c,v}\frac{\langle\psi_{v,\mathbf{k}}|\mathbf{r}|\psi_{c,\mathbf{k}}\rangle\langle\psi_{c,\mathbf{k}}|(\partial V_{SCF}/\partial E_\alpha)|\psi_{v,\mathbf{k}}\rangle}{\epsilon_{v,\mathbf{k}} - \epsilon_{c,\mathbf{k}}}. \qquad (1.57)$$

This result can be equivalently obtained by considering the density response to a perturbation of finite wavevector, $\mathbf{q}$: $\Delta n(\mathbf{r}) = \mathrm{e}^{i\mathbf{q}\cdot\mathbf{r}}\sum_{\mathbf{G}} C_{\mathbf{G}}(\mathbf{q})\,\mathrm{e}^{i\mathbf{G}\cdot\mathbf{r}}$. It is easy to see that—for small $\mathbf{q}$— one has: $C_{\mathbf{G}=0}(\mathbf{q}) \approx -i\mathbf{q}\cdot\mathbf{P}$, and obtain from this Eq. (1.57). Eq. (1.57) is well-defined and boundary-insensitive,[30] provided that the matrix elements of $\mathbf{r}$ are dealt with as prescribed by Eq. (1.52).

Eq. (1.57) can be used to obtain the screened electric field $\mathbf{E} = \mathbf{E}_0 - 4\pi\mathbf{P}$ at each iteration of the self-consistent process. However, for computational purposes,

it is more convenient to keep the value of the screened electric field fixed during self-consistency, and let only the microscopic components of the potential vary. The macroscopic polarization is then calculated from Eq. (1.57), once self-consistency is achieved. Physically, this amounts to calculating the polarization response to a given *screened* electric field, $\mathbf{E}$, instead of to the *bare* electric field $\mathbf{E}_0$.

Let us introduce the following notation for the response of the wavefunction $|\psi_{v,\mathbf{k}}\rangle$ to an applied screened electric field:

$$\left|\frac{\partial\psi_{v,\mathbf{k}}}{\partial E_\beta}\right\rangle = P_c G_0\big(\epsilon_{v,\mathbf{k}}\big) P_c \frac{\partial V_{SCF}}{\partial E_\beta}|\psi_{v,\mathbf{k}}\rangle, \tag{1.58}$$

where $\partial V_{bare}(\mathbf{r})/\partial E_\beta = -r_\beta$. The induced polarization is obtained through Eq. (1.57) and the dielectric tensor ϵ^∞ is finally given by:

$$\epsilon^\infty_{\alpha\beta} = \delta_{\alpha\beta} + \frac{16\pi e^2}{N\Omega}\sum_{\mathbf{k}}\sum_{v}\left\langle \phi^\alpha_{v,\mathbf{k}}\middle|\frac{\partial\psi_{v,\mathbf{k}}}{\partial E_\beta}\right\rangle. \tag{1.59}$$

1.4.2 Calculation of the Born effective charges

The calculation of the Born effective charges proceeds along similar lines. The Born effective charges are simply related to the total (ionic + electronic) macroscopic polarization, $\mathbf{P}^{tot}$, induced by a zone-center phonon with zero EBC:[31,32]

$$Z^*_{i,\alpha\beta} = \frac{\Omega}{e}\frac{\partial P^{tot}_\alpha}{\partial u_{\beta i\mathbf{q}=0}}, \tag{1.60}$$

where $u_{\beta i\mathbf{q}=0}$ is the amplitude of the zone-center phonon, as defined by Eq. (1.27). The ionic contribution to the polarization is trivial, whereas the electronic contribution is obtained from the linear response to a zone-center phonon as in Eq. (1.57). In our notations one has:

$$Z^*_{i,\alpha\beta} = Z_i + \frac{4}{N}\sum_{\mathbf{k}}\sum_{v}\left\langle \phi^\alpha_{v,\mathbf{k}}\middle|\frac{\partial\psi_{v,\mathbf{k}}}{\partial u_{\beta i\mathbf{q}=0}}\right\rangle, \tag{1.61}$$

where Z_i is the ionic (pseudo)charge for the i-th ion, and $\partial\psi/\partial u$ is the linear variation of the electronic wavefunction, upon lattice distortion.

Chapter 2

Phonons in Pure Bulk Semiconductors

In the previous chapter we have developed the theoretical tools necessary to calculate the linear response of semiconductor crystals to external perturbations. In this chapter we present the application of this method to some group-IV crystal: C, Si, Ge, and to some binary compound semiconductors (groups III-V: AlAs, GaAs, AlSb, GaSb).

Our calculations are performed in the framework of the local-density approximation (LDA) using the plane-wave pseudopotential method. The exchange-correlation energy and potential are taken from Ref. [33]. We have generated norm-conserving pseudopotentials using a scheme proposed by von Barth and Car.[25] This scheme consists essentially in a fitting minimization of the squared differences between the atomic all-electron and pseudo eigenvalues and eigenfunctions (beyond a given core radius r_c), as functions of a few parameters upon which the pseudopotential depends. Particular attention must be paid to the choice of the reference configuration for atomic d states, which were found to be rather important for assuring the correct lattice mismatch among the different semiconductors.

The equilibrium structure of a crystal is determined by minimizing the total

energy of the system as a function of the lattice parameters. In doing that, one has to decide how the dimension of the plane wave (PW) basis set depends on the volume of the unit cell. The most common choice[34] is to fix the kinetic energy cutoff E_{cut} defined in Section 1.3.3. In this case the dimension of the PW basis set will depend on the volume, but the real space resolution, related to the modulus of the maximum wavevector included in the basis, remains the same for the different values of the lattice parameters. Due to the finite dimension of the basis sets, this choice can cause discontinuities in the total energy. This problem can be avoided by fitting the dependence of the total energy upon the volume with an appropriate equation of state.

We use plane-wave basis sets up to a kinetic-energy cutoff of 16 Ry. These basis sets are complete enough to guarantee a convergence on the calculated phonon frequencies to better than 5 cm^{-1} for all the materials we have studied except diamond. In this case, due to the relative larger "hardness" of the pseudopotential of carbon one needs a cutoff of 55 Ry to achieve the same accuracy as in the other materials.

The sums over electronic eigenstates in the reciprocal space have been performed using an uniform grid of 256 points in the Brillouin Zone (BZ). Using the point symmetry of the lattice, only points belonging to the so called irreducible wedge need to be sampled. In the present case, they reduce to the set of ten Chadi-Cohen k-points.[35]

2.1 Equilibrium properties

All the systems we have studied crystallize in the diamond or zincblende structures,

which have two atoms per unit cell. The two atoms have coordinates $\tau_1 = (0,0,0)$ and $\tau_2 = a(\frac{1}{4},\frac{1}{4},\frac{1}{4})$. The equilibrium lattice parameter has been determined by minimizing the crystal total energy calculated for different values of the lattice parameter. The values so obtained have been fitted to Murnaghan's equation of state[36]:

$$P = \frac{B_0}{B_0'}\left[\left(\frac{\Omega_0}{\Omega}\right)^{B_0'} - 1\right], \tag{2.1}$$

or

$$E = \frac{\Omega_0 B_0}{B_0'}\left[\frac{1}{B_0' - 1}\left(\frac{\Omega_0}{\Omega}\right)^{B_0'-1} + \frac{\Omega}{\Omega_0}\right] + \text{const}\ , \tag{2.2}$$

where B_0 is the bulk modulus, B_0' is the derivative of the bulk modulus with respect to the pressure, and Ω_0 is the equilibrium crystal volume. A particular attention has been payed to ensure that the parameters resulting from the fit are well converged with respect to both the kinetic energy cutoff and the number of k-points in the BZ. Following the equation of state approach it is possible to achieve the equilibrium condition of the crystal with an accuracy of $1 \div 2$ %. This accuracy is comparable with the errors introduced by the use of the LDA and of the pseudopotentials. Within the whole range of crystal volumes we have considered, the root-mean-square deviation of the fit to the equation of state is less than 2×10^{-5} Ry.

Results for the equilibrium parameters at convergence are shown in Table I. From the comparison with the experimental values we can see that the agreement is generally good both for the lattice parameter and for the bulk modulus.

TABLE I. Equilibrium lattice parameter (a, [a.u.]) used in the present calculations, and calculated Born effective charges (Z^*), and static dielectric constants (ϵ_∞). Parentheses denote experimental data.

	C	Si	Ge	GaAs	AlAs	GaSb	AlSb
a	6.67 (6.74)	10.20 (10.26)	10.60 (10.68)	10.60_5 (10.68)	10.60_5 (10.69)	11.40 (11.49)	11.51 (11.58)
B_0	4544 (4420)	957 (978)	774 (758)	777 (769)	767 (773)	519 (580)	603 (582)
Z^*				2.07 (2.07)	2.17 (2.18)	1.73 (1.88)	1.91 (2.18)
ϵ_∞	5.7 (5.7)	13.6 (12.1)	18.7 (16.5)	12.3 (10.9)	9.2 (8.2)	18.1 (14.4)	12.2 (10.2)

2.2 Lattice dynamical properties

In order to span the entire BZ, we have calculated dynamical matrices onto uniform grids in the reciprocal space defined by the $\mathbf{q}$ points:

$$\mathbf{q}_{lmn} = \frac{l}{L}\mathbf{G}_1 + \frac{m}{L}\mathbf{G}_2 + \frac{n}{L}\mathbf{G}_3 \qquad 0 \leq l < L-1,\ 0 \leq m < L-1,\ 0 \leq n < L-1\ , \tag{2.3}$$

$\mathbf{G}_1, \mathbf{G}_2, \mathbf{G}_3$ being a basis of the reciprocal-space of an FCC lattice, which is a body-centered cubic grid.

In particular, we have calculated the dynamical matrices at all the points $\mathbf{q}$ belonging to the $(L = 4)$ grid. Phonon frequencies along low-symmetry lines have been obtained interpolating the dynamical matrices using the force constants obtained with the method of Fourier deconvolution described in Section 4.1. Along the high-symmetry lines Δ (Γ–X) and Λ (Γ–L) we have calculated the dynamical

matrices at additional points (all those belonging to the ($L = 8$) FCC mesh). One-dimensional Fourier analysis of the dynamical matrices yields the *interplanar* force constants. Interpolation of the dynamical matrices using these *interplanar* force constants gives the same phonon dispersion which would be obtained from a full 3D calculation onto an ($L = 8$) FCC mesh. Optical branches are found to be insensitive to the choice between the two meshes, whereas the ($L = 8$) mesh turns out to improve somewhat the agreement of our calculated dispersions with experiment, in the acoustic region. For polar materials, the long-range interaction—which was implicitly eliminated by the real-space force constants by subtracting the non analytic part of $\widetilde{C}(\mathbf{q})$, before Fourier analysis—was restored using an Ewald sum similar to that used to evaluate $\widetilde{C}^{ion}$, (see Section 1.2), where the ionic charges Z_i have to be replaced by $Z_i^*/\sqrt{\epsilon^\infty}$).

2.2.1 Phonon dispersions

In Table I we also report the calculated values of the effective charges and dielectric constants, which have been used for treating long-wavelength modes. Similar values for these quantities had been previously obtained [37] by the same technique, but using different pseudopotentials. The reported values of the effective charges are obtained by imposing the Acoustic Sum Rule (ASR):

$$\sum_i Z^*_{i,\alpha\beta} = 0 \tag{2.4}$$

In approximate calculations, the ASR is violated. The magnitude of such a violation strongly depends on the mesh of $\mathbf{k}$-points used for the sum over the BZ: it is large if few $\mathbf{k}$-points are used, and it tends to zero as the size of the mesh increases. Notwithstanding—if the ASR is imposed by subtracting to each effective charge

one half of their sum—good results are obtained with few **k**-points, and the data reported in Table I should be considered converged to the figures quoted. The values of the dielectric constants are overestimated with respect to experiments by $\simeq 10\%$. This is a well-known drawback of LDA known since a certain time,[29a] and discussed in some detail in Ref. [37].

Our results for the bulk phonon dispersions along several symmetry lines together with the corresponding density of states are displayed in Figs. 2.1 and 2.2, for non polar and polar materials respectively. Some numerical values at the high-symmetry points Γ, X, and L are also reported in Table II. The phonon dispersions of the two elemental semiconductors, Si and Ge, are very similar apart from the obvious scaling of the frequencies due to the mass difference between Si and Ge. It is remarkable to notice that even very delicate features of the spectra which have long escaped a proper theoretical understanding—as the flatness of the transverse acoustic (TA) modes near the BZ boundaries—are well reproduced by our calculations. This behaviour of TA branches essentially depends on the long range of the force constants along the bonds [40,41], and it is the origin of the strong structures of the density of states found in the acoustical frequencies region.

The case of diamond is quite different: the TA branches are no longer flat near zone border, thus determining the lack of sharp features in the corresponding region of the phonon density of states. Another very interesting peculiarity has been found in the phonon spectrum of diamond. In fact, the maximum of the optical branches is not at zone-center as it is the case of silicon and germanium. Along the different high-symmetry lines of diamond we have investigated, a maximum at $\mathbf{q} \neq 0$ has been found. This originates the sharp peak in the phonon density of states above the Γ-point optical frequence. Experimental evidence of this sharp

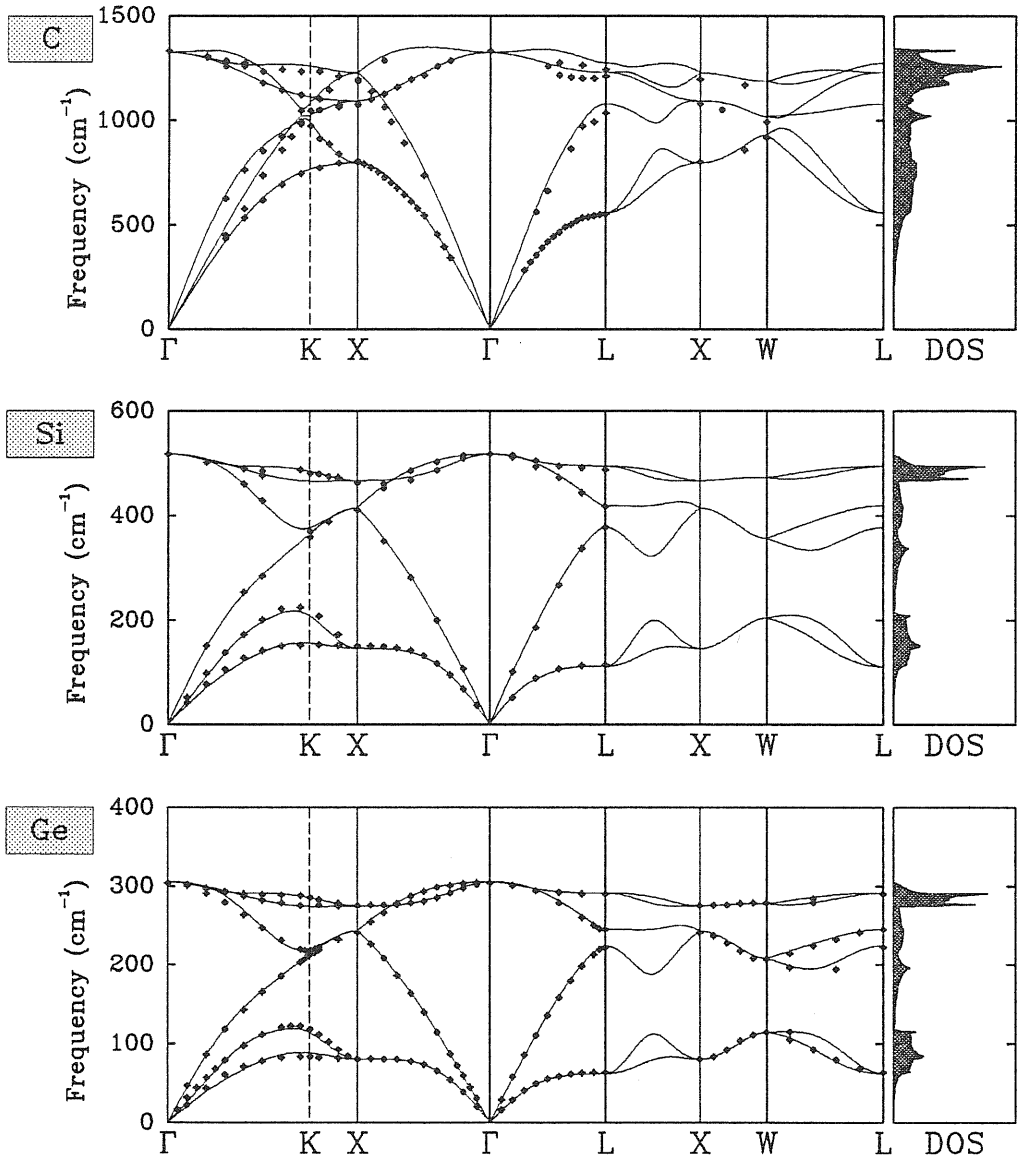

Figure 2.1. Calculated phonon dispersions and density of states of group IV elements, C, Si and Ge. Experimental data are denoted by diamonds (from Refs. [43], [42] and [44]).

peak has been found in the second order Raman spectrum of diamond[48].

Many neutron-diffraction and Raman scattering data[42,8,43–38] are available for all the materials considered here, with the exception of AlAs, for which only a

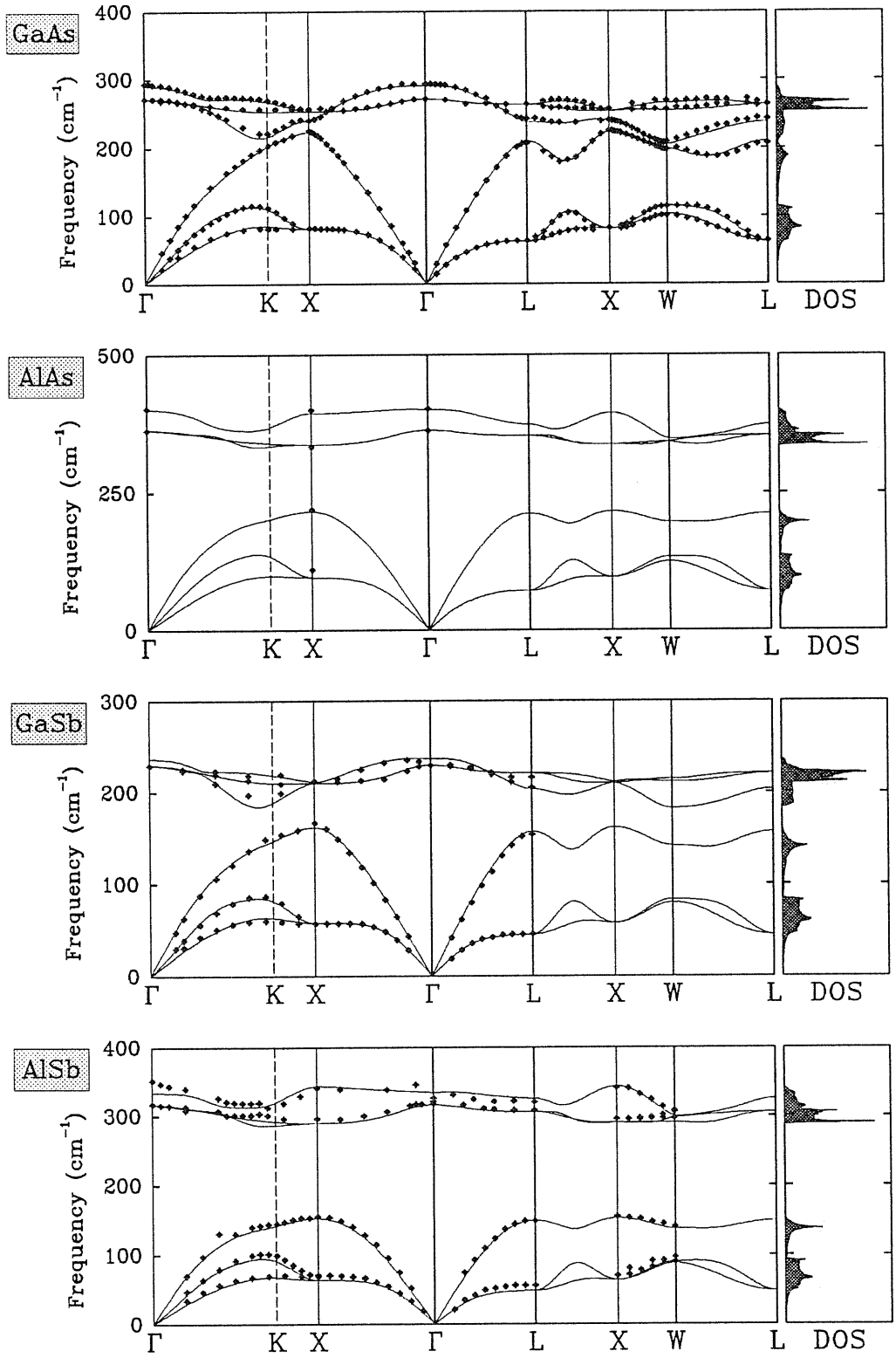

Figure 2.2. Calculated phonon dispersions and density of states for binary semiconductors, GaAs, AlAs, GaSb, and AlSb. Experimental data are denoted by diamonds (from Refs. [45], [46], [47], and [8]).

TABLE IIa. Phonon frequencies calculated at the high-symmetry points Γ, X, and L, for six semiconductors among those studied in this thesis [cm^{-1}]. Experimental data are in parenthesis. Data tagged with an asterisk are from Ref. [38]

	Si[a]	Ge[b]	GaAs[c]	AlAs[d]	GaSb[e]	AlSb[f]
Γ_{TO}	517 (517)	306 (304)	271 (271)	363 (361)	230 (224)*	316 (323)*
Γ_{LO}	517 (517)	306 (304)	291 (293)	400 (402)	237 (233)*	334 (344)*
X_{TA}	146 (150)	80 (80)	82 (82)	95 (109)	57 (57)	64 (70)
X_{LA}	414 (410)	243 (241)	223 (225)	216 (219)	162 (166)	153 (155)
X_{TO}	466 (463)	275 (276)	254 (257)	337 (333)	210 (212)	290 (296)
X_{LO}	414 (410)	243 (241)	240 (240)	393 (399)	211 (212)	343 (341)
L_{TA}	111 (114)	62 (63)	63 (63)	71 (-)	45 (46)	49 (56)
L_{LA}	378 (378)	224 (222)	210 (207)	212 (-)	157 (153)	149 (148)
L_{TO}	494 (487)	291 (290)	263 (264)	352 (-)	203 (205)	306 (308)
L_{LO}	419 (417)	245 (245)	238 (242)	372 (-)	221 (216)	327 (320)

[a]Experimental data from Ref. [43]
[b]Experimental data from Ref. [44]
[c]Experimental data from Ref. [45]
[d]Experimental data from Ref. [46]
[e]Experimental data from Ref. [47]
[f]Experimental data from Ref. [8]

TABLE IIb. Phonon frequencies at the high-symmetry points Γ, X, and L, for Carbon [cm^{-1}]. Experimental data are from Ref. [42]

	Γ_O	X_{TA}	X_{TO}	X_L	L_{TA}	L_{LA}	L_{TO}	L_{LO}
Th.	1324	800	1094	1228	561	1080	1231	1275
Exp.	1331	803	1077	1194	552	1035	1210	1242

few Raman experiments exist.[46] The agreement between calculations and available experiments is excellent. This fact is of particular importance in view of the fact that this is the first time that phonon dispersions of some real materials have been calculated completely from first principles, throughout the entire Brillouin zone. In the case of AlAs, where a direct comparison with experiments is not possible, our calculation is the first reliable prediction of the phonon dispersions. Previous calculations were in fact either limited to very few high-symmetry points,[49] or based on semiempirical models which were fitted to the phonon dispersions of GaAs. The present calculations predict that the AlAs LO branch along the Δ direction is much flatter than hitherto suspected. This fact—which is relevant for understanding the physics of phonons in GaAs/AlAs superlattices[7]—seems to be confirmed by the agreement between our calculations and the available experimental data at the X point.[46b] The reliability of those experimental data are however somewhat questionable, and the agreement perhaps fortuitous. More meaningful is that the present predictions for AlAs are indirectly confirmed by the good agreement between our calculations and recent experiments for the closely related compound AlSb.[8] Even in the case of GaAs, for which phonon dispersions along the high-symmetry Δ and Λ lines had already been calculated using *interplanar* force constants,[50] the present calculations represent an important step forward both because they have been performed for much more (low-symmetry) directions, and also because they are considerably more accurate, resulting in a much better agreement with experiments. This is particularly true for effective charges and LO–TO splittings, and the flatness of the TA branch near the X point.

The main features of our method which have made possible these improvements are the following. First of all, our Green's function technique avoids the

use of supercells, thus allowing us to calculate force constants of longer range, not limited to the high-symmetry directions; still, accurate, norm-conserving (non local, instead of local) pseudopotentials can be used without special difficulties; last but not least the overall numerical efficiency of our method allows to use a high number of special points and large plane-wave basis sets, thus permitting us to obtain fully-converged results.

2.2.2 Vibrational eigenvectors

A complete description of lattice dynamics of crystals cannot be given by just the phonon frequencies. On the other hand, recent inelastic neutron scattering experiments have been able to measure the phonon eigenvectors along some high-symmetry lines in the BZ[51,52]. The ab-initio calculation of phonon eigenvectors is important not only for its intrinsic interest (for example, matrix elements for phonon-assisted electronic, or other, transitions requires their knowledge), but also as a benchmark of the soundness of different phenomenological models.

In the zincblende or in the diamond structure we have two atoms in the unit cell. Along high symmetry lines such as the (111) or (100) direction vibrational modes may be divided into purely transverse or longitudinal ones. In such cases the eigenvector of the dynamical matrix at $\mathbf{q}$ belonging to the j-th branch may be written in the following form:

$$\begin{aligned} \boldsymbol{u}_1^j(\mathbf{q}) &= \tilde{c}_1(\mathbf{q},j)\,\boldsymbol{e}_j \\ \boldsymbol{u}_2^j(\mathbf{q}) &= \tilde{c}_2(\mathbf{q},j)\,\boldsymbol{e}_j \ , \end{aligned} \tag{2.5}$$

where the $\tilde{c}_s$ $(s = 1,2)$ are complex numbers and $\boldsymbol{e}_j$ is a real longitudinal $(j = L)$ or transverse $(j = T)$ unit vector: $\boldsymbol{e}_j \cdot \boldsymbol{e}_j = 1$. Due to the normalization conditions

in Eq. (1.15) we have:

$$\sum_{s=1}^{2} |\tilde{c}_s(\mathbf{q},j)|^2 = 1 \ . \tag{2.6}$$

Then with an appropriate choice of the overall phase factor we can put:

$$\begin{aligned} \tilde{c}_1(\mathbf{q},j) &= |\tilde{c}_1(\mathbf{q},j)| = c_1(\mathbf{q},j) \\ \tilde{c}_2(\mathbf{q},j) &= |\tilde{c}_2(\mathbf{q},j)| \ \exp[i\phi_j(\mathbf{q})] = c_2(\mathbf{q},j) \ \exp[i\phi_j(\mathbf{q})] \ , \end{aligned} \tag{2.7}$$

where both $c_s(\mathbf{q},j),(s = 1,2)$ and the phase function $\phi_j(\mathbf{q})$ are real. In the diamond structure the two atoms in the unit cell are equal, so that one has:

$$c_1(\mathbf{q},j) = c_2(\mathbf{q},j) = \frac{1}{\sqrt{2}} \ . \tag{2.8}$$

Thus we obtain the eigenvectors in the following form:

$$\begin{aligned} \boldsymbol{u}_1^j(\mathbf{q}) &= \pm \frac{1}{\sqrt{2}} \boldsymbol{e}_j \\ \boldsymbol{u}_2^j(\mathbf{q}) &= \frac{1}{\sqrt{2}} \exp[i\phi_j(\mathbf{q})] \ \boldsymbol{e}_j \ , \end{aligned} \tag{2.9}$$

where the phase function is defined in such a way as to vanish at $\mathbf{q} = 0$, so that the plus sign holds for acoustic modes, the minus for optical ones. In the zincblende structure the atoms in the unit cell are not equal; hence the relation (2.8) is no longer valid, but the phase function may still be defined following the same lines. In Figs. 2.3 and 2.4 we report the phase functions of carbon and some semiconductors along the Λ (111) and Δ (100) directions, and we compare the theoretical results with the available experimental data.

Also in this case the behaviour of the phase function in the diamond is different from the other semiconductors. In particular, the main difference concerns the longitudinal eigenvectors along the Λ direction. At the L point the phase is equal to π leading to an opposite sign in the atomic displacements in the unit cell.

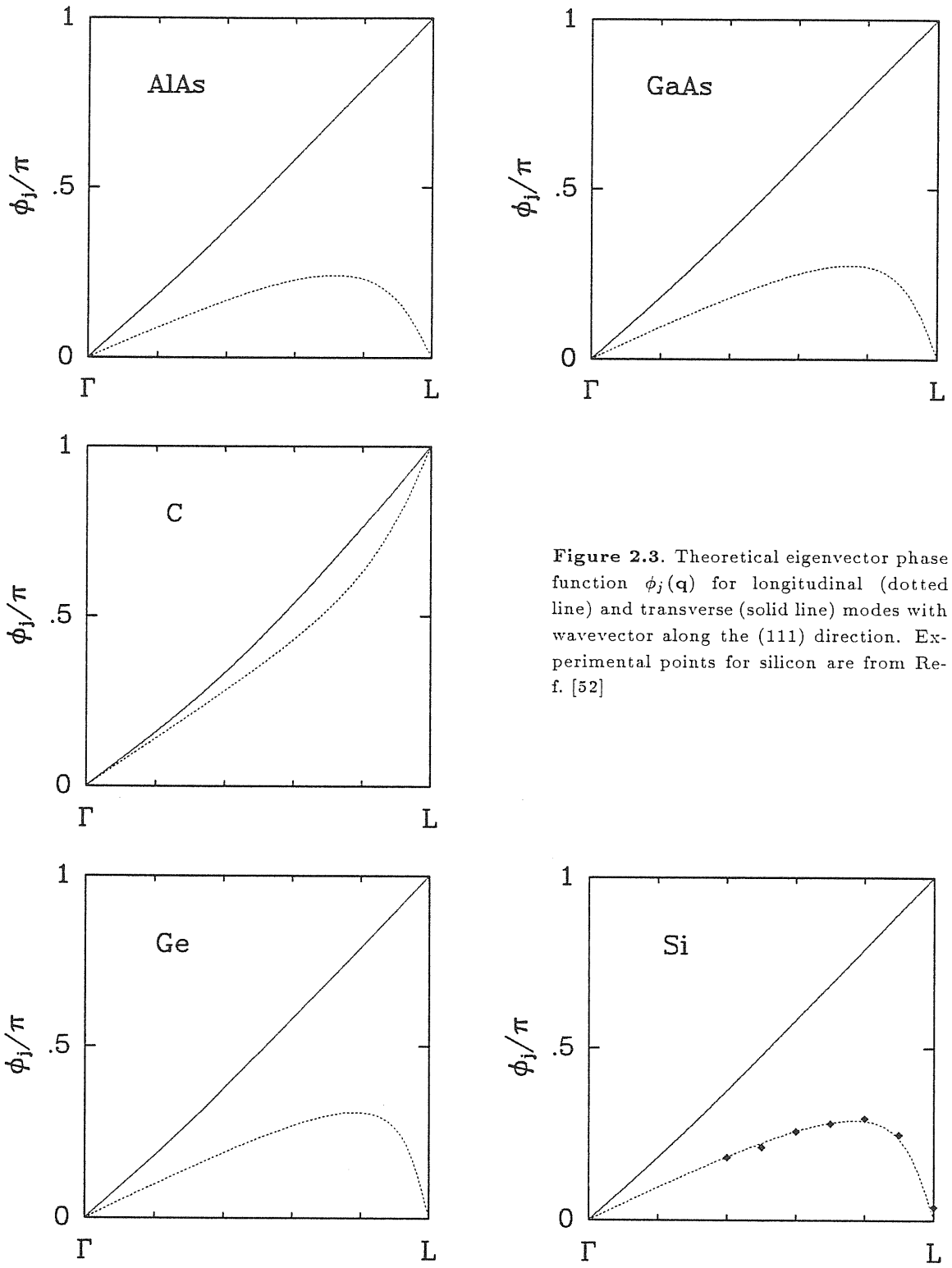

Figure 2.3. Theoretical eigenvector phase function $\phi_j(\mathbf{q})$ for longitudinal (dotted line) and transverse (solid line) modes with wavevector along the (111) direction. Experimental points for silicon are from Ref. [52]

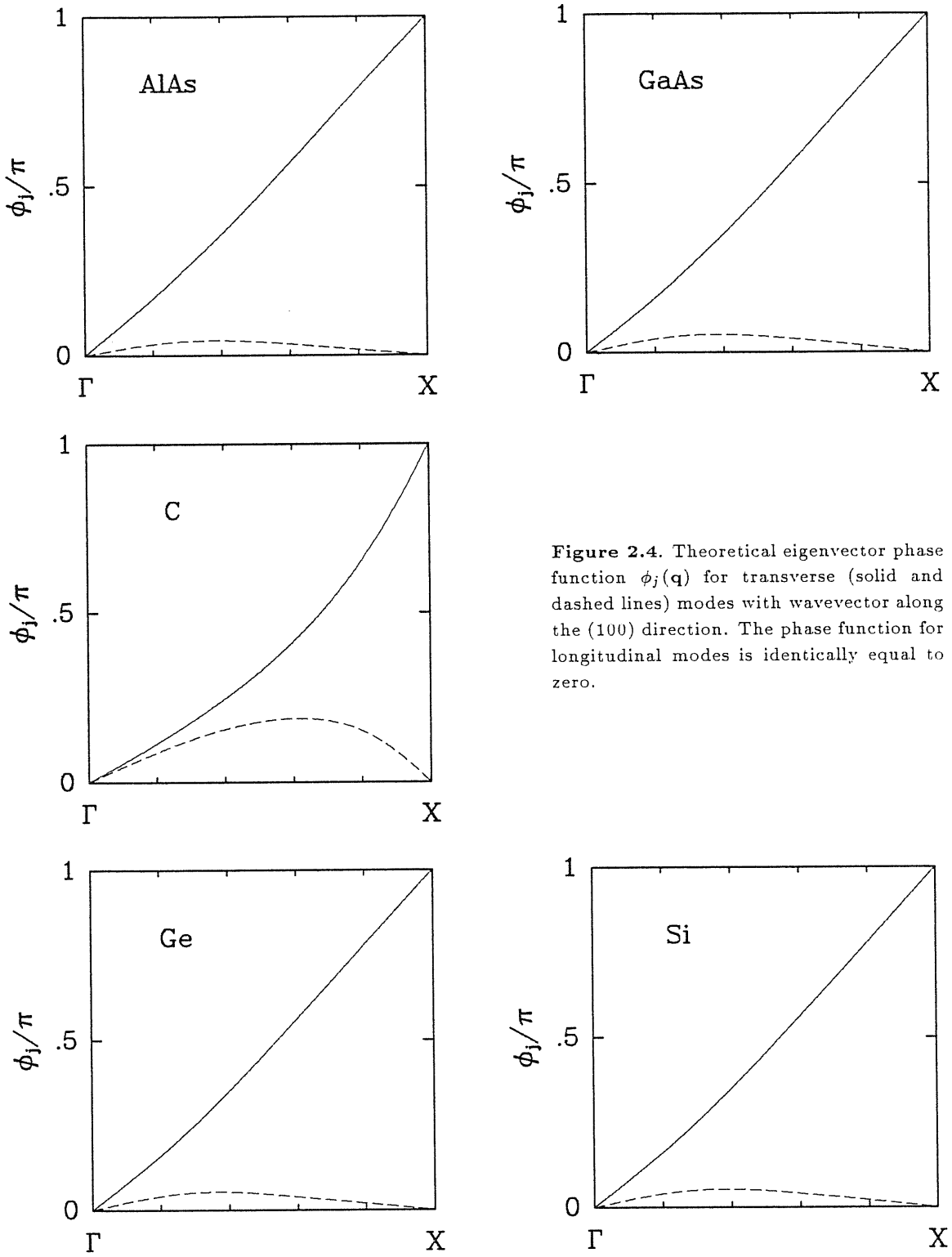

Figure 2.4. Theoretical eigenvector phase function $\phi_j(\mathbf{q})$ for transverse (solid and dashed lines) modes with wavevector along the (100) direction. The phase function for longitudinal modes is identically equal to zero.

This may be erroneously considered in disagreement with the acoustic or optical character of the eigenmodes. In fact, a real distinction between acoustic and optical modes holds only at the Γ-point. Due to symmetry reasons the eigenvectors at the L-point are real, so that both the values 0 and π are allowed for the phase factor. Actually, the unit cell associated with a phonon at the L-point is twice as large as the unit cell of the unperturbed crystal and the eigenvectors have opposite phases in the two cells. Thus, the difference between the two longitudinal modes is that the $\phi = \pi$ mode involves the stretching of the (111) bond whereas the other bonds remain unchanged (bond-stretching mode); on the contrary in the $\phi = 0$ mode the length of the (111) bond remains unchanged and the angles between the other three bonds are changed (bond-bending mode). The situation is schematically depicted in Fig. 2.5. In diamond the bond-bending mode has higher frequency than the bond-stretching one. The converse holds for the other semiconductors. This particular behaviour shows that in diamond the ratio k_b/k_s between the force constants respectively associated to the bond-bending and bond-stretching mode, is significantly larger than in the other cases. This interpretation agrees with results extracted from the force constants fitted to experimental data in the Keating model.[53]

At the Brillouin-zone center and boundary (X or L) the knowledge of the phase functions $\phi_j(\mathbf{q})$ completely determines the eigenvectors in the diamond structure. For zincblende systems, on the contrary, there is one more degree of freedom, thus the longitudinal optical eigenvectors are obtained as:

$$\begin{aligned} \overset{o}{\boldsymbol{u}}_1(\mathbf{q}) &= e_L(\mathbf{q})\, \boldsymbol{e}_o \\ \overset{o}{\boldsymbol{u}}_2(\mathbf{q}) &= -\sqrt{1 - e_L^2(\mathbf{q})}\, \boldsymbol{e}_o \ , \end{aligned} \tag{2.10}$$

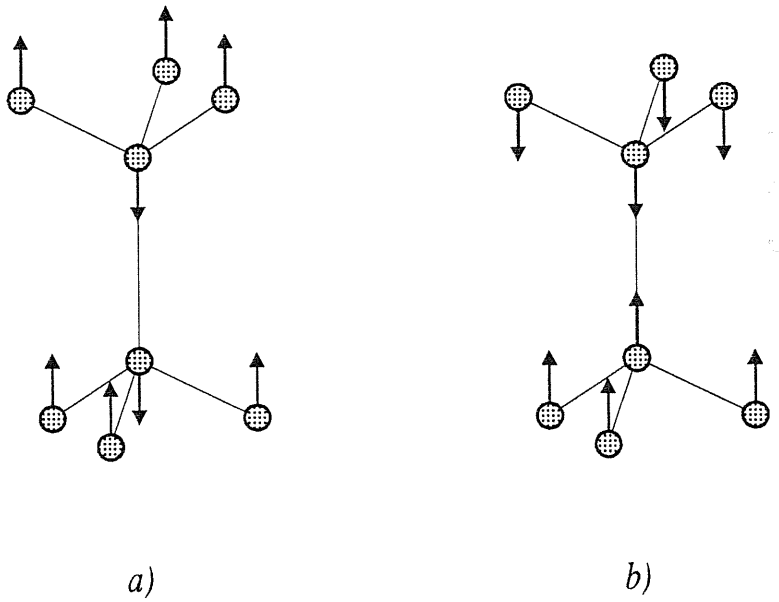

Figure 2.5. Schematic longitudinal eigendisplacements at the L-point. *a*) ϕ=0. *b*) ϕ=π.

where 1 $\equiv$ cation, 2 $\equiv$ anion. For acoustic modes one has:

$$\begin{aligned} \boldsymbol{u}_1^A(\mathbf{q}) &= \sqrt{1 - e_L^2(\mathbf{q})}\, \boldsymbol{e}_A \\ \boldsymbol{u}_2^A(\mathbf{q}) &= e_L(\mathbf{q})\, \boldsymbol{e}_A \ , \end{aligned} \tag{2.11}$$

analogous expressions hold for transverse modes. In Table III we show the calculated eigenvectors for the zincblende structure semiconductors that we have studied. It is worth noting that, in the case of GaAs, the predicted vibrational eigendisplacements at the X and L points are in good agreement with experiments and with previous ab-initio calculations,[50,54] but at variance with some results of empirical models.[45]

TABLE III. Vibrational eigenvectors at the X and L points of the Brillouin zone for III-V semiconductors. e is the cationic component of the optic mode. The indexes L and T indicate longitudinal and transverse modes, respectively. The experimental data reported in parenthesis are from Ref. [45].

	GaAs	AlAs	GaSb	AlSb
$e_T(X)$	0.66	0.85	0.91	0.77
$e_T(L)$	0.70	0.86	0.91	0.79
$e_L(X)$	1 (1)	1	1	1
$e_L(L)$	0.74 (0.56 or 0.81)	0.99	0.97	1.00

2.2.3 Internal strain parameter

Under the action of a uniform strain η, the position of a small but *macroscopic* portion of a crystal, originally located at $\mathbf{R}$, transforms according to:

$$\mathbf{R}' = (1 + \eta)\,\mathbf{R} \ . \tag{2.12}$$

The *microscopic* positions of the atoms in the unit cell $\{\tau_i\}$, instead, do not transform according to Eq. (2.12) unless this is required by symmetry. In the general case the τ 's transform according to:

$$\tau_i{}' = (1 + \eta)\,\tau_i + \mathbf{d}(i) \ . \tag{2.13}$$

To leading order, the sublattice displacements $\mathbf{d}$ are linear in the strain:

$$\mathrm{d}_\alpha(i) = -\sum_{\beta\nu} \gamma_{\alpha\beta\nu}(i)\ \eta_{\beta\nu} \ . \tag{2.14}$$

In the case of the diamond and of the zincblende structure symmetry requires that γ has only one independent component:

$$\gamma_{\alpha\beta\nu}(1) = -\gamma_{\alpha\beta\nu}(2) = -\zeta\,\frac{a}{4}\,|\epsilon_{\alpha\beta\nu}| \ , \tag{2.15}$$

where ζ is the so called internal-strain parameter and $\epsilon_{\alpha\beta\delta}$ is the fully antisymmetric Levi-Civita tensor.

The parameter ζ, which was first introduced by Kleinman,[55] has a simple physical interpretation. If we consider a uniform strain ($\eta_{xy} = \eta_{xz} = \eta_{yz} \equiv \eta$) along the (111) direction, the bond in that direction will be no longer equivalent to the other three bonds. Under the action of this strain the position of the nearest neighbour along (111) becomes:

$$\tau_2{}' = \tau_2 + (1-\zeta)\,\eta\frac{a}{4}(\eta,\eta,\eta)\ . \tag{2.16}$$

In particular, one has $\zeta = 0$ if the the atoms follows the macroscopic strain, and $\zeta = 1$ if the crystal deforms keeping the nearest neighbour bond length rigid.

A useful formal expression for the internal strain tensor is obtained by the expression of the crystal energy up to second order in the (periodic) ionic displacements, $\boldsymbol{u}_i$, and strain tensor $\boldsymbol{\eta}$:

$$\mathcal{W} = \mathcal{W}_0 + \frac{1}{2}\sum_{i,j,\alpha,\beta} u_{i\alpha}\,\Phi^{ij}_{\alpha\beta}\,u_{j\beta} + \frac{\Omega}{2}\sum_{\alpha,\beta,\nu,\tau}\eta_{\alpha\beta}\,\lambda^0_{\alpha\beta,\nu\tau}\,\eta_{\nu\tau} - \Omega\sum_{i,\alpha,\nu,\tau} u_{i\alpha}\,\Delta^i_{\alpha,\nu\tau}\,\eta_{\nu\tau}\ , \tag{2.17}$$

where the $\Phi^{ij}_{\alpha\beta} = \sum_{\mathbf{R}} C_{i\alpha,j\beta}(\mathbf{R})$ describe the restoring harmonic forces on the atoms, $\boldsymbol{\Delta}^i$ is a third-rank tensor which describes the stress generated by an unit displacement of the atom i or the force acting on it due to an unit strain, and λ^0 is the tensor of the electronic contributions to the elastic constants when the atomic displacements follow rigidly the macroscopic strain according to Eq. (2.12). When only macroscopic perturbations act on the system, the $\boldsymbol{u}$'s are not independent variables. Their value is instead determined by the condition that the force acting on each atom i vanishes:

$$F_{i\alpha} = -\frac{\partial\mathcal{W}}{\partial u_{i\alpha}} = -\sum_{j,\beta}\Phi^{ij}_{\alpha\beta}\,u_{j\beta} + \Omega\sum_{\nu\tau}\Delta^i_{\alpha,\nu\tau}\,\eta_{\nu\tau} = 0\ . \tag{2.18}$$

Imposing this condition, the energy as a function of the macroscopic strain only reads:

$$\mathcal{W} = \mathcal{W}_0 + \frac{\Omega}{2} \sum_{\alpha,\beta,\nu,\tau} \eta_{\alpha\beta}\, \lambda_{\alpha\beta,\nu\tau}\, \eta_{\nu\tau} \ , \tag{2.19}$$

where

$$\lambda = \lambda^0 - \Omega \sum_{i,j} \left(\Delta^i\right)^T \Phi_{ij}^{-1}\, \Delta^j \ , \tag{2.20}$$

are the (renormalized) elastic constants of the crystal. The macroscopic stress is defined by the relations:

$$\sigma_{\nu\tau} = -\frac{1}{\Omega}\frac{\partial \mathcal{W}}{\partial \eta_{\nu\tau}} = -\sum_{\alpha\beta} \lambda^0_{\nu\tau,\alpha\beta}\, \eta_{\alpha\beta} + \sum_{i\alpha} \Delta^i_{\alpha,\nu\tau} u_{i\alpha} \ . \tag{2.21}$$

Thus, from the equality of the second derivatives of the energy $\mathcal{W}$:

$$\Delta^i_{\alpha,\nu\tau} = -\left(\frac{\partial F_{i\alpha}}{\partial \eta_{\nu\tau}}\right)_{u=0} = -\Omega \left(\frac{\partial \sigma_{\nu\tau}}{\partial u_{i\alpha}}\right)_{\eta=0} \ . \tag{2.22}$$

For the crystal structures that we are considering we obtain from the transformation (2.20):

$$\begin{aligned} \lambda_{xx,xx} &= \lambda^0_{xx,xx} \\ \lambda_{xx,yy} &= \lambda^0_{xx,yy} \\ \lambda_{xy,xy} &= \lambda^0_{xy,xy} - \Omega \frac{(\Delta^2_{x,yz})^2}{\mu\, \omega^2_{TO}(\Gamma)} \end{aligned} \tag{2.23}$$

where μ is the reduced mass and $\omega_{TO}(\Gamma)$ the transverse optical frequency at Γ. The internal strain constant is hence obtained from the relation:

$$\zeta = a^2 \frac{\Delta^2_{x,yz}}{\mu\, \omega^2_{TO}(\Gamma)} \ . \tag{2.24}$$

Therefore, due to Eq. (2.22) we obtain two equivalent ways to calculate ζ: from the derivative of the force acting on the atom i with respect to the strain at zero

$\boldsymbol{u}$, and from the derivative of the stress with respect to the atomic displacement at zero strain.

An alternative expression of the internal strain parameter can be obtained from the dependence of the phase function ϕ, introduced in the previous paragraph, upon $\mathbf{q}$ for $\mathbf{q} \to 0$.[52] Let $\mathbf{q} \equiv (2\pi/a)(\xi, \xi, \xi)$ be a wavevector along the (111) direction. The set of displacements corresponding to a longitudinal acoustic phonon with wavevector $\mathbf{q}$ and eigenvectors in the form of Eq. (2.9) can be written as:

$$\mathbf{U}_s(\xi, \mathbf{R}) = \frac{1}{\sqrt{M_s}} \widetilde{\boldsymbol{u}}_s(\xi)\, \mathrm{e}^{i\mathbf{q}\cdot(\boldsymbol{\tau}_s + \mathbf{R})} , \tag{2.25}$$

where

$$\widetilde{\boldsymbol{u}}_s(\xi) = \boldsymbol{u}_s(\xi)\, \mathrm{e}^{-i\mathbf{q}\cdot\boldsymbol{\tau}_s} . \tag{2.26}$$

These latter quantities can be expanded up to the first-order in the parameter ξ:

$$\widetilde{\boldsymbol{u}}_s(\xi) = \widetilde{\boldsymbol{u}}_s^0 + \xi\, \widetilde{\boldsymbol{u}}_s^1 + \mathcal{O}(\xi^2). \tag{2.27}$$

In the diamond structure the zeroth-order eigenvectors do not depend on s, then:

$$\widetilde{\boldsymbol{u}}_s^0 = \sqrt{M}\mathbf{w} , \tag{2.28}$$

where M is the mass of the atoms; the first-order term reads:

$$\begin{aligned} \widetilde{\boldsymbol{u}}_1^1 &= 0 \\ \widetilde{\boldsymbol{u}}_2^1 &= i\sqrt{M} \left(\left.\frac{\partial\phi}{\partial\xi}\right|_0 - \frac{3}{2}\pi \right) \mathbf{w} . \end{aligned} \tag{2.29}$$

Within a region small compared with a/ξ, the lattice will be essentially in a state of homogeneous strain. Thus, within such a region, the particle displacements in Eq. (2.25) due to the zeroth-order term in the expansion (2.27) can be seen as being due to the homogeneous deformation:

$$\mathbf{U}(\xi, \mathrm{x}) = \mathbf{w}\, \mathrm{e}^{i\mathbf{q}\cdot\mathrm{x}} , \tag{2.30}$$

which can be described to the first-order by the strain tensor

$$\eta_{\beta\nu} = \frac{\partial U_\beta}{\partial x_\nu} = i\frac{2\pi}{a} w_\beta \xi \; e^{iq\cdot x} \simeq i\frac{2\pi}{a} w_\beta \xi \; . \tag{2.31}$$

To the leading order in ξ the sublattice displacement will be given in this case by:

$$\mathbf{d}(2) = i\xi \left(\left.\frac{\partial \phi}{\partial \xi}\right|_0 - \frac{3}{2}\pi \right) \mathbf{w} \; . \tag{2.32}$$

By inserting Eqs. (2.15), (2.31) and (2.32) into Eq. (2.14) finally we arrive at the following result:

$$\zeta = \frac{3}{2} - \frac{1}{\pi} \left. \frac{\partial \phi(\xi)}{\partial \xi} \right|_0 \; . \tag{2.33}$$

In the zincblende structure the two atoms are no longer equal; in this case following the same procedure we find a *real* correction to the sublattice displacements:

$$\Delta\mathbf{d}(2) = \left[\frac{1}{\sqrt{M_2}} \left. \frac{\partial c_2(\xi)}{\partial \xi} \right|_0 - \frac{1}{\sqrt{M_1}} \left. \frac{\partial c_1(\xi)}{\partial \xi} \right|_0 \right] \xi \, \hat{\mathbf{q}} \; . \tag{2.34}$$

However, by noting that to first-order the strain in Eq. (2.31) is purely imaginary we conclude that $\Delta\mathbf{d}(s)$ identically vanishes and that the relation (2.33) still holds in this case.

We have calculated the internal stain parameter of carbon and some semiconductors with all of the three methods we have described. A first estimate was made starting from the phase function in the (111) direction evaluated in the previous section. The eigenvectors of the dynamical matrix have been calculated using the same interplanar force constant used to interpolate the phonon dispersions.

Then we calculated the stress tensor with the crystal in the undistorted structure (i.e. at zero macroscopic strain), with one of the two atoms in the unit cell displaced in the direction (111) by the vectors:

$$\boldsymbol{u} = \pm 2 \times 10^{-4} a(1,1,1)$$

TABLE IV. Internal strain parameter for some semiconductors. (*a*) values derived from the slope of the phase function at $\mathbf{q}=0$. (*b*) values obtained from the linearization of the stress vs. the displacement. (*c*) values obtained from the linearization of the force vs. the strain. The experimental data reported are from Refs. [56, 57].

	C	Si	Ge	GaAs	AlAs
(*a*)	0.09	0.54	0.51	0.55	0.61
(*b*)	0.10	0.53	0.50	0.52	0.60
(*c*)	0.09	0.55	0.54	0.54	0.62
Exp.	0.13	0.54	0.54	0.76	

Such a displacement was found to be an appropriate compromise to guarantee linearity without affecting the results with numerical noise.

Finally the force acting on the atoms at the equilibrium in a strained structure along the Λ direction have been calculated. Strain components

$$\eta_{yz} = \eta_{xz} = \eta_{yx} = \pm(1 \div 4) \times 10^{-3}$$

have been used, the lowest value referring to the case of carbon, the higher to the other semiconductors. Furthermore, we have checked the convergence of our results for the latter two methods. For elemental and compound semiconductors we have found that the same kinetic energy cutoff used in the calculation of phonon dispersion was large enough to guarantee convergence of ζ to within 5%. To achieve the same accuracy in the case of diamond, whose pseudopotential is *harder* than the ones of the other elements, we needed a kinetic energy cutoff of 75 Ry.

The obtained results for the three methods are shown in Table IV in comparison with the available experimental data.

Chapter 3

Thermal Expansion

So far we have described how the harmonic properties of semiconductors can be predicted from first principles. However, real crystals are not completely harmonic, and anharmonic effects are in fact responsible for very important phenomena such as e.g. thermal conductivity and the dependence of the crystal volume and elastic constants upon temperature.

Crystal volume normally increases with temperature, and so behave tetrahedral semiconductors at room temperatures.[58] At low temperatures, however, tetrahedral semiconductors display a *negative* thermal expansion coefficient, as illustrated in Fig. 3.1 in the case of silicon. Very few attempts have been made to explain this behaviour on realistic grounds.[11,12,13]

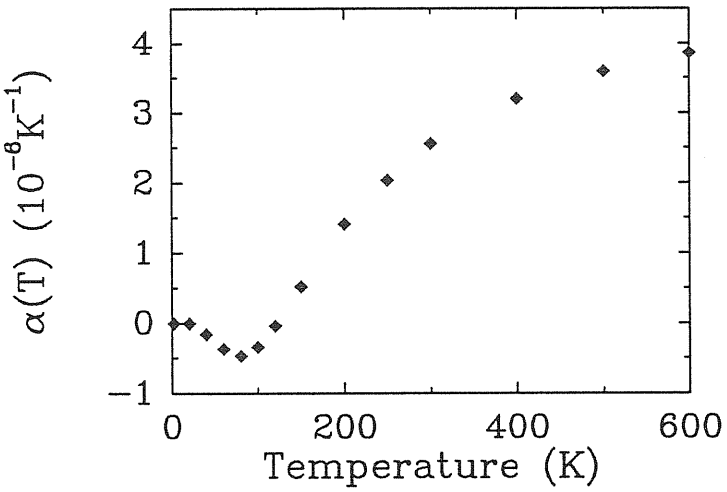

Figure 3.1. Experimental data for the linear thermal expansion coefficient in silicon as a function of temperature.[9]

In this chapter we will show how thermodynamical properties related to anharmonic effects can be derived and accurately predicted within the so called *Quasi Harmonic Approximation* (QHA) by employing the same first principles numerical techniques developed in the previous part of this thesis.

3.1 The quasi-harmonic approximation

At $T = 0$ the atomic equilibrium positions in a crystal are defined by the minimum of the potential energy $U(T = 0, V)$. At finite temperature and in the absence of an applied pressure the equilibrium condition requires the minimization of the appropriate thermodynamical potential, in this case the Helmholtz free energy defined as:

$$F(T,V) = U(T,V) - T\,S(T,V)\ , \tag{3.1}$$

where $S(T,V)$ is the entropy of the crystal. In the harmonic approximation the crystal can be considered as a collection of independent harmonic oscillators, so that the Helmholtz free energy can be expressed in terms of vibrational quantities only:

$$F_{\rm har}(T,V) = F^0(V) + F_{\rm vib}(T,V)\ . \tag{3.2}$$

The term $F^0(V)$ in Eq. (3.2) corresponds to the free energy at $T = 0$ and can be written in the following way:

$$F_0(V) = \mathcal{E}(V) + U^0_{\rm vib}(V)\ , \tag{3.3}$$

where $\mathcal{E}(V)$ is the internal energy of the static lattice at volume V, i.e. the so-called *total* energy which can be evaluated with the methods described in Chapter 1, and

$U^0_{\rm vib}(V)$ is the zero-point vibrational energy. On the other hand, the vibrational contribution in the harmonic approximation is given by:

$$F_{\rm vib}(T) = k_B T \sum_{n,\mathbf{q}} \ln\left[1 - \exp\left(-\frac{\hbar\omega_n(\mathbf{q})}{k_B T}\right)\right] \tag{3.4}$$

where the $\omega_n(\mathbf{q})$ are the normal-mode frequencies at $T = 0$.

In the harmonic approximation phonon-phonon interactions are completely neglected. The relevant consequences of this fact are that the normal-mode frequencies at $T = 0$ do not depend on the crystal volume, and that the equilibrium volume do not depend on the temperature. In this case the linear thermal expansion coefficient, which for cubic systems is defined as:

$$\alpha(T) = \frac{1}{3V}\left(\frac{\partial V}{\partial T}\right) , \tag{3.5}$$

obviously vanishes. However, the equilibrium volume of real crystals depends on temperature as a consequence of the phonon-phonon interaction. A simple approach to thermal expansion consists in simulating anharmonic effects by allowing for the dependence of the normal-mode frequencies upon the volume, and retaining for the vibrational part of the free energy the same functional form as in Eq. (3.4):

$$F_{\rm vib}(T,V) = k_B T \sum_{n,\mathbf{q}} \ln\left[1 - \exp\left(-\frac{\hbar\omega_n(\mathbf{q},V)}{k_B T}\right)\right] . \tag{3.6}$$

This approximation is known as the *Quasi-Harmonic Approximation*. Hence, the thermal expansion of the system can be obtained from the equation of state:

$$\left(\frac{\partial F(T,V)}{\partial V}\right)_T = 0 \qquad \Longrightarrow \qquad V = V(T) . \tag{3.7}$$

To evaluate Eq. (3.7) we expand the Helmholtz free energy around the equilibrium volume at $T = 0$:

$$F(T,V) = F(T,V_0) + \left(\frac{\partial F(T,V)}{\partial V}\right)_{T,V_0}(V - V_0) + \frac{1}{2}\left(\frac{\partial^2 F(T,V)}{\partial V^2}\right)_{T,V_0}(V - V_0)^2, \tag{3.8}$$

where the coefficients in the expansion are:

$$\begin{aligned}\left(\frac{\partial F(T,V)}{\partial V}\right)_{T,V_0} &= \left(\frac{\partial F_0(V)}{\partial V}\right)_{V_0} + \left(\frac{\partial F_{\rm vib}(T,V)}{\partial V}\right)_{T,V_0} \\ \left(\frac{\partial^2 F(T,V)}{\partial V^2}\right)_{T,V_0} &= \left(\frac{\partial^2 F_0(V)}{\partial V^2}\right)_{V_0} + \left(\frac{\partial^2 F_{\rm vib}(T,V)}{\partial V^2}\right)_{T,V_0}\end{aligned} . \tag{3.9}$$

Due to the equilibrium condition, one has:

$$\left(\frac{\partial F_0(V)}{\partial V}\right)_{V_0} = 0 . \tag{3.10}$$

In the QHA the coefficients in Eq. (3.9) involve the evaluation of the derivatives of the frequencies up to the second order in the volume. Assuming that the phonon dispersions depend smoothly on the volume, we can consider in Eq. (3.9) only those terms in which the derivatives of the frequencies appear up to the first order. Hence we can write:

$$\left(\frac{\partial^2 F(T,V)}{\partial V^2}\right)_{T,V_0} \simeq \left(\frac{\partial^2 F_0(V)}{\partial V^2}\right)_{V_0} \simeq \frac{B_0}{V_0} , \tag{3.11}$$

where B_0 is the Bulk modulus of the crystal at equilibrium:

$$B_0 = -V_0\left(\frac{\partial P}{\partial V}\right)_{V_0} . \tag{3.12}$$

Following Eq. (3.7) we arrive at the equation of state:

$$V(T) = V_0 - \frac{V_0}{B_0}\left(\frac{\partial F_{\rm vib}(T,V)}{\partial V}\right)_{T,V_0} , \tag{3.13}$$

including the vibrational free energy in the QHA we get the final expression for the thermal expansion coefficient:

$$\alpha(T) = -\frac{V_0}{3B_0} \sum_{\mathbf{q},n} \frac{c_{vn}(\mathbf{q},T)}{\omega_n(\mathbf{q},V_0)} \left(\frac{\partial \omega_n(\mathbf{q},V)}{\partial V} \right)_{V_0} , \tag{3.14}$$

where the $c_{vn}(\mathbf{q},T)$ are the mode contributions to the specific heat at constant volume:

$$c_{vn}(\mathbf{q},T) = \frac{\hbar\omega_n(\mathbf{q},V_0)}{V_0} \frac{\mathrm{d}}{\mathrm{d}T} \left[\exp\left(\frac{\hbar\omega_n(\mathbf{q},V_0)}{k_B T} \right) - 1 \right]^{-1} . \tag{3.15}$$

3.2 Mode Grüneisen parameters

Equation (3.14) can be recast in a simpler form by introducing the mode Grüneisen parameters defined as:

$$\gamma_n(\mathbf{q}) = -\frac{V_0}{\omega_n(\mathbf{q},V_0)} \left. \frac{\partial \omega_n(\mathbf{q},V)}{\partial V} \right|_{V=V_0} , \tag{3.16}$$

which describe how each single phonon mode varies with the volume of the system. Inserting Eq. (3.16) in Eq. (3.15) we obtain the following result:

$$\alpha(T) = -\frac{1}{3B_0} \sum_{\mathbf{q},n} \gamma_n(\mathbf{q})\, c_{vn}(\mathbf{q},T) . \tag{3.17}$$

3.2.1 Mode Grüneisen parameters at $\mathbf{q} = 0$

Approaching the Γ point ($\mathbf{q} = 0$) both the acoustic frequencies and their derivatives with respect to the volume vanish. In fact, mode Grüneisen parameters are non analytic at $\mathbf{q} = 0$ and the value they assume in the limit $\mathbf{q} \to 0$ depends on the direction of the vector $\mathbf{q}$. Thus to properly account for the behaviour of the

Grüneisen parameter near Γ it is necessary to find an appropriate expansion of both frequencies and their derivatives to the correct order. Let us expand the acoustic frequence $\omega(\mathbf{q},\Omega)$ (where Ω is the unit cell volume and for the sake of simplicity we have suppressed the band index) up to linear order in $\mathbf{q}$:

$$\omega(\mathbf{q},\Omega) = v_{\widehat{\mathbf{q}}}(\Omega)\,|\mathbf{q}| \ . \tag{3.18}$$

where the sound velocity in the direction $\widehat{\mathbf{q}} = \mathbf{q}/|\mathbf{q}|$ is:

$$v_{\widehat{\mathbf{q}}}(\Omega) = \lim_{|\mathbf{q}|\to 0} \frac{\partial\omega(\mathbf{q},\Omega)}{\partial\mathbf{q}} \cdot \widehat{\mathbf{q}} \ . \tag{3.19}$$

Hence the derivatives of the frequencies with respect to the volume read:

$$\frac{\partial\omega(\mathbf{q},\Omega)}{\partial\Omega} = \frac{\partial v_{\widehat{\mathbf{q}}}(\Omega)}{\partial\Omega}\,|\mathbf{q}| + v_{\widehat{\mathbf{q}}}(\Omega)\,\frac{\mathrm{d}|\mathbf{q}|}{\mathrm{d}\Omega} + \mathcal{O}(|\mathbf{q}|^2) \ . \tag{3.20}$$

Finally the expression for the Grüneisen parameter at Γ is:

$$\begin{aligned}\gamma_{\widehat{\mathbf{q}}}(\Gamma) &= \lim_{|\mathbf{q}|\to 0}\left\{\frac{\Omega_0}{v_{\widehat{\mathbf{q}}}(\Omega_0)\,|\mathbf{q}|}\left[\left.\frac{\partial v_{\widehat{\mathbf{q}}}(\Omega)}{\partial\Omega}\right|_{\Omega=\Omega_0}|\mathbf{q}| + v_{\widehat{\mathbf{q}}}(\Omega_0)\left.\frac{\mathrm{d}|\mathbf{q}|}{\mathrm{d}\Omega}\right|_{\Omega=\Omega_0}\right]\right\} \\ &= \frac{\Omega_0}{v_{\widehat{\mathbf{q}}}(\Omega_0)}\left.\frac{\partial v_{\widehat{\mathbf{q}}}(\Omega)}{\partial\Omega}\right|_{\Omega=\Omega_0} + \omega_0 \lim_{|\mathbf{q}|\to 0}\left\{\frac{1}{|\mathbf{q}|}\left.\frac{\mathrm{d}|\mathbf{q}|}{\mathrm{d}\Omega}\right|_{\Omega=\Omega_0}\right\} \ .\end{aligned} \tag{3.21}$$

We are mainly interested in crystals with the diamond and zincblende structures; in this case we can write explicitly the dependence on the equilibrium lattice parameter a_0:

$$\Omega_0 = \frac{1}{4}a_0^3 \ ; \qquad\qquad \mathrm{q} = \frac{2\pi}{a_0}x \ , \tag{3.22}$$

where x is a dimensionless number. We finally obtain:

$$\gamma_{\widehat{\mathbf{q}}}(\Gamma) = \frac{1}{3}\left[1 - \frac{a_0}{v_{\widehat{\mathbf{q}}}(a_0)}\left.\frac{\mathrm{d}v_{\widehat{\mathbf{q}}}(a)}{\mathrm{d}a}\right|_0\right] \ . \tag{3.23}$$

TABLE V. Convergence test of the Grüneisen parameter of Si for increasing values of the cutoff energy. Energies are expressed in Rydberg.

$E_{\rm cut}$	12	16	20	24
$\gamma(\Gamma_O)$	0.90	1.01	0.98	0.97
$\gamma(X_{TA})$	-2.42	-1.95	-2.19	-2.09
$\gamma(X_L)$	0.90	1.02	0.99	0.97
$\gamma(X_{TO})$	1.36	1.54	1.51	1.47

3.3 Results for Si, Ge, GaAs, AlAs

Dynamical matrices at any point in the Brillouin Zone (BZ) can be efficiently obtained using the density functional perturbation theory derived in Chapter 1. In particular, using the interpolation procedure described in Section 4.1 it is straightforward to perform sums in reciprocal space, such as in Eq. (3.17), over a practically unlimited number of points in the BZ. The technical details of the calculation are the same which are reported in the introduction to Chapter 2.

Phonon frequencies have been evaluated by diagonalizing the dynamical matrix $\widetilde{D}_{ss'}(\mathbf{q},\Omega)$ near the equilibrium volume $\Omega_0 = a_0^3/4$, and derivatives have been calculated numerically using quadratic interpolation.

In Table V we report an example of a convergence test for the $\gamma(\mathbf{q})$ at some high-symmetry point in the case of Si. Analogously to the case of the phonon frequencies, we have evaluated the complete dispersions of the mode Grüneisen parameters along several symmetry lines. The results we have obtained for several semiconductors are shown and compared with available experimental data in Fig. 3.2. Most of the branches in the dispersions of Grüneisen parameters are

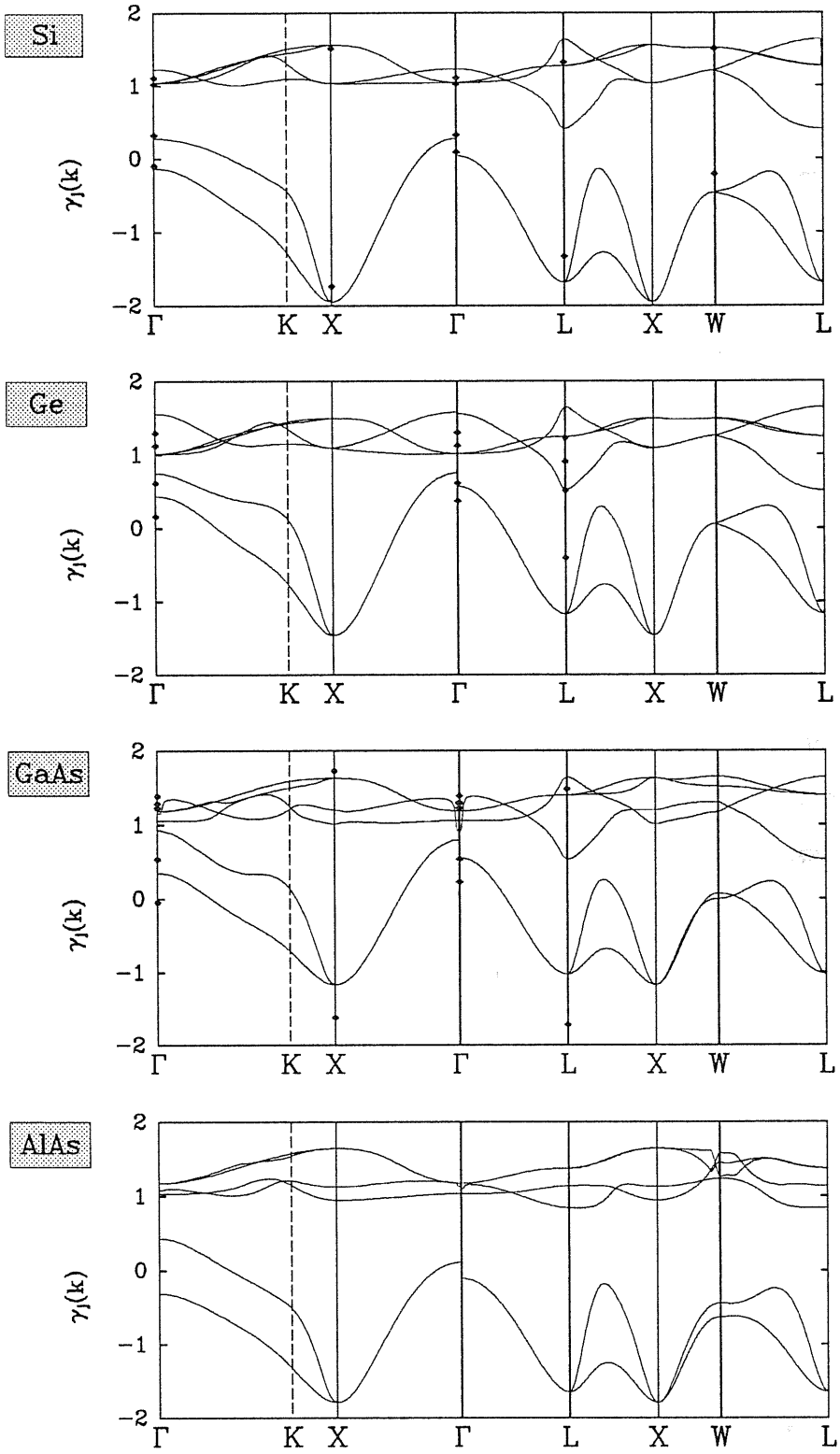

Figure 3.2. Calculated dispersions of the mode Grüneisen parameters. Experimental data are denoted by diamonds (from Refs. [59], [60], and [61]).

contained within a small strip of values around $\gamma = 1$. On the other hand, the lowest branches, corresponding to transverse acoustic (TA) modes, are spread over a larger region, ranging from positive values at Γ and to negative values at the BZ boundaries. The negative values of the $\gamma_{TA}(\mathbf{q})$ at the edges of the BZ can be related to competition effects between the contributions to the force acting on the atoms. This restoring force can be described as a sum of a contribution from central forces and a noncentral angular part coming from the directional covalent bonds. At the zone boundaries these terms originate respectively a negative and a positive contribution to the Grüneisen parameters of the TA modes. In the case of silicon and of the other tetrahedral semiconductors we have considered, the negative central-force contributions are dominant.[13]

Thermal expansion coefficients have then been evaluated following Eq. (3.6). The sum over phonon modes has been performed using 182 points in the irreducible wedge of the Brillouin Zone; further increasing the number of k-points does not change significantly our results. The dependence upon temperature of the coefficient $\alpha(T)$ for some diamond (Si, Ge) and zincblende (GaAs, AlAs) structure semiconductors is displayed in Figs. 3.3 and 3.4. Our result correctly predict a negative thermal expansion at low temperatures. The insert shows the details at very low temperatures, where positive thermal expansion coefficients have been found except for AlAs. Also in this case experiments are predicted with remarkable accuracy by our calculations. No experimental data is, to date, available for AlAs. The anomalies in the thermal expansion at low temperatures of tetrahedral semiconductors are due to the behaviour of the TA mode Grüneisen parameters at the zone boundaries. Our results support this interpretation. At low temperatures strongly negative values of $\gamma_{TA}(\mathbf{q} \approx 0)$ near the edges of the BZ originate

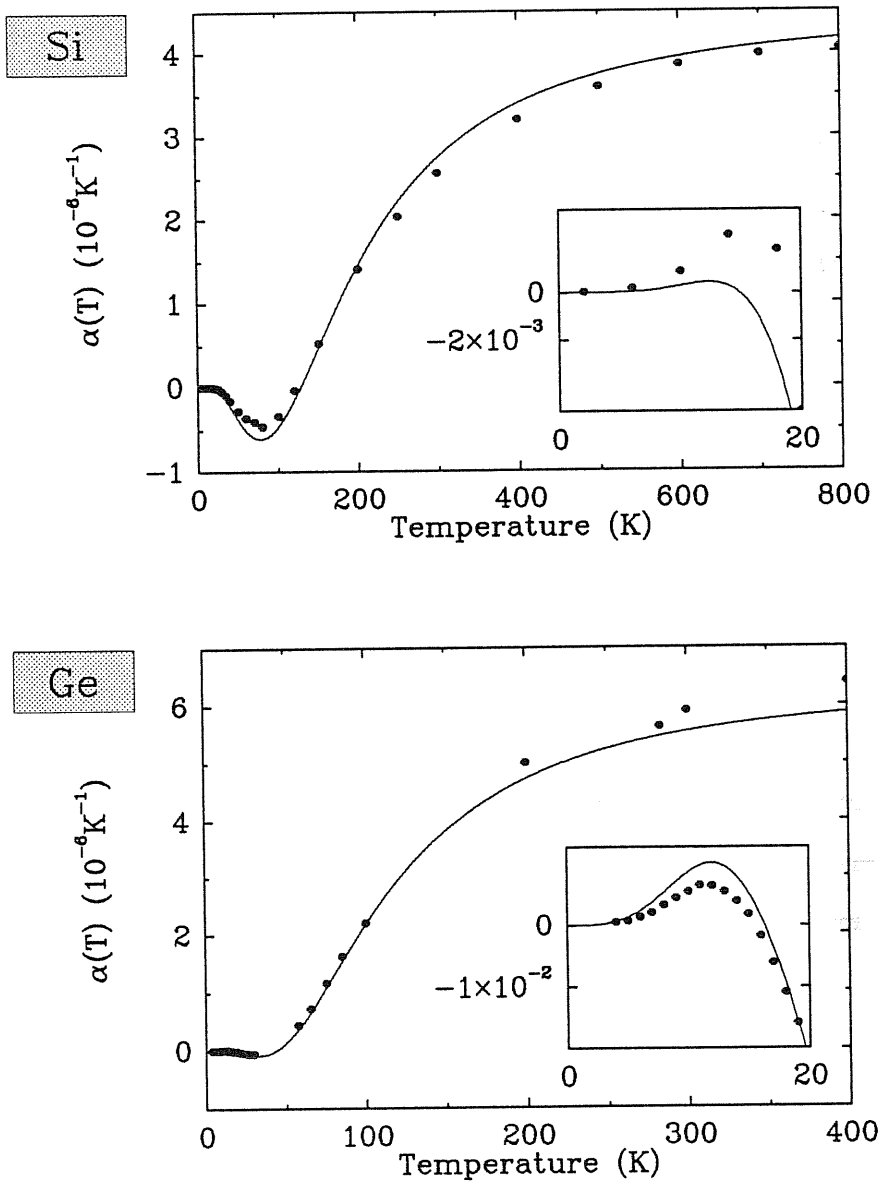

Figure 3.3. Thermal expansion coefficient as a function of temperature for elemental semiconductors. The insert shows the details at very low temperatures. Experimental data are denoted by full circles (from Refs. [9], and [10]).

the dominant contribution to Eq. (3.6) in relation to the large density of states in the corresponding region of frequencies.

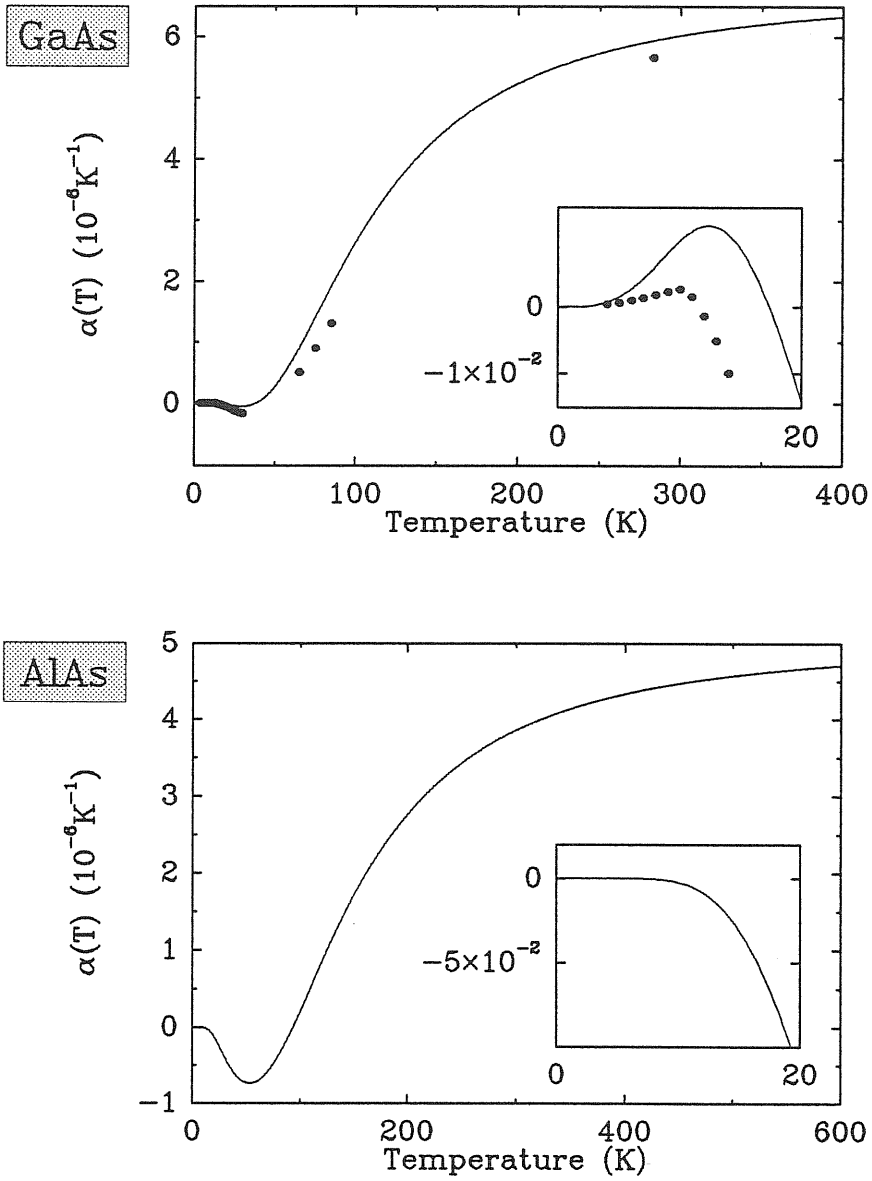

Figure 3.4. Thermal expansion coefficient as a function of temperature for compound semiconductors. The insert shows the details at very low temperatures. Experimental data are denoted by full circles (from Ref. [10]).

The behaviour of the thermal expansion coefficient as a function of temperature can be simply interpreted in the following way. At very low temperatures only

acoustic phonons in a small region in proximity of the Γ-point are excited. The sign of the thermal expansion coefficient near $T = 0$ depends on the values of the mode Grüneisen parameters of the acoustic branches very close to Γ: when all the $\gamma_{TA}(\mathbf{q})$ at $\mathbf{q} \approx 0$ are positive the $\alpha(T \approx 0)$ is also positive. According to this interpretation, most of the semiconductors we have studied show a positive $\alpha(T)$ for T very close to zero. This is is not the case of AlAs, where the thermal expansion coefficient is always negative. Unlike the other semiconductors we have considered, AlAs can have negative $\gamma_{TA}(\mathbf{q})$ when approaching Γ along some direction (e.g. the (111) direction), this fact originates competition effects in the sum in Eq. (3.6) which can explain the obtained behaviour. Far from the zone-center the $\gamma_{TA}(\mathbf{q})$ become negative, thus in the range of temperatures where only acoustic phonons are excited there exists a value at which the coefficient $\alpha(T)$ changes its sign. With increasing temperature the positive contributions dominate expression (3.17) and the crystal expands relatively to the $T = 0$ volume. In the QHA at temperatures of the order of the Debye temperature all the phonon modes in the crystal are excited and the $\alpha(T)$ displays a tendency to saturate to a constant value. The residual dependence of α upon T is due to the dependence of the γ's upon volume which is determined by higher-order anharmonic effects.

Chapter 4

From Pure Bulk Semiconductors to Superlattices and Alloys

In the previous chapters we have seen that accurate lattice dynamical properties, such as bulk phonon dispersions spectra and thermal expansion coefficients, can be obtained in simple semiconductors with a modest investment of supercomputer time. More complex semiconductor structures, such as alloys, superlattices, and other quantum microstructures, could in principle be dealt with in the same way as simple semiconductors, by studying appropriate "supercells". Some calculations for GaAs/AlAs ultrathin superlattices have been actually done in this way,[7] but the required amount of supercomputer time is no longer modest. Already the simplest among such structures—ideal superlattices—are described by supercells containing several atoms in the unit cell. As the computer time required by first-principles DFPT phonon calculations grows as the fourth power of the number of atoms in the unit cell, systems larger than 10-20 atoms cannot be presently treated in a straightforward "brute-force" approach. It is evident that such small supercells will not lead to clearcut answers in complex systems.

In this chapter we show how an accurate description of lattice dynamics in mixed semiconductors can be achieved using the information gained from ab-initio calculations on pure materials. Such an apparently unreachable goal can in fact

be achieved, at least for those systems which differ from a perfect crystal for the (partial) substitution of one of its atomic species with another chemically very similar. This is the case of GaAs/AlAs.

Phonon frequencies in mixed systems can be obtained from real-space interatomic force constants of pure materials within the so-called *Mass Approximation* (MA). The MA consists in neglecting the dependence of the interatomic force constants, Eq. (1.19), upon composition. Within the MA, therefore, the interatomic force constants can be calculated once for all in the pure materials, and used then for mixed systems. In practice, real-space interatomic force constants are calculated by Fourier analysing the dynamical matrices obtained for the pure crystals on a fine grid in reciprocal space, as explained below. In GaAs/AlAs systems, the mass approximation is shown to be very accurate, thus giving the possibility of studying with high accuracy and low computational effort the vibrational properties of very large SL or alloy samples.

As a further development, in the second part of this chapter we present a perturbative approach to first-order Raman scattering in AlAs/GaAs systems in which the dielectric susceptibility is expanded in terms of "chemical variables" defined on each cationic site of the lattice and specifying the presence at that site of an Al or Ga atom.

4.1 Phonon frequencies from real-space interatomic force constants

In non polar materials (such as elemental semiconductors), the range of the interatomic forces constants (Eq. (1.19)) is short, typically some shells of neighbours.

For this reason, interatomic force constants offer a convenient way of storing the information contained in the dynamical matrices $\widetilde{D}_{\alpha i,\beta j}(\mathbf{q})$ at any $\mathbf{q}$, into a few (typically some tens) independent parameters. Real-space force constants are conveniently obtained by discrete Fourier analysis of their reciprocal-space counterpart, Eq. (1.24), calculated onto a finite uniform grid in the BZ. This yields a finite set of interatomic force constants in real space up to a maximum range essentially given by $2\pi/\Delta q$, where Δq is the spacing between neighbouring points in the BZ. Mathematically, the number of force constants so obtained is equal to the number of $\mathbf{q}$ points in the finite grid. The discrete BZ sampling is equivalent to solving the problem directly with a supercell whose linear dimensions are of the order of $2\pi/\Delta q$, thus containing a number of atoms proportional to the number of $\mathbf{q}$-points. Such equivalence is *exact* if all the $\mathbf{q}$ points in the mesh can be obtained as differences of the $\mathbf{k}$ points used for the BZ sampling of the electronic wavefunctions necessary to calculate Eq. (1.37); otherwise, it is only approximate. In any case, the error made in the discretization is negligible, provided that the $\mathbf{q}$-space grid is dense enough to yield force constants in real space up to their typical range. For typical semiconductors, this can be achieved by calculating the dynamical matrix in $\simeq 100$ points, which is computationally feasible. The advantage of this approach with respect to a supercell approach is evident: the computational workload scales linearly with the number of $\mathbf{q}$-points in our approach, as opposed to as the third power of the number of atoms when using supercells.

Once real-space constants have been obtained in this way, reciprocal-space dynamical matrices can be calculated by inverse Fourier transform at any point of the BZ (i.e. even at a point not contained in the original grid). For this reason, real-space force constants are a powerful tool for interpolating dynamical matrices throughout the BZ. We remark that the discrete Fourier analysis can be performed

in an extremely efficient way using Fast-Fourier-Transform algorithms.

In polar materials (such as compound semiconductors), the range of the interatomic force constants is not short, due to dipolar interactions associated with non vanishing effective charges. Mathematically, the long-range character of the force constants is the origin of the non analytic behavior of $\widetilde{C}(\mathbf{q})$, as $\mathbf{q} \to 0$. As the non analytic part of $\widetilde{C}(\mathbf{q})$ can be expressed in terms of the ionic effective charges and dielectric tensor of the system through Eq. (1.51), the former is easily separated out of $\widetilde{C}(\mathbf{q})$, once ϵ_∞ and the Z^*'s have been calculated. Once this is done, the remaining analytic term can be treated as in non polar materials. Note that subtracting Eq. (1.51) from the matrix of the force constants, $\widetilde{C}(\mathbf{q})$, and expressing the resulting difference in terms of real-space force constants, effectively maps the lattice-dynamical problem onto a rigid-ion model whose interaction constants, however, are not necessarily restricted to a small number of neighbours.

As has been already mentioned in Section 2.2, we have calculated the dynamical matrices at all the points $\mathbf{q}$ belonging to the $(L = 4)$ grid. Fourier deconvolution on this mesh yields real-space interatomic force constants up to the 9-th shell of neighbors. This procedure is equivalent to calculating real-space force constants using an FCC supercell whose linear dimensions are four times larger than the primitive zincblende cell, thus containing 128 atoms.

The qualitative behavior of the obtained real-space force constants for Si and Ge is similar to that previously obtained by dielectric matrices and local pseudopotentials.[62] In particular, we have found that the force constants decay slowly in the direction of the bond chains, $\langle 110 \rangle$. A similar behavior has been observed also in III-V compounds, once the long-range tails of the force constants are removed.

4.2 Transferability of the force constants

We wish now to assess to which extent the force constants calculated for one material are able to describe the lattice dynamics of another material or a mixture of the two (such as an alloy or a microstructure). To this end, we have calculated the phonon dispersions of several materials using the force constants obtained for different materials which differ from the former for the cationic or anionic species. Our results are displayed in Fig. 4.1, where the notation [A]→B indicates that phonons of material B have been obtained with the force constants appropriate to material A, just replacing the relevant masses (*mass approximation*). In the case of GaAs and AlAs—which differ for the cationic species and have practically the same lattice parameter—the mass approximation gives phonon dispersions practically indistinguishable from the real ones in the acoustical and transverse optic regions, while they differ by less than 10 cm^{-1} in the LO region. Such an accuracy is achieved without any empirical adjustment of the effective charges. In fact, the small discrepancies are almost entirely due to the small difference between the effective charges of the two materials.

It turns out that ab-initio force constants calculated for GaAs are indeed capable of describing rather accurately phonon dispersions in AlAs, while semiempirical dynamical matrices (such as those from the bond-charge or other models), fitted to the GaAs dispersions, give an AlAs LO band width along ΓX which is much larger that calculated from first principles. This indicates that the agreement between the calculated frequencies and experiments is by no means a sufficient criterion for judging the quality of a model. A similar accuracy is obtained also for Sb compounds, where the lattice mismatch is larger. These results clearly indicate that the use of the mass approximation for systems which differ for the cationic

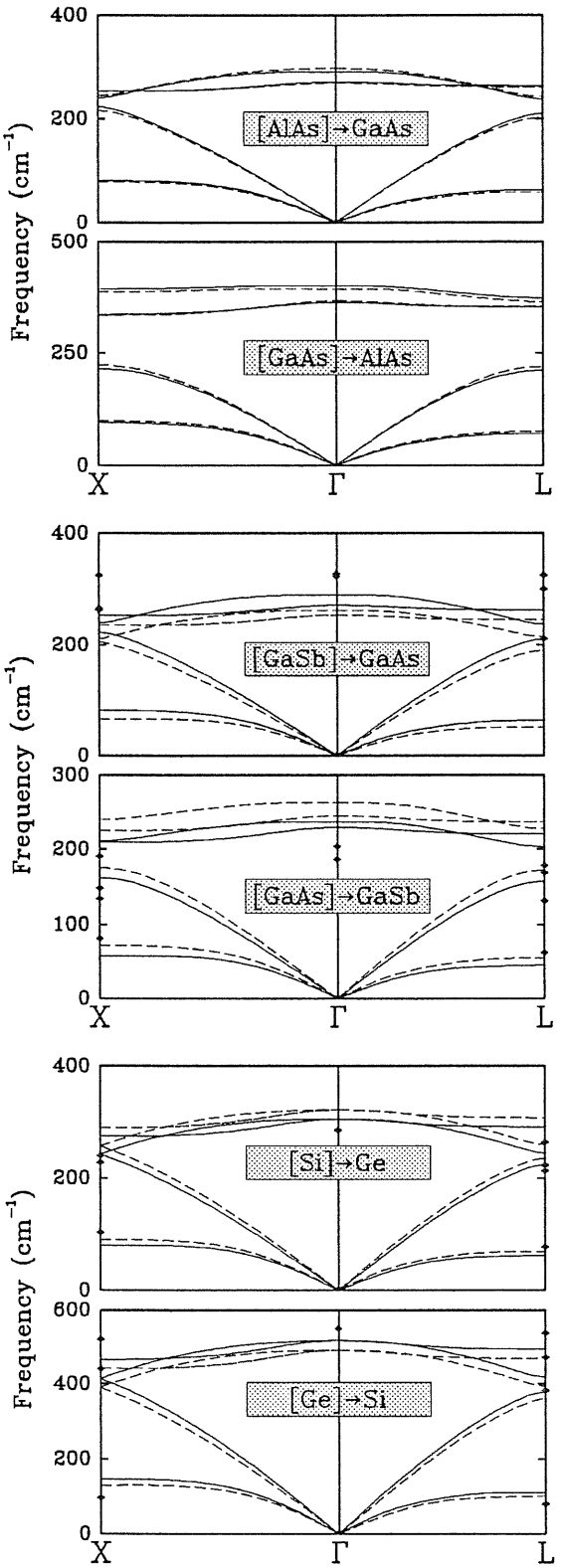

Figure 4.1. Comparison between the phonon dispersions calculated with (dashed line) and without (full line) the mass approximation. The notation [A]⟶B indicates that phonon dispersions of material B have been obtained with the force constants appropriate to material A, just replacing the relevant masses. The diamonds indicate the frequencies obtained calculating the dynamical matrices of material A at the lattice parameter appropriate for material B.

species is well justified, provided accurate force constants are used.

In the case of GaAs and GaSb (which differ for the anionic species and have a rather large lattice mismatch) the mass approximation gives poorer results, with errors larger than 30 cm^{-1}. This fact had been already noted and attributed to the larger polarizability of the anions.[15] One could think that the main source of inaccuracy lies in the large lattice mismatch. To verify this issue, we have also calculated some representative phonon frequencies for system B, using the force constants of system A, calculated at the lattice parameter of system B. The results are indicated by diamonds at the X, Γ, and L points in Fig. 4.1. We see that even worse results are obtained in this case. Similar results have been obtained for Al compounds as well. We conclude that the mass approximation is much less accurate when the systems differ by their anions, than when they differ by their cations.[15] Finally, in the case of Si and Ge, the accuracy of the mass approximation is somewhat intermediate between the above two cases, as expected.

The use of the mass approximation in GaAs/AlAs systems is not new,[15] nor even recent. However—in the lack of any reliable information on the phonon dispersions of AlAs—its validity has always been assumed, rather than demonstrated. Our results definitely show that the interatomic force constants in GaAs and in AlAs are very similar. The use of equal interatomic force constants for AlAs and GaAs, however, may lead to sizeable errors, when GaAs force constants are obtained from semiempirical models, rather that from first principles. The BCM, for instance, provides a very good fit to phonon dispersions of GaAs—quite close to our results, in fact. The same BCM force constants for GaAs, when applied to AlAs with the mass approximation, yield much worse results. The reason

for this apparent contradiction is that semiempirical models are almost invariably obtained from a fit to experimental phonon dispersions; 'good' force constants, however, should reproduce both the eigenvalues (the dispersions) and the eigenvectors (the displacement pattern) of the dynamical matrix. As the latter are usually poorly known from experiments, ab-initio calculation appear to be the only reliable source of information for the interatomic force constants.

We used the mass approximation and the force constants calculated for the virtual crystal $(Ga_{0.5}Al_{0.5})As$ to calculate the phonon frequencies at $\mathbf{q} = 0$ of $(AlAs)_n(GaAs)_n$ $(n = 1, 2)$ superlattices grown along the (001) direction. The obtained frequencies are displayed and compared with results from full ab-initio calculations in Table VI. The overall agreement is very good.

4.3 First-order Raman scattering

First-order (one-phonon) Raman scattering due to a normal mode ν can occur when the macroscopic crystal electric polarizability, χ, exhibits a linear dependence on the normal coordinate ξ_ν.[63] Therefore, if we expand χ to the linear order in ξ_ν we obtain:

$$\chi = \chi_0 + \sum_\nu \Delta\chi_\nu \, \xi_\nu + \mathcal{O}(\xi^2) \, , \tag{4.1}$$

where χ_0 is the ground state susceptibility, and $\Delta\chi_\nu$ is modulated by the mode ν at the frequency ω_ν. When the crystal is exposed to a monochromatic light beam of frequency ω (usually in the visible region of the spectrum) the associated electric field $\mathbf{E}$ sets up an electric moment per unit cell $\mathbf{M}_\nu$, equal to $\Delta\chi_\nu \cdot \mathbf{E}$. Since $\Delta\chi_\nu$ and $\mathbf{E}$ are modulated at the frequencies ω_ν and ω respectively, the resulting dipole moment per unit cell oscillates at the frequency $\omega_S = \omega - \omega_\nu$ or

TABLE VI. Calculated ab-initio phonon frequencies at q=0 for (1-1) and (2-2) Sl's in comparison with values obtained within the mass approximation from the force constants of the virtual crystal. The symmetry of each longitudinal mode is also reported: modes $A1$ are invariant relative to the 2-fold rotation axis perpendicular to the growth direction, modes $B2$ are antisymmetric relative to the same axis. Units are cm^{-1}.

SL 1-1	$\omega_{ab-initio}$	$\omega_{mass\ app.}$	symmetry
T_1	88	87	
L_1	222	222	$A1$
T_2	253	261	
L_2	265	269	$B2$
T_3	358	352	
L_3	397	394	$B2$

SL 2-2	$\omega_{ab-initio}$	$\omega_{mass\ app.}$	symmetry
T_1	74	73	
T_2	77	77	
T_3	90	91	
L_1	141	142	$A1$
L_2	143	145	$B2$
L_3	221	222	$B2$
T_4	251	257	
T_5	259	263	
L_4	261	264	$A1$
L_5	284	288	$B2$
T_6	344	341	
T_7	359	355	
L_6	396	393	$A1$
L_7	399	396	$B2$

$\omega_A = \omega + \omega_\nu$. This means that the crystal radiates (scatters) these two frequencies which fall close to ω (since $\omega_\nu << \omega$). They are commonly known as the "Stokes" and "anti-Stokes" components respectively of first-order Raman scattering by the mode ν. From a microscopical point of view one can also regard the Stokes process as a sequence of elementary processes involving the emission and the absorption of photons and phonons: (i) absorption of a photon ω through an electro-photon interaction, (ii) creation of a phonon ω_ν through an electron-phonon interaction, and (iii) emission of a photon $\omega_S = \omega - \omega_\nu$ through an electron-photon interaction. An analogous sequence of elementary processes may be invoked to describe an anti-Stokes scattering.

Off resonance the Raman cross section related to first-order scattering is given essentially by the derivative of the macroscopic crystal polarizability of the system with respect to the vibrational normal coordinates:

$$\sigma_R^{IF}(\omega) \propto \sum_\nu \delta(\omega^2 - \omega_\nu^2) \left| \widehat{e}_F^* \cdot \frac{\partial \chi}{\partial \xi_\nu} \cdot \widehat{e}_I \right|^2 . \tag{4.2}$$

where $\widehat{e}_{IF}$ are the polarization vectors of the incoming and scattered photons, and ω_ν is the frequency corresponding to the normal mode ν. The derivative of the polarizability can be written in terms of the atomic displacements $u_\gamma^s(L)$, of the s-th atoms in the L-th unit cell, from equilibrium:

$$\frac{\partial \chi_{\alpha\beta}}{\partial \xi_\nu} = \sum_{L,s,\gamma} \mathcal{P}^s_{\alpha\beta\gamma} \frac{\partial u_\gamma^s(L)}{\partial \xi_\nu} , \tag{4.3}$$

where we define the third-rank tensor

$$\mathcal{P}^s_{\alpha\beta\gamma} = \frac{\partial \chi_{\alpha\beta}}{\partial u_\gamma^s(L)} , \tag{4.4}$$

as the *Raman tensor* of the crystal, which is independent of the index L due to the periodicity of the crystal. In the case of pure tetrahedral semiconductors the

independent components of the Raman tensor reduce to only one due to symmetry reasons:

$$\mathcal{P}^{s}_{\alpha\beta\gamma} = P\,(-)^{s}|\epsilon_{\alpha\beta\gamma}| \ . \tag{4.5}$$

The Raman tensor for elemental and binary semiconductors can be easily calculated from first-principles. To this end, we calculate the electronic polarizability tensor for the crystal as a function of phononlike distorsions of the form

$$\boldsymbol{u}^{s} = \pm u a(1,1,1) \ , \tag{4.6}$$

where a is the lattice constant. The derivatives of the polarizability tensor have been calculated numerically. Due to the tetrahedral symmetry the expansion of the susceptibility in terms of u reads:

$$\begin{aligned}\chi(u) = &\begin{pmatrix} \chi^{(0)} & 0 & 0 \\ 0 & \chi^{(0)} & 0 \\ 0 & 0 & \chi^{(0)} \end{pmatrix} + u \begin{pmatrix} 0 & \chi^{(1)} & \chi^{(1)} \\ \chi^{(1)} & 0 & \chi^{(1)} \\ \chi^{(1)} & \chi^{(1)} & 0 \end{pmatrix} \\ &+ u^2 \begin{pmatrix} \chi^{(2)} & 0 & 0 \\ 0 & \chi^{(2)} & 0 \\ 0 & 0 & \chi^{(2)} \end{pmatrix} + \mathcal{O}(u^3) \ .\end{aligned} \tag{4.7}$$

A typical value of the amplitude u, providing good linearity and still giving no cancellation problems, is $u = 2 \times 10^{-4}$. Then, the value of P can be evaluated from the linear term of Eq. (4.7):

$$P = \frac{a^2}{8}\,\chi^{(1)} \ . \tag{4.8}$$

In order to have a correct description of the relative intensities of the peaks in the Raman spectrum of mixed systems, we are not interested in the absolute

TABLE VII. Calculated Raman tensor for pure bulk semiconductors. The reported values are expressed in units $10^{-2}\,a^2$, where a is the corresponding lattice parameter.

	Si	Ge	GaAs	AlAs
P	77.4	219.0	59.4	19.5

values of the Raman intensities but in the relative ones. To this purpose, a kinetic energy cutoff of 12 Ry was large enough to guarantee a convergence of the relative intensities to an accuracy of 5%, even if the the accuracy for the absolute values is not yet as good. The results we have obtained for Si, Ge, GaAs and AlAs are shown in Table VII.

4.4 Raman intensities in complex systems from a perturbative approach

When one has to deal with systems, such as superlattices, with many atoms in the unit cell, the calculation of the Raman tensor from first-principles is no longer feasible: the computational effort may become a very hard and, in most cases, impossible task. Thus, one has to device alternative approaches. We present in the following a microscopic model of the first-order Raman spectroscopy in AlAs/GaAs mixed systems. As stated in the previous sections, the force constants in AlAs and GaAs are very similar, furthermore the two bulk constituents are nearly lattice matched; this allows us to neglect lattice relaxation. Thus, we expect that in AlAs/GaAs a perturbative expansion of the Raman activity in terms of chemical composition to be rapidly convergent. Therefore, a model is developed by expanding the dielectric susceptibility in terms of the difference between the

actual structure for a given composition and that of the "virtual" crystal, where only fictitious cations $X \equiv (Al_{0.5}Ga_{0.5})$ are present.

The various situations corresponding to SL's or to any other possible configuration of the system may be described by specifying the atomic species which occupies each given cationic site. Each configuration is described by a set of Ising-like variables $\{\sigma_L\}$ associated to the cationic sites of the L-th unit cell of the corresponding virtual crystal. The σ_L are defined in such a way that $\sigma_L = 0$ corresponds to the "virtual" cation $(Ga_{0.5}Al_{0.5})$ and the values $\sigma_L = 1$ and $\sigma_L = -1$ correspond to the Ga and the Al atom respectively. The bare pseudopotential of the cation sitting on lattice position R_L is given by:

$$V^C(\mathbf{r}, \sigma_L) = V^C_{\rm virt}(\mathbf{r} - \mathbf{R}_L) + \sigma_L \, \Delta V(\mathbf{r} - \mathbf{R}_L) \ , \tag{4.9}$$

where

$$\begin{aligned} V^C_{\rm virt}(\mathbf{r} - \mathbf{R}_L) &= \frac{1}{2}\left(V_{Ga}(\mathbf{r} - \mathbf{R}_L) + V_{Al}(\mathbf{r} - \mathbf{R}_L)\right) \\ \Delta V(\mathbf{r} - \mathbf{R}_L) &= \frac{1}{2}\left(V_{Ga}(\mathbf{r} - \mathbf{R}_L) - V_{Al}(\mathbf{r} - \mathbf{R}_L)\right) \ . \end{aligned} \tag{4.10}$$

Hence, for a given underlying structure the dielectric susceptibility may be considered a function of the set of atomic displacements and of the composition variables:

$$\chi = \chi(\{u^s_\gamma(L)\}, \{\sigma_L\}) \ . \tag{4.11}$$

As we have shown in the previous section, in first-order Raman scattering the relevant quantity is the linear variation of χ with the displacements $u^s_\gamma(L)$:

$$\Delta\chi^{(1)}_{\alpha\beta} = \sum_{L,s,\gamma} \frac{\partial\chi_{\alpha\beta}}{\partial u^s_\gamma(L)} \, u^s_\gamma(L) \ . \tag{4.12}$$

The derivatives with respect to the atomic displacements may be expanded in terms of the composition variables σ_L:

$$\frac{\partial\chi_{\alpha\beta}}{\partial u^s_\gamma(L)} = \widetilde{\mathcal{P}}^s_{\alpha\beta\gamma} + \sum_{L'} \mathcal{T}^s_{\alpha\beta\gamma}(\mathbf{R}_L, \mathbf{R}_{L'}) \, \sigma_{L'} + \mathcal{O}(\sigma^2) \ . \tag{4.13}$$

where $\widetilde{\mathcal{P}}^s_{\alpha\beta\gamma}$ is the Raman tensor of the virtual crystal, and

$$\mathcal{T}^s_{\alpha\beta\gamma}(\mathbf{R}_L, \mathbf{R}_{L'}) \equiv \left. \frac{\partial^2 \chi_{\alpha\beta}}{\partial u^s_\gamma(L) \partial \sigma_{L'}} \right|_{\sigma=0} . \tag{4.14}$$

The indexes L and L' label the unit cells of the virtual crystal: due to the periodicity of the lattice in this case, one obtains:

$$\mathcal{T}^s_{\alpha\beta\gamma}(\mathbf{R}_L, \mathbf{R}_{L'}) = \mathcal{T}^s_{\alpha\beta\gamma}(\mathbf{R}_L - \mathbf{R}_{L'}, 0) \equiv \mathcal{T}_{\alpha\beta\gamma}(\mathbf{R}^s_L - \mathbf{R}_{L'}) . \tag{4.15}$$

The above equations allow us to rewrite Eq. (4.12) to first-order in σ in the following form:

$$\Delta\chi^{(1)}_{\alpha\beta} = \sum_{L,s,\gamma} \widetilde{\mathcal{P}}^s_{\alpha\beta\gamma} u^s_\gamma(L) + \sum_{L',\gamma,k} \sigma_{L'} \left[\sum_{\mathbf{R} \in n^k(L')} \mathcal{T}_{\alpha\beta\gamma}(\mathbf{R}) u_\gamma(\mathbf{R}) \right] + \mathcal{O}(\sigma^2) , \tag{4.16}$$

where $n^k(L')$ is the set of all the neighbours of the cation in $\mathbf{R}_{L'}$ of order k. In fact, the perturbative approach so far described is useful to practical purposes if only the linear order in σ has to be retained in the expansion in Eq. (4.16) to achieve the desired accuracy. Such assumption of linearity should be checked for the systems we are considering. Furthermore, the same considerations suggest that the applicability of the methods relies on the possibility of truncating the sum over the shells of neighbours in Eq. (4.16) to some limit value k_{max}, or alternatively of fitting to a known analytic expression, which should depend on very few parameters, the terms with $k > k_{max}$.

The dielectric susceptibility of a crystal remains obviously unchanged if all the atoms are displaced by the same amount. This must be true at any order in the σ variables. As a consequence of that we obtain relations which reduce the number of independent components of $\widetilde{\mathcal{P}}^s_{\alpha\beta\gamma}$ and $\mathcal{T}_{\alpha\beta\gamma}(\mathbf{R})$. To the zeroth-order in σ the following relation must hold:

$$\sum_s \widetilde{\mathcal{P}}^s_{\alpha\beta\gamma} = 0 . \tag{4.17}$$

The relation we obtain for the first-order is:

$$\sum_{L',k} \sigma_{L'} \left[\sum_{\mathbf{R} \in n^k(L')} \mathcal{T}_{\alpha\beta\gamma}(\mathbf{R}) \right] = 0 \ , \tag{4.18}$$

this condition must be true for any choice of the $\{\sigma_{L'}\}$, therefore

$$\sum_{k=0}^{\infty} \sum_{\mathbf{R} \in n^k(0)} \mathcal{T}_{\alpha\beta\gamma}(\mathbf{R}) = 0 \ . \tag{4.19}$$

The independent components of the tensors $\widetilde{\mathcal{P}}$ and $\mathcal{T}$ may be deduced using standard group theoretical methods.[64,65] The quantities $\widetilde{\mathcal{P}}^s_{\alpha\beta\gamma}$ transform as a third-rank tensor (symmetric in the indexes α, β) in the point group of the zincblende, (T_d). Then it follows[65] that the general reducible representation $D(\widetilde{\mathcal{P}}) = D(\boldsymbol{\chi}) \otimes D(\boldsymbol{u})$ can be decomposed within the group T_d in the following form:

$$D(\widetilde{\mathcal{P}}) = (D_2^+ + D_0^+) \otimes D_1^- \Rightarrow \Gamma_1 + \Gamma_3 + 2\Gamma_4 + 3\Gamma_5 \ . \tag{4.20}$$

where $(D_2^+ + D_0^+)$ and D_1^- are representations in the group of rotations in the three-dimensional space of a symmetric second-rank tensor, $(\boldsymbol{\chi})$, and of a polar vector, $(\boldsymbol{u})$, respectively. The number of independent components of the tensor $\widetilde{\mathcal{P}}$ is equal to the number of times that the identity representation Γ_1 occurs in the reduction of representation $D(\widetilde{\mathcal{P}})$.[64] Thus, we have in this case only one independent component. Without entering into further details the final expression we achieve is:

$$\widetilde{\mathcal{P}}^s_{\alpha\beta\gamma} = \widetilde{P}\,(-)^s |\epsilon_{\alpha\beta\gamma}| \ . \tag{4.21}$$

The same symmetry arguments we have exposed here have been used to derive Eq. (4.5). Analogous symmetry properties hold for the tensor $\mathcal{T}_{\alpha\beta\gamma}(\mathbf{R} = 0) \equiv \mathcal{T}^C_{\alpha\beta\gamma}$:

$$\mathcal{T}^C_{\alpha\beta\gamma} = c\,|\epsilon_{\alpha\beta\gamma}| \ . \tag{4.22}$$

The symmetry analysis of the tensor $\mathcal{T}_{\alpha\beta\gamma}(\mathbf{R})$ in the other cases is more complicated, but formal results may still be obtained with the above procedure. As an illustrative and important example we report in Table VIII the explicit form of the tensor $\mathcal{T}^{A}_{\alpha\beta\gamma}(i)$, where i labels the nearest-neighbour anions to the cation at $\mathbf{R} = 0$. In this particular case only 4 independent components, c_k $(k = 1, \ldots, 4)$, have been found.

Let us now examine the contribution to $\Delta\chi^{(1)}_{\alpha\beta}$ of order σ, which contains derivatives of the susceptibility to perturbations localized at two sites $\mathbf{R}^s_L$ and $\mathbf{R}_{L'}$ of the lattice:

$$\mathcal{T}_{\alpha\beta\gamma}(\mathbf{R}^s_L - \mathbf{R}_{L'}) = \frac{\partial^2 \chi_{\alpha\beta}}{\partial u^s_\gamma(L)\partial\sigma_{L'}} \ . \tag{4.23}$$

In the case of AlGaAs, the electronic response of the virtual crystal to a ionic substitution is almost entirely contained in the Wigner-Seitz cell.[66] On the other hand, due to long range Coulomb interactions, the perturbation caused by a displacement of an atom in a polar system, such as that we are interested in, is surely not short range. However, for non polar systems contributions as in Eq. (4.23) should quickly decrease with increasing distance $\mathbf{R}^s_L - \mathbf{R}_{L'}$.

The extent to which such terms cannot be considered negligible in non polar systems has been checked via the ab-initio calculation of the derivatives of the susceptibility in fictitious SL's formed by virtual atoms ($Si_{0.5}Ge_{0.5}$). We have considered (001) SL's with 4 (2-2 SL's) and 8 (4-4 SL's) atoms in the unit cell. The lattice parameter of the underlying diamond structure has been taken as that of the (Si-Ge) virtual crystal: $a_{\rm virt} = 10.40$ (a.u.). In order to extract linear and quadratic contribution in σ to the Raman tensor, we calculated the derivatives of the polarizability with respect to atomic displacements in SL's in which we have placed at the origin a Si atom ($\sigma = -1$) or a Ge atom ($\sigma = 1$). The results

TABLE VIII. Explicit form of the tensor $\mathcal{T}^A(\mathbf{r})$ for $\mathbf{r}$ belonging to the nearest neighbours of the site at $\mathbf{R}=0$.

$\mathcal{T}^A(-1,\ 1,\ 1)$

$(\alpha\beta x)$	$(\alpha\beta y)$	$(\alpha\beta z)$
$\begin{pmatrix} c_1 & c_4 & c_4 \\ & c_2 & c_3 \\ & & c_2 \end{pmatrix}$	$\begin{pmatrix} -c_2 & -c_4 & c_3 \\ & -c_1 & c_4 \\ & & -c_2 \end{pmatrix}$	$\begin{pmatrix} -c_2 & c_3 & -c_4 \\ & -c_2 & c_4 \\ & & -c_1 \end{pmatrix}$

$\mathcal{T}^A(-1,-1,-1)$

$(\alpha\beta x)$	$(\alpha\beta y)$	$(\alpha\beta z)$
$\begin{pmatrix} c_1 & -c_4 & -c_4 \\ & c_2 & c_3 \\ & & c_2 \end{pmatrix}$	$\begin{pmatrix} c_2 & -c_4 & c_3 \\ & c_1 & -c_4 \\ & & c_2 \end{pmatrix}$	$\begin{pmatrix} c_2 & c_3 & -c_4 \\ & c_2 & -c_4 \\ & & c_1 \end{pmatrix}$

$\mathcal{T}^A(\ 1,\ 1,-1)$

$(\alpha\beta x)$	$(\alpha\beta y)$	$(\alpha\beta z)$
$\begin{pmatrix} -c_1 & c_4 & -c_4 \\ & -c_2 & c_3 \\ & & -c_2 \end{pmatrix}$	$\begin{pmatrix} -c_2 & c_4 & c_3 \\ & -c_1 & -c_4 \\ & & -c_2 \end{pmatrix}$	$\begin{pmatrix} c_2 & c_3 & c_4 \\ & c_2 & c_4 \\ & & c_1 \end{pmatrix}$

$\mathcal{T}^A(\ 1,-1,\ 1)$

$(\alpha\beta x)$	$(\alpha\beta y)$	$(\alpha\beta z)$
$\begin{pmatrix} -c_1 & -c_4 & c_4 \\ & -c_2 & c_3 \\ & & -c_2 \end{pmatrix}$	$\begin{pmatrix} c_2 & c_4 & c_3 \\ & c_1 & c_4 \\ & & c_2 \end{pmatrix}$	$\begin{pmatrix} -c_2 & c_3 & c_4 \\ & -c_2 & -c_4 \\ & & -c_1 \end{pmatrix}$

of this calculation are shown in Table VIII. They confirm the linearity in σ for such structures. Furthermore, it can be seen that "effective" interactions in the direction (001) extend their range up to the third neighbours.

A check of the linearity in σ for polar structures has also been done in $(Al_{\frac{1}{2}(1+\sigma)}Ga_{\frac{1}{2}(1-\sigma)})As(Al_{\frac{1}{2}(1-\sigma)}Ga_{\frac{1}{2}(1+\sigma)})As$ superlattices along the 001 direction, which are grown in the zincblende structure with lattice parameter $a_0 = 10.605$ (a.u.). The calculated values of $\partial\chi_{xy}/\partial u_z(X)$, where the atom X is $(Al_{\frac{1}{2}(1+\sigma)}Ga_{\frac{1}{2}(1-\sigma)})$, have been reported in Fig. 4.2. Also in this case quadratic contributions are fairly small. Thus, we may argue that the assumption of linearity in these systems is well verified.

In polar materials, due to dipolar interactions associated with non vanishing effective charges, the $\mathcal{T}_{\alpha\beta\gamma}(\mathbf{R})$ defined in Eq. (4.23) are not short range. However, the other contribution to $\mathcal{T}_{\alpha\beta\gamma}(\mathbf{R})$ vanishes more quickly than the dipolar ones with increasing $|\mathbf{R}|$. Therefore, the asymptotic expression of $\mathcal{T}_{\alpha\beta\gamma}(\mathbf{R}_i - \mathbf{R}_L)$ at long distances (i.e. for large $|\mathbf{R}_i - \mathbf{R}_L|$) can be explicitly written as:

$$\mathcal{T}_{\alpha\beta\gamma}(\mathbf{R}_i - \mathbf{R}_L) = \frac{\partial^2 \chi_{\alpha\beta}}{\partial u^i_\gamma \partial \sigma_L} = \sum_\tau \frac{\partial^2 \chi_{\alpha\beta}}{\partial E_\tau \partial \sigma_L} \frac{\partial E^i_\tau(L)}{\partial u^i_\gamma} \ , \tag{4.24}$$

where $\mathbf{E}^i(L)$ is the electric field generated by the dipole $\mathbf{p}_i = \mathbf{Z}^*_i \boldsymbol{u}^i$ calculated at the site L:

$$\mathbf{E}(\mathbf{p}_i, L) = \frac{1}{\widetilde{R}_i^5} \left[3(\mathbf{p}_i \cdot \widetilde{\mathbf{R}}_i)\, \widetilde{\mathbf{R}}_i - \widetilde{R}_i^2\, \mathbf{p}_i \right] \ , \tag{4.25}$$

with $\widetilde{\mathbf{R}}_i = \mathbf{R}_i - \mathbf{R}_L$.

Thus, in polar materials we can separate the long range "Coulomb" contributions from "effective" short range interactions, in a way which is similar to that used for the force constants in Section 4.1:

$$\mathcal{T}_{\alpha\beta\gamma}(\mathbf{R}) = \mathcal{T}^{\text{short}}_{\alpha\beta\gamma}(\mathbf{R}) + \mathcal{T}^{\text{long}}_{\alpha\beta\gamma}(\mathbf{R}) \ , \tag{4.26}$$

TABLE IX. Calculated values of $\partial\chi_{xy}/\partial u_z(X_i)$, where $(i{=}0,n)$ for 2-2 $(n{=}2)$ and 4-4 $(n{=}4)$ SL's. Atom X_0 is Si or Ge as specified, atoms X_i $(i{=}1,n)$ are "virtual" atoms ($Si_{0.5}Ge_{0.5}$). The linear and the quadratic components in σ are also reported. The reported values are expressed in units $10^{-2}\, a^2_{virt}$.

SL 2-2	$X_0 = $ Si	$X_0 = $ Ge	σ	σ^2
0	113.1	127.2	7.1	-0.4
1	-111.6	-129.3	-8.9	0.1
2	110.2	131.8	10.8	0.5

SL 4-4	$X_0 = $ Si	$X_0 = $ Ge	σ	σ^2
0	113.0	126.3	6.7	-0.9
1	-113.5	-125.9	-6.2	0.8
2	114.4	125.0	5.3	-0.8
3	-116.2	-122.5	-3.2	1.2
4	119.2	120.1	0.9	-0.9

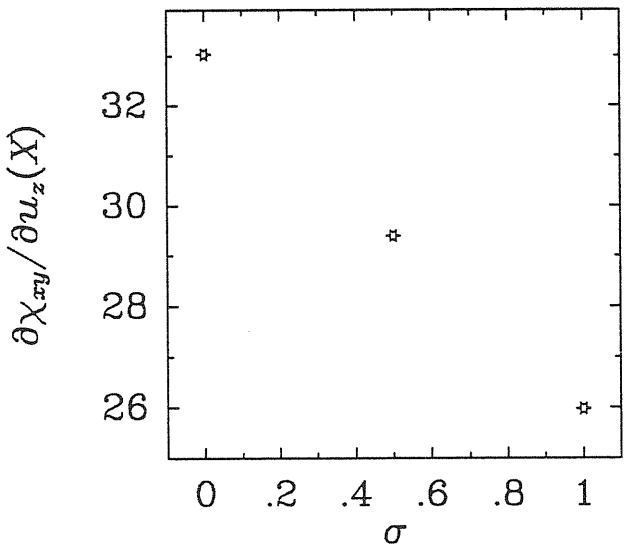

Figure 4.2. Test of linearity of the calculated values of $\partial\chi_{xy}/\partial u_z(X)$, where $X \equiv (Al_{\frac{1}{2}(1+\sigma)}Ga_{\frac{1}{2}(1-\sigma)})$ in superlattices $(Al_{\frac{1}{2}(1+\sigma)}Ga_{\frac{1}{2}(1-\sigma)})As(Al_{\frac{1}{2}(1-\sigma)}Ga_{\frac{1}{2}(1+\sigma)})As$ along the (001) direction. The reported values are expressed in units $10^{-2}\, a_0^2$.

where the term $\mathcal{T}^{\text{long}}_{\alpha\beta\gamma}(\mathbf{R})$ is entirely due to electric field effects. From a chemical point of view, GaAs and AlAs are much more similar than Si and Ge, as we have seen in the previous section for the transferability of the force constants. Assuming that in AlAs/GaAs systems $\mathcal{T}^{\text{short}}_{\alpha\beta\gamma}(\mathbf{R})$ extends its range only up to the first neighbours, and including the Coulomb part for $\mathbf{R}$ up to the nearest neighbours of the site at $\mathbf{R} = 0$ in the short range term, we have:

$$\mathcal{T}_{\alpha\beta\gamma}(\mathbf{R}) = \begin{cases} \mathcal{T}^{\text{short}}_{\alpha\beta\gamma}(\mathbf{R}) & \text{for } \mathbf{R} \in n^k(0) \text{ with } k \leq 1 \\ \mathcal{T}^{\text{long}}_{\alpha\beta\gamma}(\mathbf{R}) & \text{otherwise .} \end{cases} \tag{4.27}$$

An explicit expression for $\mathcal{T}^{\text{long}}_{\alpha\beta\gamma}(\mathbf{R})$ together with a general explicit analysis of the various effects of electric fields in polar material will be described in the following subsection.

4.4.1 Role of electric fields in polar systems

As has been already pointed out, in a polar system the displacement of an atom creates an electric dipole proportional to the displacement. The presence of such long range interactions has to be taken into account both for the macroscopic and microscopic (or "local") effects they have.

In fact, in polar materials the dielectric susceptibility depends on the macroscopic electric field $\mathbf{E}$ generated by the displacements:

$$\chi^E = \chi\left(\{u^s_\gamma(L)\}, \{\sigma_L\}, \mathbf{E}\left(\{u^s_\gamma(L)\}\right)\right) . \tag{4.28}$$

In such a case the term of the polarizability which is linear in the displacements should be rewritten:

$$\frac{\partial \chi^E_{\alpha\beta}}{\partial u^s_\gamma} = \left.\frac{\partial \chi^E_{\alpha\beta}}{\partial u^s_\gamma}\right|_{\mathbf{E}=0} + \sum_\tau \mathcal{B}^s_{\alpha\beta\gamma\tau} E_\tau , \tag{4.29}$$

where we have introduced the "hyperpolarizability":

$$\mathcal{B}^s_{\alpha\beta\gamma\tau} = \left.\frac{\partial^2 \chi^E_{\alpha\beta}}{\partial E_\tau \partial u^s_\gamma}\right|_{\mathbf{E}=0} . \tag{4.30}$$

As has already been mentioned, electric boundary conditions (EBC) determine the macroscopic electric field. In any supercell ab-initio calculations periodic boundary conditions are imposed. In this case, which implicitly corresponds to zero EBC, we have $\mathbf{E} = 0$. As we have seen in Chapter 1, only transverse phonons may be completely described in this case. Thus, a supercell geometry does not allow the calculation of the hyperpolarizability $\mathcal{B}^s_{\alpha\beta\gamma\tau}$, which should be analyzed and fitted separately to the available experimental data. However, our present purpose is to obtain and test a model based on first-principles calculations. Therefore, in the following we always assume the condition of vanishing macroscopic electric field.

Local electric fields, which are not negligible even at $\mathbf{E} = 0$, are responsible for the long range interactions in Eq. (4.24). If they are explicitly taken into account, the long range part of the linear term in the expansion of $\Delta\chi_{\alpha\beta}$ is given by:

$$\Delta\chi^{(E)}_{\alpha\beta} = \sum_{L,\tau} \sigma_L \left.\frac{\partial^2 \chi_{\alpha\beta}}{\partial E_\tau \partial \sigma_0}\right|_{\sigma=0} \left[\sum_\gamma \sum_{i \notin \mathcal{N}(L)} \left.\frac{\partial E^i_\tau(L)}{\partial u^i_\gamma}\right|_{\sigma=0} u^i_\gamma \right] . \tag{4.31}$$

where $\mathcal{N}(L) \equiv n^0(L) \cup n^1(L)$. It may be easily recognized that the expression in square brackets in Eq. (4.31) coincides with the component τ of the "local" electric field $\mathbf{E}^{\rm loc}(L)$ generated by an array of dipoles localized on all the sites of the lattice except those which fall into the range of the nearest neighbours of the site L. Usual methods of electrostatics allow us to calculate the local field[67]:

$$\mathbf{E}^{\rm loc}(L) = \mathbf{E}^{\rm loc}_{\rm in}(L) + \mathbf{E} + \frac{4}{3}\pi\mathbf{P} , \tag{4.32}$$

where $\mathbf{P}$ is the polarization density:

$$\mathbf{P} = \frac{1}{\Omega_M} \sum_{s \in \mathcal{U}_M} \mathbf{p}^s , \tag{4.33}$$

$\mathcal{U}_M$ being the set of the M atoms in unit cell of the structure we are considering and Ω_M the corresponding volume. $\mathbf{E}$ is the macroscopic electric field which is identically zero if, as in our case, periodic boundary conditions (PBC) are imposed. Finally, $\mathbf{E}_{\rm in}^{\rm loc}(L)$ is the microscopic local field appropriate to a spherical region $\mathcal{S}(L)$ whose center is taken to be on the site L on which the field acts. Obviously, in our case sites within the nearest neighbours distance are not contained in $\mathcal{S}(L)$. The final expression for the local field reads:

$$\mathbf{E}^{\rm loc} = \sum_{s\in\mathcal{U}_M} \boldsymbol{W}^s(L)\,\mathbf{p}^s \ , \tag{4.34}$$

where the tensor $\boldsymbol{W}^s$ is defined by:

$$W^s_{\alpha\beta}(L) = \frac{4}{3}\frac{\pi}{\Omega_M}\delta_{\alpha\beta} + \sum_{i\in\mathcal{S}(s,L)} \frac{1}{\widetilde{R}_i^5}[3\widetilde{R}_{i\alpha}\widetilde{R}_{i\beta} - \widetilde{R}_i^2\delta_{\alpha\beta}] \ , \tag{4.35}$$

$\mathcal{S}(s,L)$ being the set of the equivalent sites of type s which belong to $\mathcal{S}(L)$. Finally, we obtain the following expression for the long range contribution to the variation of the susceptibility.

$$\Delta\chi^{(E)}_{\alpha\beta} = \sum_{L,\tau}\sigma_L \left.\frac{\partial^2\chi_{\alpha\beta}}{\partial E_\tau \partial\sigma_0}\right|_{\sigma=0} \sum_{s\in\mathcal{U}_M}\sum_{\gamma} W^s_{\tau\gamma}(L)\,p^s_\gamma \ , \tag{4.36}$$

where

$$p^s_\gamma = Z^*_s u^s_\gamma \qquad\qquad Z^*_s = Z^*(-)^{\kappa(s)} \ , \tag{4.37}$$

with

$$\kappa(s) = \begin{cases} 1 & \text{for} \quad s \equiv \text{anion} \\ 2 & \text{for} \quad s \equiv \text{cation} \ . \end{cases} \tag{4.38}$$

The symmetry analysis of the derivatives appearing in Eq. (4.36) gives us:

$$Z^* V \left.\frac{\partial^2\chi_{\alpha\beta}}{\partial E_\tau \partial\sigma_0}\right|_{\sigma=0} = q\,|\epsilon_{\alpha\beta\gamma}| \ . \tag{4.39}$$

4.5 Applications to some $(AlAs)_n(GaAs)_n$ superlattices

We applied the model described in the previous section to (001) $(AlAs)_n(GaAs)_n$ superlattices with $n = 1, 2$. A schematic representation of these two SL's is reported in Fig 4.3.

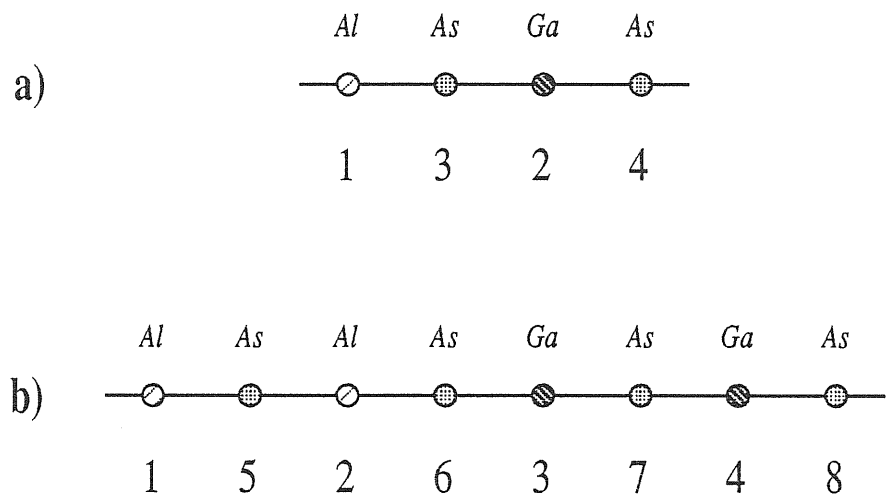

Figure 4.3. Schematic representation of the SL's we have studied. a) SL (1-1); b) SL (2-2). Notice that atoms in real structures are not aligned.

We have then calculated the variation of the polarizability χ with respect to the displacement of one of the atoms in the unit cell of the superlattice. The magnitude of the displacements has been chosen to be equal to $u = \pm 2 \times 10^{-4}\, a$, where $a = 10.605$ (a.u.) is the lattice parameter of the corresponding zincblende structure. The obtained values of the component of the first-order Raman tensor are shown in Table X.

For an (n-n) superlattice Eq. (4.36) may be expressed in the form:

$$\Delta\chi^E_{\alpha\beta} = \frac{q}{2n\Omega} \sum_{\tau\gamma} |\epsilon_{\alpha\beta\gamma}| \sum_{s \in \mathcal{U}_{AI}} (-)^{\kappa(s)}\, V^s_{\tau\gamma}\, u^s_\gamma \tag{4.40}$$

TABLE X. Calculated ab-initio values of the components of the first-order Raman tensor. Atoms are labelled as in Fig. 4.3. The reported values are expressed in units $10^{-2}a^2$.

SL 1-1	(xy,z)	(xz,y)	(yz,y)
Al(1)	25.98	25.14	
Ga(2)	40.16	45.90	
As(3)	-33.07	-35.52	-20.32

SL 2-2	(xy,z)	(xz,y)	(yz,y)
Al(1)	20.22	27.20	
Ga(3)	47.67	41.69	
As(5)	-18.60	-30.32	
As(6)	-31.49	-35.00	-22.27
As(7)	-54.19	-37.46	

where we have defined:

$$V^s_{\tau\gamma} = \sum_{i \in \mathcal{U}^C_M} \sigma_i \, W^s_{\tau\gamma}(i) \tag{4.41}$$

where the sum is limited to the cations in the unit cell. By symmetry reasons the only independent components $V^s_{\tau\gamma}$ we have found for (1-1) SL's are:

$$V^1_{xx} = -\alpha \qquad V^3_{xy} = -2\beta \ , \tag{4.42}$$

and for (2-2) SL's:

$$V^1_{xx} = -\gamma \qquad V^5_{xx} = -\delta \qquad V^6_{xy} = -\lambda \ , \tag{4.43}$$

the upper index labels atoms as in Fig. 4.3. Let us define the quantity $\Delta_{ij,k}$ as the variation of $\Delta\chi^E_{ij}$ due to displacements along the k-axis. The independent

components of the tensor $\Delta_{ij,k}$ we have obtained in the case of (1-1) SL's are:

$$\begin{aligned}
\Delta_{xy,z} &= \frac{q}{2\Omega}(-2\alpha)\,[u_z^2 - u_z^1] \\
\Delta_{xz,y} &= \frac{q}{2\Omega}\,\alpha\,[u_y^2 - u_y^1] \\
\Delta_{xz,z} &= \frac{q}{2\Omega}(-2\beta)\,[u_x^4 - u_x^3]\ ,
\end{aligned} \tag{4.44}$$

and for (2-2) SL's:

$$\begin{aligned}
\Delta_{xy,z} &= -\frac{q}{4\Omega}\left\{2\gamma\,[u_z^3 + u_z^4 - u_z^1 - u_z^2] + \delta\,[u_z^5 - u_z^7]\right\} \\
\Delta_{xz,y} &= \frac{q}{4\Omega}\left\{\gamma\,[u_y^3 + u_y^4 - u_y^1 - u_y^2] + \delta\,[u_y^5 - u_y^7]\right\} \\
\Delta_{yz,y} &= \frac{q}{4\Omega}\,\lambda\,[u_y^6 - u_y^8]\ .
\end{aligned} \tag{4.45}$$

Retaining short range interaction in Eq. (4.23) up to the first neighbours only, we obtain a model which is described by the following list of parameters:

$$\widetilde{P},\ c,\ c_1,\ c_2,\ c_3,\ c_4,\ q\ . \tag{4.46}$$

On the other hand, due to the condition (4.19) we have

$$-4c_3 = c\ . \tag{4.47}$$

Therefore, only 6 parameters $(\widetilde{P}, c, c_1, c_2, c_4, q)$ appears in our model. The parametrized expression of the components of the Raman tensor is given in Table XI. The Raman cross section in Eq. (4.2) can be expressed in terms of the so-called Raman activity, defined by

$$\mathcal{A}_{\tau\mu}^{\nu} = \frac{\partial \chi_{\tau\mu}}{\partial \xi_\nu}\ . \tag{4.48}$$

where ξ_ν is the normal coordinate of the mode ν. Hence, we apply our model to the calculation of $\mathcal{A}_{xy}$ in the case of the Ga- and Al-like $B2$ modes in (2-2) SL's.

TABLE XI. Parametrization of the first-order Raman tensor for (1-1) and (2-2) superlattices. Atoms are labelled as in Fig. 4.3.

SL 1-1	(xy,z)	(xz,y)	(yz,y)
Al(1)	$\widetilde{P}-c+2\alpha q$	$\widetilde{P}-c-\alpha q$	
Ga(2)	$\widetilde{P}+c-2\alpha q$	$\widetilde{P}+c+\alpha q$	
As(3)	$-\widetilde{P}$	$-\widetilde{P}$	$-4c_4$
As(4)	$-\widetilde{P}$	$-\widetilde{P}$	$4c_4$

SL 2-2	(xy,z)	(xz,y)	(yz,y)
Al(1)	$\widetilde{P}-c+2\gamma q$	$\widetilde{P}-c-\gamma q$	
Al(2)	$\widetilde{P}-c+2\gamma q$	$\widetilde{P}-c-\gamma q$	
Ga(3)	$\widetilde{P}+c-2\gamma q$	$\widetilde{P}+c+\gamma q$	
Ga(4)	$\widetilde{P}+c-2\gamma q$	$\widetilde{P}+c+\gamma q$	
As(5)	$-\widetilde{P}+c-2\delta q$	$-\widetilde{P}+c+\delta q$	
As(6)	$-\widetilde{P}$	$-\widetilde{P}$	$-4c_4+\lambda q$
As(7)	$-\widetilde{P}-c+2\delta q$	$-\widetilde{P}-c-\delta q$	
As(8)	$-\widetilde{P}$	$-\widetilde{P}$	$4c_4-\lambda q$

In this particular case only 4 parameters $(\widetilde{P}, c, c_4, q)$ are involved in the calculation of $\mathcal{A}_{xy}$. A fitting procedure of the expression in Table XI has been used to extract, from the ab-initio calculation of Table X, the values of the parameters reported in Table XII. The corresponding values of the component of the Raman tensor are shown in Table XIII. Finally, the obtained results for the Raman activity are displayed in Table XIV and compared with those of full ab-initio calculations. The

TABLE XII. (a) Values of the calculated independent components of $V^s_{\tau\gamma}$. (b) Parameters obtained from the fit of the ab-initio values in Table X, the units are the same as in Table X.

(a)	
α	8.68
β	3.39
γ	12.85
δ	16.68
λ	7.93

(b)	
$\widetilde{P}$	34.68
c	9.52
c_4	5.03
q	-0.16

agreement is good also in this case.

TABLE XIII. Components of the first-order Raman tensor derived from the expression in Table XI using the parameters reported in Table XII. Atoms are labelled as in Fig. 4.3. The reported values are expressed in units $10^{-2}a^2$.

SL 1-1	(xy,z)	(xz,y)	(yz,y)
Al(1)	22.38	26.55	
Ga(2)	46.98	42.81	
As(3)	-34.68	-34.68	-20.12

SL 2-2	(xy,z)	(xz,y)	(yz,y)
Al(1)	21.05	27.22	
Ga(3)	48.31	42.14	
As(5)	-19.82	-27.83	
As(6)	-34.68	-34.68	-18.85
As(7)	-49.53	-41.53	

TABLE XIV. Comparison between the Raman activity of the Ga- and Al-like $B2$ modes in (2-2) SL's, calculated from first principles and from our model.

	$\mathcal{A}_{xy}^{(ab-initio)} \times 10^{-2}$	$\mathcal{A}_{xy}^{(fitted)} \times 10^{-2}$
Ga-like	-23.4	-24.7
Al-like	35.6	35.3

Conclusions

In this thesis we have shown that the accurate calculation of lattice dynamical properties of semiconductors is by now well within the scope of computational methods based on density-functional theory.

The phonon dispersions of diamond and several pure bulk semiconductors have been calculated within the framework of the Density Functional Perturbation Theory. The results so obtained compare very favorably with experiments. In fact, when experimental informations are missing or are not reliable, ab-initio calculations represent the only realistic approach. The predictive power of first-principles methods in describing harmonic lattice dynamics has been also tested in determining the eigenvectors of the dynamical matrix as well as the internal strain parameters in diamond and some pure bulk semiconductors. The agreement with the available experiments is always remarkable.

Accurate thermal expansion coefficients in pure semiconductors have been also calculated. Our results are able to reproduce even fine details of several sets of experimental data.

Thus, we can conclude that theoretical calculations are able to provide an unbiased and very reliable picture of the vibrational properties of semiconductors, provided that they are carried out by accurate first-principles techniques. When such techniques are no longer applicable, namely if the system becomes very large,

one has to devise methods which provide an accuracy similar to the one of ab-initio calculations.

In this context the concept of *interatomic* force constants is very useful not only for interpolating vibrational properties throughout the Brillouin zone, but also for using the information gained in simple systems (such as elemental or binary semiconductors) in rather complex ones, such as alloys and quantum structures: this is feasible in a straightforward way in the case of pseudobinary systems presenting different cationic species, and, to a minor extent, for Si/Ge. The case of pseudobinary systems with different anions may require some semiempirical adjustment of the force constants, in order to achieve a comparable accuracy.

Applications of these ideas to GaAs/AlAs systems have been presented. We have shown that within the so-called *mass approximations* phonon frequencies can be obtained in such systems within an accuracy comparable to that of full ab-initio calculation. Furthermore, we devised a model for Raman spectroscopy which, allowing to take into account the difference in the atomic polarizabilities of each cationic species, can reasonably predict relative Raman intensities in GaAs/AlAs mixed semiconductors.

Appendix A

Ewald energy

The ion-ion term in the expression of the total energy of a system of electrons and ions may be easily calculated in the form:

$$\begin{aligned}\mathcal{E}_{Ewald} = \frac{4\pi N}{\Omega}\frac{e^2}{2}\left(\sum_{\mathbf{G}\neq 0}\frac{\mathrm{e}^{-\mathrm{G}^2/4\eta}}{\mathrm{G}^2}\left|\sum_l Z_l \mathrm{e}^{i\mathbf{G}\cdot\boldsymbol{\tau}_l}\right|^2 - \frac{1}{2\eta}\left(\sum_l Z_l\right)^2\right) + \\ + \frac{Ne^2}{2}\sum_{l,m}\sum_{\mathbf{R}}\frac{Z_l Z_m}{|\boldsymbol{\tau}_l - \boldsymbol{\tau}_m - \mathbf{R}|}\Big(1 - \mathrm{erf}(\sqrt{\eta}|\boldsymbol{\tau}_l - \boldsymbol{\tau}_m - \mathbf{R}|)\Big) \\ - \frac{Ne^2}{2}\sqrt{\frac{2\eta}{\pi}}\sum_l Z_l^2 \ ,\end{aligned}$$

where eZ_i indicates the bare ionic (pseudo)charges for the i-th ion in the cell, and η is a parameter whose arbitrary value can be chosen large enough to allow the neglect of the real space term.

Appendix B

Matrix elements of nonlocal pseudopotentials

The plane-wave matrix elements of the nonlocal pseudopotentials defined in Eq. (1.44) are given by:

$$\langle \mathbf{k}+\mathbf{G}|v_i|\mathbf{k}+\mathbf{G}'\rangle = \widetilde{v}_{i,loc}(\mathbf{G}-\mathbf{G}') + \sum_l \widetilde{v}_{i,l}(\mathbf{k}+\mathbf{G},\mathbf{k}+\mathbf{G}') \ ,$$

where:

$$\widetilde{v}_{i,loc}(\mathbf{G}) = \frac{1}{\Omega}\int v_{i,loc}(r)\, \mathrm{e}^{-i\mathbf{G}\cdot\mathbf{r}}\, \mathrm{d}\mathbf{r} \ ,$$

and

$$\begin{aligned}\widetilde{v}_{i,l}(\mathbf{k}_1,\mathbf{k}_2) &= \frac{1}{\Omega}\int \mathrm{e}^{-i\mathbf{k}_1\cdot\mathbf{r}}\, v_{i,l}(\mathbf{r},\mathbf{r}')\, \mathrm{e}^{i\mathbf{k}_2\cdot\mathbf{r}'}\, \mathrm{d}\mathbf{r}\, \mathrm{d}\mathbf{r}' \\ &= \frac{4\pi}{\Omega}(2l+1)\, P_l(\hat{\mathbf{k}}_1\cdot\hat{\mathbf{k}}_2)\int_0^\infty r^2\, j_l(k_1 r)\, j_l(k_2 r)\, v_{i,l}(r)\, \mathrm{d}\mathbf{r} \ .\end{aligned}$$

The matrix elements of the the linear variation of the external ionic pseudopotential (1.23) upon a lattice distortion of the form:

$$u_{\alpha i}(\mathbf{R}) = u_{\alpha i\mathbf{q}}\, \mathrm{e}^{i\mathbf{q}\cdot\mathbf{R}} \ ,$$

are

$$\begin{aligned}\left\langle \mathbf{k}+\mathbf{q}+\mathbf{G}\left|\frac{\partial V_{ion}}{\partial u_{\alpha i\mathbf{q}}}\right|\mathbf{k}+\mathbf{G}'\right\rangle &= -i(\mathrm{q}_\alpha+\mathrm{G}_\alpha-\mathrm{G}'_\alpha)\, \mathrm{e}^{-i(\mathbf{q}+\mathbf{G}-\mathbf{G}')\cdot\boldsymbol{\tau}_i}\times \\ &\times\left(\widetilde{v}_{i,loc}(\mathbf{q}+\mathbf{G}-\mathbf{G}') + \sum_l \widetilde{v}_{i,l}(\mathbf{k}+\mathbf{q}+\mathbf{G},\mathbf{k}+\mathbf{G}')\right) \ .\end{aligned}$$

The screening contribution to $\partial V_{SCF}/\partial u_{\alpha i\mathbf{q}}$, which is a local potential in DFT, can be advantageously evaluated in real space and transformed back to reciprocal space using the Fast-Fourier Transform. The matrix elements of the second derivative of the electron-ion interaction potential are given by

$$\left\langle \mathbf{k}+\mathbf{G}\left|\frac{\partial^2 V_{ion}}{\partial u_{\alpha i\mathbf{q}=0}\partial u_{\beta i\mathbf{q}=0}}\right|\mathbf{k}+\mathbf{G}'\right\rangle = -(\mathrm{G}_\alpha-\mathrm{G}'_\alpha)(\mathrm{G}_\beta-\mathrm{G}'_\beta)\,\mathrm{e}^{-i(\mathbf{G}-\mathbf{G}')\cdot\boldsymbol{\tau}_i} \times\left(\widetilde{v}_i(\mathbf{G}-\mathbf{G}')+\sum_l \widetilde{v}_{i,l}(\mathbf{k}+\mathbf{G},\mathbf{k}+\mathbf{G}')\right) .$$

Acknowledgements

I spent four years of my life at Sissa. This was a very enjoyable period in which my experience both as a physicist and as a man went beyond any previous expectations. I am so very indebted to so many people that it is impossible to give here an explicit acknowledgement to all of them. Thus I apologize in advance for any omission.

First of all I would like to thank Stefano Baroni who not only introduced me to the research field of this thesis, but who has also patiently encouraged me with his continuous suggestions. Furthermore I wish to thank Paolo Giannozzi and Stefano De Gironcoli. Part of the work presented in this thesis is the result of a fruitful collaboration with them.

When four years ago I came to Trieste for the first time, to start my Ph.D. studies at Sissa, I was sure to find a very good place to pursue my research in physics. However, at the same time I was afraid to find a "cool" atmosphere among the people. Fortunately, I was wrong. The "Sissa way of life", as my old friend Daniele would say, is one of the most pleasant I know. A great part of the merit of creating this nice atmosphere may be attributed to some old friends of mine: Simonetta Abenda, Annarita Bizzarri, Alfio Borzí and Anni Koubek, Virginia De Cicco, Kurt Lechner, Jorge and Clarisa Kohanoff and Daniele Tommasini.

In a strict alphabetic order I have to mention for the frequent friendly dis-

cussions, both scientific and not, all my "Solid State" friends: Marco Bernasconi, Marco Buongiorno Nardelli, Michela Di Stasio, Guido Goldoni, Miklos Gulacsi, Michele Fabrizio, Andrea Ferrante, Vincenzo Fiorentini, José "Pepe" Lorenzana, Giorgio Mazzeo, Roman Martonak, Lucia Reggiani and Pierino Silvestrelli.

Many people shared with me a lot of enjoyable experiences during these four years, among the others: Fabio Bagarello, Enrico Nardi, Marcelo Guzzo and Norma Reggiani.

I am also very grateful to Valeria Bonservizi and Stefano Borgani for the help they gave me in some "dark" period.

Paul Haines merits a honour place in these acknowledgements for his efforts in trying to make acceptable the English of this thesis.

I hope that the friendly atmosphere of these years at Sissa will not be lost. I trust "young people" will preserve it. Among the others I remember Pietro Donatis, Nicola Marzari, Marta Nolasco, Elena, and Prospero "The Great" Simonetti.

Life is not only Sissa, I would like to thank here Irene and Paola who even if not directly involved in my work, deserve special mention for having had made even more enjoyable my stay in Trieste.

And to clarify a mystery I would like to thank Manuela (my old password), who even at long distance gave me strong moral support.

Finally, I owe very special thanks to Anna.

Bibliography

[1] For a recent review, see for instance: W. E. Pickett, Computer Phys. Reports **9**, 115 (1989).

[2] S. Baroni, P. Giannozzi, and A. Testa, Phys. Rev. Lett. **58**, 1861 (1987).

[3] For an independent derivation of the technique exposed in Ref. [2], see also N. E. Zein, Sov. Phys.: Solid State **26**, 1825 (1984). An hybrid linear-response/supercell method for lattice-dynamical calculations has also been developed by D. King-Smith and R. J. Needs, J. Phys.: Condens. Matter **2**, 3431 (1990).

[4] P. Giannozzi, S. de Gironcoli, P. Pavone and S. Baroni, Phys. Rev. B **43**, 7231 (1991).

[5] For a recent review, see for instance: B. Jusserand and M. Cardona, in *Light Scattering in Solids V*, edited by M. Cardona and G. Güntherodt (Springer, Berlin, 1989), p. 49.

[6] See A. Fasolino and E. Molinari, Surf. Sci. **228**, 112 (1990), and references quoted therein.

[7] S. Baroni, P. Giannozzi, and E. Molinari, Phys. Rev. B **41**, 3870 (1990).

[8] D. Strauch, B. Dorner, and K. Karch, in *Proceedings of the Third International Conference on PHONON PHYSICS*, edited by S. Hunklinger, W. Ludwig, and

G. Weiss, (World Scientific Publishing Co, Singapore, 1990), p. 82.

[9] P. W. Sparks and C. A. Swenson, Phys. Rev. **163**, 779 (1967); and H. Ibach, Phys. Status Solidi **31**, 625 (1969).

[10] T. F. Smith and G. K. White, J. Phys. C: Solid State Phys. **8**, 2031 (1975); and G. A. Slack and S. F. Bartram, J. Apll. Phys. **46**, 89 (1975).

[11] S. Biernacki and M. Scheffler, Phys. Rev. Lett. **63**, 290 (1989).

[12] A. Fleszar and X. Gonze, Phys. Rev. Lett. **64**, 2961 (1990).

[13] C. H. Xu, C. Z. Wang, C. T. Chan, and K. M. Ho, Phys. Rev. B **43**, 5024 (1991).

[14] S. Baroni, S. de Gironcoli, and P. Giannozzi, Phys. Rev. Lett. **65**, 84 (1990).

[15] N. Meskini and K. Kunc, Université P. et M. Curie, Technical Report n. 5 (1978), unpublished.

[16] H. Böttger, *Principles of the Theory of Lattice Dynamics*, Akademie-Verlag Berlin (1983).

[17] P.D. De Cicco and F.A. Johnson, Proc. R. Soc. London Ser. A **310**, 111 (1969).

[18] R. Pick, M.H. Cohen and R.M. Martin, Phys. Rev B **1**, 910 (1970).

[19] H. Hellmann, *Einführung in die Quantenchemie* (Deuticke, Leipzig, 1937); R.P. Feynman, Phys. Rev. **56**, 340 (1939).

[20] X. Gonze and J.P. Vigneron, Phys. Rev. B **39**, 13120 (1989).

[21] P. Hohemberg and W. Kohn, Phys. Rev. **136**, B864 (1964).

[22] W. Kohn and L. J. Sham, Phys. Rev. **140**, A1133 (1965).

[23] G. B. Bachelet, D. R. Hamann and M. Schlüter, Phys. Rev. B **26**, 4199 (1982).

[24] D.R. Hamann, M. Schlüter, and C. Chiang, Phys. Rev. Lett. **43**, 1494 (1979).

[25] U. von Barth and R. Car, unpublished.

[26] G. B. Bachelet and N. E. Christensen, Phys. Rev. B **31**, 879 (1985).

[27] M. Born and K. Huang, *Dynamical Theory of Crystal Lattices* (Oxford University Press, Oxford, 1954).

[28] W. Cochran and R. A. Cowley, J. Chem. Phys. Solids **23**, 447 (1962).

[29] (a) S. Baroni and R. Resta, Phys. Rev. B **33**, 7017 (1986); (b) M.S. Hybertsen and S.G. Louie, Phys. Rev. B **35**, 5585 (1987).

[30] P. Giannozzi, S. de Gironcoli, and R. Resta, in *Proceedings of the Third International Conference on PHONON PHYSICS*, edited by S. Hunklinger, W. Ludwig, and G. Weiss, (World Scientific Publishing Co, Singapore, 1990), p. 205.

[31] P. B. Littlewood, J. Phys. C **13**, 4893 (1980).

[32] P.Vogl, J. Phys. C **11**, 251 (1978).

[33] J. Perdew and A. Zunger, Phys. Rev. B **23**, 5048 (1981).

[34] M. T. Yin in *Proceedings of the 17th International Conference on the Physics of Semiconductors*, ed. by D. J. Chadi and W. A. Harrison, (Springer, New York, 1985). See also M. T. Yin Phys. Rev. **B** 27, 7769 (1983).

[35] D.J. Chadi and M.L. Cohen, Phys. Rev. B **8**, 5747 (1973).

[36] F. D. Murnaghan, Proc. Nat. Acad. Sci. USA, **50** 697 (1944).

[37] S. de Gironcoli, S. Baroni, and R. Resta, Phys. Rev. Lett. **62**, 2843 (1989).

[38] (a) P.B. Klein, R.K. Chang, Phys. Rev. B **14**, 2498 (1976); (b) A. Mooradian, G.B. Wright: Solid State Comm. **4** 431 (1966).

[39] R. Landolt-Börnstein, *Zahlenwerte und Funktionen aus Naturwissenschaft und technik*, N. S. Vol III 17a, Springer (1982) and references quoted therein.

[40] A. Fleszar and R. Resta, Phys. Rev. B **34**, 7140 (1986).

[41] K. Kunk and P. Gomes Dacosta, Phys. Rev. B **32**, 2010 (1985).

[42] J. L. Warren, J. L. Yarnell, G. Dolling and R. A. Cowley, Phys. Rev. **158**, 805 (1967).

[43] G. Dolling, in *Inelastic Scattering of Neutrons in Solids and Liquids* IAEA, Vienna 1963, Vol. II, p. 37. G. Nilsson, G. Nelin, Phys. Rev. B **6**, 3777 (1972).

[44] G. Nilsson, G. Nelin, Phys. Rev. B **3**, 364 (1971).

[45] D. Strauch and B. Dorner, J. Phys.: Condens. Matter **2**, 1457 (1990).

[46] (a) A. Onton, in *Proc. 10th Int. Conf. Phys. Semiconductors*, USAEC, New York (1970), p. 107; (b) B. Monemar, Phys. Rev. B **8**, 5711 (1973).

[47] M.K. Farr, J.G. Traylor, S.K. Sinha, Phys. Rev. B **11**, 1587 (1975).

[48] M. A. Washington and H. Z. Cummins, Phys. Rev. B **15**, 5840 (1940).

[49] The only previous *ab-initio* calculation on phonons in *AlAs* are by K.J. Chang and M.L. Cohen, in *Proceedings of the* 17^{th} *International Conference on the Physics of Semiconductors*, edited by J.D. Chadi and W.A. Harrison (Springer, New York, 1985), p. 1151. This calculation only provided results for $TO(\Gamma)$, and X modes.

[50] K. Kunc and R.M. Martin, in *Ab Initio Calculation of Phonon Spectra*, edited by J.T. Devreese, V.E. van Doren, and P.E. van Camp (Plenum, New York, 1983), p. 65.

[51] D. Strauch and B. Dorner, J. Phys. C: Solid State Phys. **19**, 2853 (1986).

[52] D. Strauch, A. P. Mayer and Dorner, Z. Phys. B - Condensed Matter 78, (1990).

[53] R. M. Martin, Phys. Rev. B **1**, 4005 (1970).

[54] K. Kunc and P. Hagège, in *Phonon Physics*, edited by J. Kollár, N. Kroó, N.

Menyhárd, and T. Siklós (World Scientific, Singapore), p. 943.

[55] L. Kleinman, Phys. Rev. **128**, 2614 (1962).

[56] C. S. G. Cousins, L. Gerward, J. Staun Olsen, B. Selsmark and B. J. Sheldon, J. Phys. C **20**, 29 (1987); C. S. G. Cousins, L. Gerward, J. Staun Olsen, and B. J. Sheldon, J. Phys. Condens. Matter **1**, 29 (1989).

[57] M. Cardona, K. Kunc and R. M. Martin, Solid State Communications **44**, 1205 (1982)

[58] E. Anastassikis, A. Cantanero, and M. Cardona, Phys. Rev. B **41**, 7529 (1990).

[59] B. A. Weinstein and G. J. Piermarini, Phys. Rev. B **12**, 1172 (1975); and J. Prechtel, J. Kalus, E. Lüscher, L. Pintschovius, and R. Ghosh, Phys. Status Solidi (b) **93** 653 (1979).

[60] R. T. Payne, Phys. Rev. Lett. **13**, 53 (1964); C. J. Buchenauer, F. Cerdeira, and M. Cardona, in *Proc. 2nd Int. Conf. Light Scattering in Solids*, ed. M. Balkanski, Flammarion, Paris 1971, p. 280; and T. Soma, J. Phys. Soc. Jpn. **42**, 1491 (1977).

[61] R. Trommer, Ph.D. thesis, University of Stuttgard 1977; and T. Soma and K. Kudo, J. Phys. Soc. Jpn. **48**, 115 (1980)

[62] A. Fleszar and R. Resta, Phys. Rev. B **34**, 7140 (1986).

[63] M. Cardona, in *Light Scattering in Solids II*, edited by M. Cardona and G. Guntherödt (Springer, New York, 1982).

[64] E. M. Anastassakis, in *Dynamical Properties of Solids*, Vol. 4, pp. 157, North-Holland Publishing Company, (1980).

[65] G. F. Koster, J. O. Dimmock, R. G. Wheeler and H. Statz, *Properties of the thirty-two point groups*, MIT Press, Cambridge, Massachusetts (1963).

[66] A. Baldereschi, S. Baroni and R. Resta, Phys. Rev. Lett. **61**, 734 (1988); and M. Peressi, S. Baroni, A. Baldereschi and R. Resta, Phys. Rev. B **41**, 12106, (1990). See also M. Peressi, Ph.D. thesis, Internationa School for Advanced Studies (SISSA), 1989.

[67] N. W. Ashcroft and N. D. Mermin, *Solid State Physics*, Ed. by Holt, Rinehart and Winston, (1976).